Lithium, Boron and Pb-Pb Isotopic Signatures of the Basement Lithologies Underlying the Eastern Athabasca Basin

A Thesis Submitted to the College of

Graduate Studies and Research

In Partial Fulfillment of the Requirements

For the Degree of Master of Science

In the Department of Geological Sciences

University of Saskatchewan

Saskatoon

By

Robert Allan Millar

© Copyright Robert Allan Millar, December, 2015. All rights reserved.

PERMISSION TO USE

In presenting this thesis in partial fulfilment of the requirements for a Postgraduate degree from the University of Saskatchewan, I agree that the Libraries of this University may make it freely available for inspection. I further agree that permission for copying of this thesis in any manner, in whole or in part, for scholarly purposes may be granted by the professor or professors who supervised my thesis work or, in their absence, by the Head of the Department or the Dean of the College in which my thesis work was done. It is understood that any copying or publication or use of this thesis or parts thereof for financial gain shall not be allowed without my written permission. It is also understood that due recognition shall be given to me and to the University of Saskatchewan in any scholarly use which may be made of any material in my thesis.

Requests for permission to copy or to make other use of material in this thesis in whole or part should be addressed to:

Head of the Department of Geological Sciences
University of Saskatchewan
114 Science Place
Saskatoon, Saskatchewan (S7N 5E2)

ABSTRACT

The eastern margin of the Proterozoic Athabasca Basin in northern Saskatchewan is host to several of the highest-grade unconformity-related (U/C-related) uranium deposits in the world. Many researchers agree that uranium deposition occurred due to oxidized basinal brines transporting uranium mixing with reducing fluids or interacting with reduced rock causing uranium to precipitate, although the source of the uranium is still an unresolved and highly debated subject. Boron isotopic signatures, preserved in refractory minerals such as tourmaline, can aid in determining the source of fluids and P-T conditions during crystallization whereas lithium isotopic fractionation is indicative of weathering, hydrothermal alteration, and/or igneous and metamorphic processes.

For this study a suite of fresh to strongly altered basement samples were selected from multiple sites below the eastern Athabasca Basin to measure the bulk δ^7Li, δ^{11}B and Pb-Pb isotopic signatures. Kinetic modelling of the Li and B isotopic systems suggest that both systems are slightly conservative of their original fluid reservoir, and by calculating the Damkohler numbers (N_D) it is predicted that δ^{11}B will be more indicative of the fluid source whereas lithium isotopes will equilibrate over shorter distance. However, both isotopic systems will fractionate with large concentration changes. Significant variations were observed for both δ^7Li and δ^{11}B, δ^7Li values ranged from 0 to 14 ‰, the range in δ^7Li was interpreted to be representative of both partial melting of metasediments to form granitic pegmatites and hydrothermal fluids. In comparison the range for δ^{11}B was much larger from -16 to +17‰, within the dataset there appeared to be regional isotopic differences but unfortunately this dataset was too small to determine regional isotopic patterns. For each region the δ^{11}B for the

pegmatites was often heavier than the metasedimentary samples suggesting a metasedimentary source for the granitic pegmatites.

Elevated U concentrations and decreasing $^{207}Pb/^{206}Pb$ ratios in both altered and unaltered samples suggest radiogenic Pb and U are present both in the basement and in fluids transporting U through the basement. Partial digestion $^{207}Pb/^{206}Pb$ ratios range from the common $^{207}Pb/^{206}Pb$ ratios of 0.7 to radiogenic $^{207}Pb/^{206}Pb$ ratios of 0.1. The radiogenic $^{207}Pb/^{206}Pb$ are indicative of either resetting of residual material during fluid migration or radiogenic fluids sources interacting with the rocks of this study.

ACKNOWLEDGMENTS

First I would like to thank my two supervisors Dr. Irvine Annesley and Dr. Kevin Ansdell for their continued support and patience throughout this project. The many invigorated discussions at the university, post conference or in the lab at SRC have helped me immensely in achieving my goal of developing into a geoscientist. Also I would like to thank my committee and especially Dr. Bruce Eglington who has provided great insight into data interpretation, sample analysis and the understanding of fluid modelling.

Without the support of both Dr. Roberta Rudnick and Dr. Xiaoming Liu, Li isotopic analysis would not have been possible. Thank you to Xiaoming who, while I was visiting the University of Maryland, made me feel as if I was one of the department while guiding me through the Li isotopic analytical procedure.

This project would not have been completed without the full support of the Saskatchewan Research Council; more specifically, the Mining and Minerals team including Bernard Gartner, Bryan Schreiner, Al Holsten and the uranium geochemistry laboratory. SRC provided the encouragement, financial assistance and freedom to pursue my academic achievements while working in the uranium exploration industry. In addition I would like to acknowledge the financial assistance provided by the NSERC Discovery Grant to Kevin Ansdell.

To all the many friends that I have made both in the department and through networking at the many conferences, your conversations benefited me in many ways.

Lastly, thank you to my family who has been very patient and encouraging throughout this entire project. Without the immediate support of my expanding family, Lucy, Fergus and my beautiful wife Heather, I could not have completed this work.

TABLE OF CONTENTS

page

LIST OF TABLES

LIST OF FIGURES

CHAPTER 1
INTRODUCTION

1.1 Introduction

The Proterozoic Athabasca Basin in northern Saskatchewan, Canada, contains the highest grade unconformity-related (U/C-related) uranium deposits in the world. Covering nearly 100,000 km^2, the Athabasca Basin is comprised of a sedimentary rock sequence underlain by Archean to Paleoproterozoic metamorphosed basement rocks, which include graphitic pelitic gneisses and granitic pegmatites (Annesley et al., 2005). Deposition of uranium occurred at approximately 1500 Ma and remobilization events have been suggested at 1270 Ma, 950 Ma and 300 Ma (Alexander et al., 2009; Fayek and Kyser., 1997; Reid et al., 2014). Many of the uranium deposits occur along major faults related initially to the Talston Magmatic Zone or the Trans Hudson Orogen. However, many of these faults were reactivated episodically and thus provided focal points for fluid flow and mixing.

Oxidized basinal brines flowed through the Proterozoic Athabasca Basin and the basement rocks below the unconformity (Hoeve and Sibbald., 1978) scavenging, remobilizing and depositing U and other metals. Mixing of oxidized basinal brines with reducing fluids or reduced rocks caused changes in the redox chemistry of oxidized fluids to precipitate uranium (Alexandre et al., 2005). Understanding both the characteristics of the fluids and the fluid pathways are critical for developing high-quality uranium deposit models. Considerable knowledge gains have been achieved in recent years due to the rapid evolution of analytical capability thus providing both exploration companies and researchers greater accessibility to tools for routine analysis of many different isotopic systems including $\delta^{37}Cl$, Pb-Pb, δD and $\delta^{18}O$ (Alexandre et al., 2005; Cloutier et al., 2010; Cloutier et al., 2011; Holk et al., 2003; Richard et al., 2011; Wilson and Kyser., 1987). With the success of traditional isotopic systems in the

interpretation of uranium deposits, further understanding of the complicated hydrothermal uranium ore deposit system is potentially achieved by combining traditional isotopic systems with other non-traditional isotopic systems such as U-Th-Pb with δ^{7}Li and δ^{11}B (Mercadier et al., 2012).

Lithium has two naturally occurring stable isotopes, ^{6}Li (7.5%) and ^{7}Li (92.5%), with a mass difference between the two isotopes of approximately 17% (Olive and Schramm., 1992). This monovalent element is often mobile in the presence of fluids, moderately incompatible and is not redox sensitive (Chacko et al., 2001; Tomascak., 2004). Fractionation of lithium isotopes can occur due to many physio-chemical processes including changes in temperature, pH or the Li-coordination in minerals, fluids and melts (Maloney et al., 2008; Teng et al., 2006; Wunder et al., 2007). Significant relative mass differences between the two isotopes and preferential fractionation during fluid-rock interactions, due to the preference of ^{7}Li for smaller coordination sites or stronger bonds and ^{6}Li to weaker bond sites and higher coordination (Tomascak., 2004), can influence natural δ^{7}Li values which range from -20‰ in peridotites to +50 ‰ in marine evaporites. The considerable range in isotopic signatures means that lithium has potential as an excellent geochemical tracer of many different geological processes. Lithium isotopic fractionation has been used to examine igneous processes from magmatic differentiation in the alkaline to peralkaline Illimaussaq plutonic system in Greenland (Marks et al., 2007) to pegmatite formation (Liu et al., 2010; Maloney et al., 2008; Teng et al., 2006) and the source of these igneous rocks(Tomascak et al., 2005). This isotopic system is not just specific to igneous processes but has also been used to interpret other geological processes including the effects of chemical weathering of the continental crust (Liu et al., 2013;Liu and Rudnick., 2011; Millot et

al., 2010), the origin of brines in the Canadian Shield (Bottomley et al., 2003), and the effects of metamorphism on metapelites around the Onawa pluton, Maine (Teng et al., 2007).

At this point there has been no significant research into lithium isotopes in the Athabasca basin other than a model proposed by Kyser et al. in 2009 (Fig. 1-1) suggesting that as hydrothermal fluids flow toward uranium deposition δ^7Li should increase within the alteration path providing vectoring towards mineralization. The investigation of lithium isotopes in relation to U/C-related uranium deposits of the Athabasca basin could aid in the determination of a source for the pegmatites (Liu et al., 2010; Maloney et al., 2008; Teng et al., 2006), and the effects of hydrothermal activity and metamorphism of the metasedimentary rocks beneath the Athabasca basin (Liesbscher et al., 2007; Teng et al., 2007). During hydrothermal activity it would be predicted that δ^7Li increases as both the temperature and the volume of fluid reacting with the host rock increases. This is because the heavier isotope ^{7}Li tends to prefer smaller coordination sites or stronger bonds in the liquid phase during fractional crystallization whereas ^{6}Li prefers higher coordination or weaker bonds in fluids and minerals, such as mica (Wunder et al., 2007). This preference for specific bond sites can be observed in the preferential partitioning of lithium into pelitic metamorphic minerals in the following order staurolite>cordierite>biotite> muscovite> garnet (Duttrow et al., 1986). During partial melting of metapelites lithium will become depleted but the δ^7Li will remain relatively constant (Teng et al., 2007). If there is a significant changes in δ^7Li of the metasedimentary rocks most likely they will occur due to interaction with hydrothermal fluids which can have δ^7Li signatures as heavy as +44‰ (Tomascak., 2004).

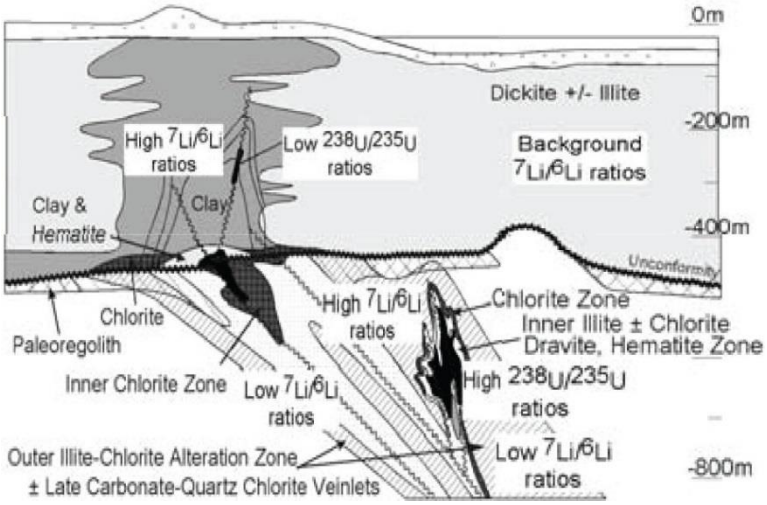

Figure 1-1. Model of potential Li isotopic ratios in relation to U/C-related uranium deposition in the Athabasca Basin. From Kyser et al. (2009).

Similar to lithium, boron has two naturally occurring stable isotopes, ^{10}B (19.9%) and ^{11}B (80.1%), and the natural $\delta^{11}B$ range is extensive from -30‰ in non-marine evaporites to +60 ‰ in marine evaporites (Mercadier et al., 2012; Tornos et al., 2012). This incompatible element is the major component of the multiple generations of tourmaline found in the Athabasca Basin and underlying basement, and due to its refractive nature tourmaline has the potential to preserve primary isotopic signatures of either igneous or metamorphic activity. Thus minimizing the effects of post-crystallization hydrothermal fluid alteration events causing fractionation (Kawakami., 2001; Marschall and Jiang., 2011; Trumbull et al., 2011; van Hinsberg et al., 2011). The B isotopic composition recorded by tourmaline will be influenced by fractionation during interaction with fluids, mineral composition and other geological processes such as degassing of magmas preferentially volatizing ^{11}B (Jiang and Palmer., 1998; van Hinsberg et al., 2011; van Hinsberg., 2011). During processes such as migmatisation, boron is lost from the source rock, and similar to lithium isotopes the heavier ^{11}B preferentially partitions into the melt during partial melting which affects both the boron isotopic composition of the source rock and the

pegmatite or leucogranite that crystallizes from the melt (Kawakami, 2001). The source rock undergoing partial melting will contain tourmalines with lower $\delta^{11}B$ whereas the fluid forming the pegmatite will have higher $\delta^{11}B$. The $\delta^{11}B$ of the residual rock and the newly formed pegmatite will retain the P-T conditions during alteration and crystallization processes (Jiang and Palmer., 1998).

Multiple studies have examined the relationship between $\delta^{11}B$ and a range of deposit types from magmatic emeralds to hydrothermal uranium deposition. Exploring for emerald deposits in both Australia and the North West Territories researchers have used $\delta^{11}B$ from tourmaline to determine the source of both the alteration and formation fluids of emerald deposits (Trumbull et al., 2009) and to differentiate whether the source of the emerald deposits was granitic or ultramafic (Galbraith et al., 2009). Similarly for hydrothermal deposits, $\delta^{11}B$ has been successful for distinguishing the evolution and source of fluids in both Brazilian IOCG deposits (Xavier et al., 2008) and Au deposits (Garda et al., 2009), and to interpret the source of fluids in hydrothermal uranium deposition (Fig. 1-2) in both India (Pal et al., 2010) and the Athabasca Basin (Mercadier et al., 2012). The studies up to now have determined that the tourmalines proximal to uranium deposits have higher $\delta^{11}B$ signatures, likely recording the influence of marine evaporites or seawaters.

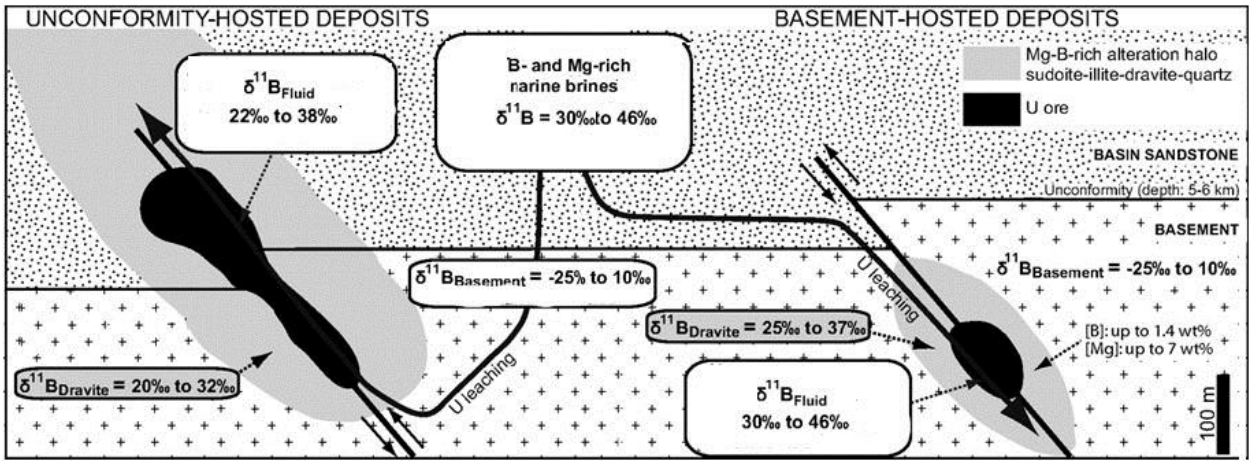

Figure 1-2. Model of potential boron isotopic ratios in relation to U/C-related uranium deposition in the Athabasca Basin. From Mercadier et al. (2012).

The source of uranium for the hydrothermal U/C-related uranium deposits in the Athabasca basin is still heavily debated (Jefferson et al., 2007). Radioactive decay of the U-Th isotopic systems provides a measurable daughter product Pb isotopic signature. If this radiogenic system is a closed system locked in an unaltered detrital zircon or monazite it is an excellent geochronometer, but if the system is open such as in a hydrothermal system in which uranium is leached from the detrital mineral it can still be used as a geochronometer but there are other potential uses as well. The radioactive decay of ^{238}U to ^{206}Pb leads to increased ratios of $^{206}Pb/^{204}Pb$, if the ratio of $^{206}Pb/^{204}Pb$ >30 the sample is considered radiogenic and could have potential as a uranium pathfinder (Holk et al., 2003). Cloutier et al (2010) determined a weak acid leach is the best mechanism to examine if the lead present is loosely bound and could be used as a geochemical pathfinder. To determine if the lead isotopes are a potential uranium pathfinder the concentration of lead can be classified as either supported or unsupported based on whether the lead can be attributed back to the concentrations of uranium in the sample. In a closed system ^{238}U decays at a known rate over time to ^{206}Pb, as the $^{206}Pb/^{204}Pb$ ratio increases over time this lead is not lost and can be used as a geochronometer. Whereas in an open system

the $^{206}Pb/^{204}Pb$ radiogenic lead ratio increases due to the interaction of hydrothermal fluids transporting lead from a uranium-rich source. Therefore in the open system if the age of mineralization and the concentrations of ^{238}U, ^{206}Pb and ^{204}Pb are known, the isotopic signature can be used as a pathfinder to mineralization (Holk et al., 2003; Marschall et al., 2007).

Experimental petrology studies have shown that in thorium-rich monazite uranium is found as a trace element and that both U and Th fractionate differently during crystallization dependent on the composition of the fluids present. During the crystallization of monazite the higher the pressure, temperature and SiO_2 in the fluids the more likely uranium is to be found in higher concentrations in monazite. Also the concentration of uranium in monazite can increase if the source of the melt is from the partial melting of metasediments (Stepanov et al., 2012). Once monazite is formed in an igneous system Th is relatively insoluble compared to HREE, U and Pb. Alteration of monazite by hydrothermal fluids will deplete the host rock in HREE, U and Pb and enrich the host rock in Th, precipitating insoluble thorium-rich minerals such as monazite, thorite or huttonite (Seydoux-Guillaume et al., 2002). The resulting geochemical signature would be an increase in the Th/U ratio relative to unaltered rock. This alteration of monazite is often a challenging process but fluids such as calcium-rich brines have demonstrated the ability to partially dissolve monazite (Seydoux-Guillaume et al., 2002). Many fluid inclusion studies of the Athabasca Basin have confirmed the presence of calcium-rich brines in the basement lithologies (Derome et al., 2005; Mercadier et al., 2009; Richard et al., 2010) and combined with the high heat production from the Trans-Hudson Orogen would have provided the right conditions to form Hudsonian granitic pegmatites from metasedimentary melt. Exposing these pegmatites to hydrothermal alteration by oxidative brines could alter monazite and provide uranium for the large U/C-related mineralization. In the Athabasca Basin both detrital minerals

in the sandstone (Hoeve and Sibbald, 1978; Hoeve and Quirt, 1984; Kotzer and Kyser, 1995; Fayek and Kyser, 1997;) and U-rich minerals of the basement including monazite and zircon have been suggested as the source of uranium (Annesley and Madore, 1999; Madore et al. 2000; Hecht and Cuney, 2000; Cuney et al. 2003; Richard et al., 2010; McKechnie et al., 2012a, 2012b; Mercadier et al., 2013). This difference in opinion is not specific to the Athabasca Basin, the uranium source in other basin type uranium regions such as Tin Mersoi Basin in Niger, detrital monazite is considered a potential source of uranium (Wagani et al., 2011) whereas the suggested uranium source for the Four Mile West mineralization, South Australia is proximal U-rich breccias, granites and gneisses (Hore and Hill, 2011).

As mentioned above all three isotopic systems are affected by hydrothermal alteration and metamorphic processes. During prograde metamorphism B, Li and Pb are all mobilized and substitute into metamorphic minerals (King et al., 2007; Marschall et al., 2006). Isotopic fractionation can be affected by the isotopic preference for partitioning into specific minerals and fluids based on the preferred coordination, similarly elemental partition coefficients determine the elemental preferences for specific minerals. For example during metamorphism metamorphic minerals in pelitic rocks preferentially partition lithium into the crystal structure in the following order staurolite>cordierite>biotite> muscovite> garnet (Duttrow et al. 1986). In regards to hydrothermal alteration lithium partitions preferentially into Mg silicates, chlorite and tourmaline whereas boron preferentially precipitates as hydrothermal tourmaline (Marschall et al., 2006). Coupling $\delta^{11}B$ and $\delta^{7}Li$ to determine the source of fluids has been effective in a number of cases. For example, $\delta^{11}B$ and $\delta^{7}Li$ was used to determine that the source of leucogranites in the Black Hills, South Dakota was adjacent metapelites (Wilke et al., 2002). Shabaga et al. (2010) inferred that Li and B isotopes can be used for interpreting provenance and

source for Cu-bearing tourmalines in different mining districts from Brazil, Nigeria and Mozambique. The combination of the three isotope systems has shown good potential in determining the source and provenance of the fluids and also understanding the metamorphic conditions of the region.

All three isotopic systems require precise and accurate measurement, especially for low mass isotope systems such as boron and lithium. Historically boron and lithium isotopic analysis were performed with great precision using thermal ionization mass spectrometry (TIMS) but this method can be costly and time consuming. More recently researchers are using more rapid and cost effective analysis techniques which include quadrupole inductively coupled plasma mass spectrometry (Q-ICPMS) (Al-Ammar et al., 2000), high resolution inductively coupled plasma mass spectrometry (HR-ICPMS)(Tirez et al., 2010; Vogl et al., 2011,) and multi-collector inductively coupled plasma mass spectrometry (MC-ICPMS) (Gangjian et al., 2013; Magna et al., 2004). Isotopic analysis for this project will be provided by both MC-ICPMS and single collector HR- ICPMS instruments that can provide both the precision and accuracy that at one time was only reserved for TIMS (Tirez et al., 2010).

1.2 Objectives

The primary objective of this study is to determine the bulk chemistry, δ^{7}Li, δ^{11}B and U-Th-Pb isotopic signatures by ICP-MS for fresh and altered basement rocks from the eastern Athabasca Basin. Furthermore investigating observed variations in isotopic composition, both locally and regionally, and determine possible explanations for the variations observed. As well if there is a relationship between Li, B and U-Th-Pb isotopic systems and U/C-related uranium deposits and thus whether there is vectoring potential of these systems for uranium exploration.

1.3 Sampling Locations and Analytical Techniques

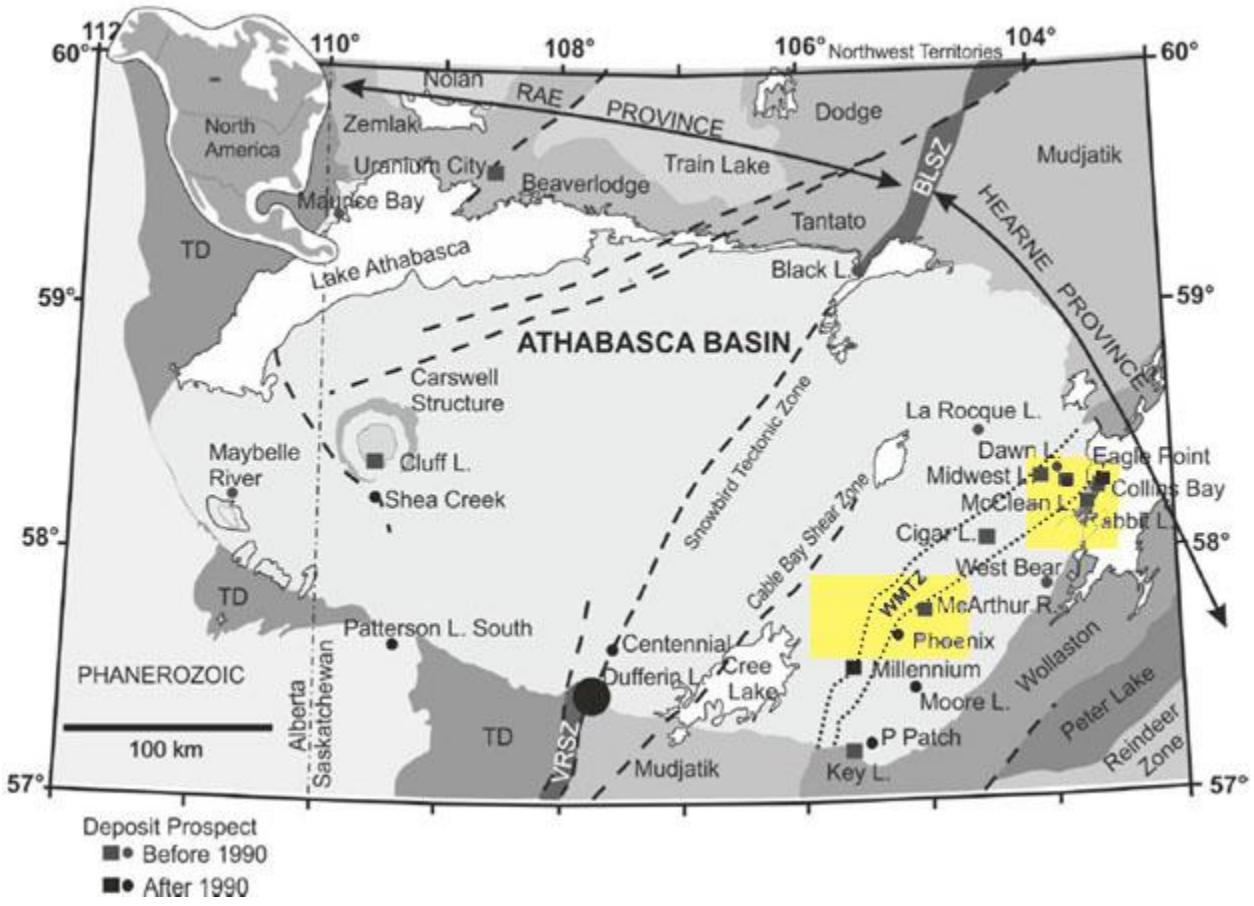

Figure 1-3. Geologic map of the Athabasca Basin (Saskatchewan, Canada) including many of the present and past uranium mines, highlighting the two sample localities of basement lithologies underlying the eastern margin of the Proterozoic sandstone. Site 1(SRC EAGLE project) was located in the NE region of the Athabasca Basin encompassing McClean Lake and Dawn Lake, site 2 (SRC EAGLE 2 project) is SW of site 1 highlighting Epp Lake, Read Lake and McArthur River. Modified from Jefferson et al. (2007), Card (2012) and Pascal (2014).

The Wollaston EAGLE and EAGLE 2 (Eastern Athabasca Geotransect/Lithoprobe Extension) projects were initiated in 1994, and over multiple years the investigators developed integrated geological interpretations/models using lithostratigraphic, geochemical, geophysical and geochronological data with the final expectation of developing new metallogenic models and exploration tools for U/C-related uranium deposits in Saskatchewan (Annesley et al. 1995, 1996,

1998, 1999). Project contributors included Cameco, Cogema Resources Inc., PNC Exploration (Canada) Co. Ltd., Uranerz and the Saskatchewan Research Council. Initial data was to be released to the contributing companies and then, with consent from all partners, the intention of Annesley, Madore, Shi, Quirt, Dyck, Hajnal and Reilkoff was to publish a series of papers summarizing their findings. All sample data, vials and core were stored at the Saskatchewan Research Council (SRC) Geoanalytical laboratories since completion of the project in 1999 (geological summary; Annesley et al., 2005).

Samples were collected from multiple locations within two areas on the eastern margin of the Athabasca Basin (Fig. 1-3). In 1995 samples were collected from site 1 of the Wollaston EAGLE project which was located approximately 300 km north of La Ronge within the 2500 km^2 NEA/IAEA Athabasca Test Area (Cameron, 1983). Two years following the original drill program samples were collected for Segment 2 of the Wollaston EAGLE 2 report from a 7500 km^2 area approximately 250 km north of La Ronge (Site 2). The sites of interest for this study included fresh and altered basement rocks from the area of known deposits including Dawn Lake (10 kt U at a grade of approximately 1.5%), Epp Lake, McClean Lake (19 kt U at a grade of approximately 2.78%), McArthur River (192 kt U at a grade of approximately 22%) and Read Lake (Jefferson et al., 2007).

After careful review of historical data, the author Millar and co-supervisor Dr. Annesley selected a suite of samples that displayed anomalous concentrations of Li, B, Th, Pb and U specifically from the Dawn Lake region. This suite of samples was made up of potential uranium source rocks including granitic pegmatites, pelitic gneisses and graphitic pelitic gneisses. A second set of sample was selected in proximity to the Epp Lake, McArthur River, McClean Lake and Read Lake uranium deposits using similar chemical criteria.

To determine the bulk isotopic and chemical compositions, pulverized drill core from previous SRC projects (Wollaston EAGLE and EAGLE 2) were retrieved from storage for chemical analysis. The bulk chemical Pb isotopes, major and trace elements, including B, Li and REE's were analyzed using ICP-OES and ICP-MS at the SRC Geoanalytical Laboratory. Boron isotopic signatures were analyzed by Dr. Ilia Rodushkin at ALS Sweden with both HR-ICPMS and MC-ICPMS. The author travelled to the University of Maryland to work with Dr. Roberta Rudnick and Dr. Xiaoming Liu at the UMD Geochemistry Plasma lab performing both the chemical separation and the Li isotopic analysis by MC-ICPMS.

1.4 Thesis Structure

The first few chapters of this thesis outline the foundation for this project. Chapter 2 is a review of the geological background of the Athabasca Basin region and U/C-type uranium deposition followed by the methods of analysis outlined in Chapter 3. The results from both the analytical work and computational modelling are presented in Chapter 4 and Chapter 5, respectively. Chapter 6 discusses the behaviour of lithium and boron isotopic systems during metamorphism, partial melting and hydrothermal fluid interaction. In addition, the relationship of δ^{7}Li and δ^{11}B variations to uranium mineralization and the potential of the basement as a uranium source is examined, as well as the feasibility of performing routine B and Li isotopic analysis by single collector HR-ICPMS. The entire body of work for the project in the Athabasca Basin along with potential future research initiatives are summarized in Chapter 7.

.

CHAPTER 2
GEOLOGICAL BACKGROUND

2.1 Geology of Archean and Proterozoic Basement

The western side of the Athabasca Basin is underlain by the southern extension of the Taltson Magmatic Zone (TMZ) (Jefferson et al., 2007). Rock types to the southwest of the basin in proximity of the Patterson Lake South deposit include predominantly Paleoproterozoic granitic gneiss, amphibolite, and pelitic gneiss of Taltson-age and post-metamorphic plutonic rocks (Fig. 1-3) (Card et al., 2007; Card et al., 2014). The earliest igneous rocks are interpreted to have formed in a continental magmatic arc at about 2.0 and underwent peak metamorphism at approximately 1.93 Ga (Card et al., 2007; Card et al., 2014).

The Rae Province is exposed around the Carswell Structure and north of Lake Athabasca, where it is subdivided into a number of domains (Fig. 1-3), including the Zemlak, Beaverlodge and Tantato domains immediately north of the basin (Ashton et al., 2009; Card et al., 2007). Metamorphic grade is up to granulite grade, and the intensity of deformation varies. Uranium mineralization in the Rae includes the vein type mineralization in the Beaverlodge domain and the U/C-related Shea Creek and Cluff Lake uranium deposits adjacent to the Carswell structure (Ashton et al., 2009; Jefferson et al., 2007).

A NE-trending structure, the Snowbird tectonic zone, separates the Rae province to the west and the Hearne province to the east (Hoffman, 1988, Hoffman, 1990). This is a significant crustal structure, which was reactivated after the formation of the Athabasca Basin, and along which uranium mineralization has been discovered (Dufferin Lake zone and Centennial deposit; Pascal, 2014; Reid et al., 2014).

The Hearne Province is divided into three major regions the Mudjatik Domain, the Wollaston Domain, and the Wollaston-Mudjatik Transition Zone (WMTZ) (Fig. 1-3). The

transition zone between the Wollaston and eastern Mudjatik basement domains underlies the majority of known U deposits located in the eastern Athabasca Basin and is a significant structural corridor (Annesley and Madore, 1989, Annesley and Madore, 1994). The Mudjatik Domain is a NE-trending belt of Archean felsic gneisses with a "dome and basin" structural character, whereas the Wollaston Domain is a NE-trending fold-thrust belt of Paleoproterozoic Wollaston Group metasedimentary rocks overlying Archean granitoid gneisses (Annesley et al., 2005; Yeo and Delaney, 2007). Collisions during the Trans-Hudson Orogen (THO) at ca. 1.8 Ga led to the development of the Wollaston fold-thrust belt, and later major structures which trend NW-WNW (Annesley et al., 2005; Portella and Annesley, 2000). The lower Wollaston Group is mainly composed of pelitic gneiss, which is often graphitic, overlain by psammitic to psammopelitic gneisses, calc-silicate gneisses and metaquartzites (Annesley et al., 2005). The Wollaston domain is intruded by syn to post peak thermal metamorphic granitic pegmatites and leucogranites. Partial melting of pelitic to psammopelitic rocks of the Wollaston Group at peak metamorphism (800 MPa, 800^{o}C) during the THO (Annesley et al., 2005, Mercadier et al., 2013) generated migmatites and pegmatite bodies in which uranium was concentrated and thus providing a potential U source in the basement (McKechnie et al., 2012).

2.2 Geology of the Athabasca Basin

The present day Proterozoic Athabasca Basin is a 1.5 km thick sequence of flat lying, unmetamorphosed and undeformed Paleoproterozoic to Mesoproterozoic sedimentary rocks, dominated by quartz arenite, and covering an area of approximately 100,000 km^2 (Ramaekers, 1990). The basin unconformably overlies Archean to Paleoproterozoic basement rocks, described above, and started being filled at about 1700 -1750 Ma (Kotzer et al., 1992). Four sedimentary sequences have been identified (Ramaekers et al., 2007). The oldest sequence is the quartz

arenite Fair Point Formation which only occurs on the west side of the basin. The Read Formation, Smart Formation and Manitou Falls Formation comprise the second sequence with varying quantities of quartz arenite, pebbly arenites and conglomerates of fluvial origin. The third sequence consists of the Lazenby Lake Formation and Wolverine Point Formation, quartz arenite with more common mudstone intervals. The upper most sequence of Locker Lake and Otherside Formations are dominated by quartz arenite and quartz pebbly arenite (Ramaekers et al., 2007). Paleocurrent directions indicate that the dominant direction of transport of detritus was from east to west, suggesting derivation from uplifted THO to the east (Ramaekers, 1990). During the Mesoproterozoic, the sedimentary rocks in the Athabasca Basin formed a 5 to 6 km thick package, based on fluid inclusion data (Pagel, 1975), whereas the current topography of the basin was controlled by the southwest advance and northwest retreat of the Quaternary Laurentide Ice Sheet (Campbell, 2007).

2.3 Review of Athabasca Basin Unconformity-Related (U/C-Related) Deposits

U/C-related uranium deposits in the Athabasca Basin occur as two main types (Fig. 2-1) 1) simple "basement-hosted" deposits composed primarily of uraninite and 2) complex "unconformity-hosted" deposits which occur typically at the unconformity and are polymetallic mineralization with sulphides, arsenides and uraninite (Cuney and Kyser, 2008; Fayek and Kyser, 1997; Thomas et al., 2000). The majority of the known U mineralization is located on the eastern side of the Athabasca Basin (Fig.1-3) at, above or below the unconformity (Fig. 2-1). This corridor is located on the Wollaston-Mudjatik transition zone and correlates to a zone of high heat production (HHP) in the basement rocks due to high radioelement (U,Th,K) contents (Madore et al., 2000). The U/C-related uranium deposits are typically structurally-controlled and uranium mineralization occurred due to redox changes in uranium-rich diagenetic hydrothermal

fluids (Hoeve and Sibbald, 1978). Oxidized basinal brines flowed through the Athabasca basin and the basement rocks, leaching and transporting uranium, and episodic reactivation of major faults provided focal points for fluid flow (Hoeve and Sibbald, 1978). Fluid inclusion studies have showed that the basinal brines were a combination of Na-Cl rich, Ca-Cl rich, and low salinity fluids (Derome et al., 2005; Derome et al., 2007; Mercadier et al., 2009; Richard et al., 2011).

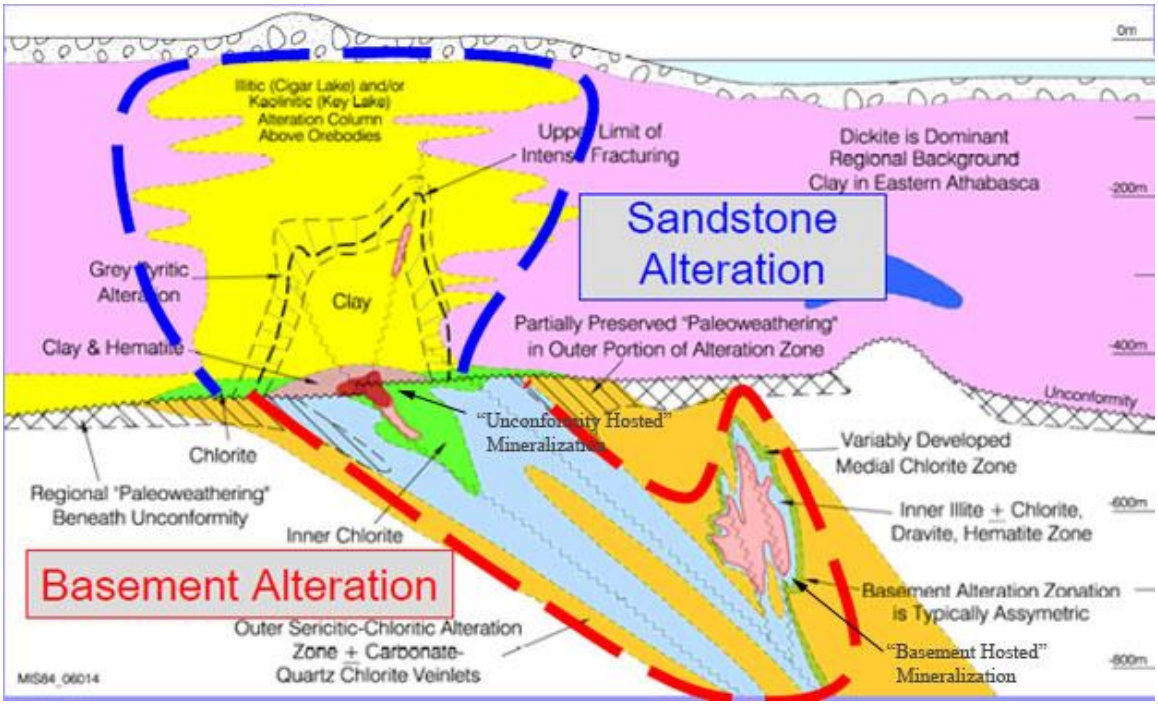

Figure 2-1. Model of both sandstone and basement alteration in relation to uranium mineralization at the unconformity from Brisbin and Cuney (2010).

Alteration haloes around the deposit represent good exploration targets but there are significant differences in alteration haloes between the two deposit types. "Unconformity hosted" tend to have extensive and intense clay rich alteration both above and below the unconformity, whereas surrounding "basement hosted" deposits clay-rich alteration is not as significant and is found only in the basement (Fig. 2-1) (Cuney and Kyser, 2008; Fayek and Kyser, 1997; Thomas et al., 2000). Alteration mineral assemblages include, but are not limited to illite, sudoite,

dravite, quartz and hematite (Hoeve and Sibbald, 1978; Kotzer and Kyser, 1995; Derome et al., 2005; Kyser and Cuney, 2008).

Paleoweathering profiles are preserved below the basin, and locally extend down to depths of 220 m along basement faults (Macdonald, 1980). Penetration of basinal brines into the basement is extensive and driven by reactivation of basement structures and thermal convection (Richard et al., 2010). There is still significant debate over the source of uranium (Jefferson et al., 2007) but the basement lithologies contain many uranium rich minerals including magmatic and metamorphic uraninite (Annesley et al., 1999; McKechnie et al., 2012; Mercadier et al., 2013), monazite (Hecht and Cuney, 2000; Madore et al., 2000) and pre-Athabasca U mineralization (Parslow and Thomas, 1982). The upper limit of uranium concentrations in the unaltered basement rocks can range from 40 ppm in pelitic rocks to as high as 2400 ppm in granitic pegmatites and leucogranites, for example Fraser Lakes Zone B (McKechnie et al., 2013). Fluid inclusion studies of basinal brines trapped in quartz contain uranium concentrations which range from < 0.2 to 600 ppm (Richard et al., 2012) which suggests infiltration into the uranium-rich basement by chloride rich brines capable of transporting uranium. Mixing of oxidized basinal brines with reducing fluids or reduced rocks caused changes in the redox chemistry of fluids transporting uranium to precipitate uranium at, above or below the unconformity (Alexandre et al., 2005).

2.4 Uranium Deposit Summary

Samples for this study were collected in the vicinity of five deposits along the WMTZ. These vary in size from uranium showings to some of the highest-grade U/C-related uranium deposits in the world (Fig. 1-3), and are described briefly below.

2.4.1 McClean Lake

McClean Lake is located 11km W/NW of Rabbit Lake and operated by Areva Resources in partnership with Denison Mines and OURD Canada Co., with an average grade of 3.28 % U_3O_8 and combined reserves of 42.7 Mlbs U_3O_8 (Jefferson et al., 2007). Mineralization occurs in six different pods with a mix of polymetallic ore and monomineralic uraninite hosted both in the sandstone and the crystalline basement. The mineralized pods are divided into the North and South regions of McClean Lake, although the largest is Pod 1 of McClean Lake North. Alteration mineral assemblages include chlorite, pyrite, illite and hematite (Wallis et al., 1983).

2.4.2 Dawn Lake

The Cameco-operated Dawn Lake uranium deposit consists of 4 zones, each zone containing 3 to 4 NE-SW cigar-shaped ore bodies with an average grade for the deposit of 1.69 % U_3O_8 and a cumulative reserve of 12.94 Mlbs U_3O_8 (Geology and uranium resources of the Dawn Lake deposit: unpublished report of Cameco Corporation). Hosted in metapelites, calc-silicate rocks, biotite gneiss and pegmatite of the Wollaston Group (Chan et al., 2000) the basement alteration is primarily chlorite and illite (Quirt, 1997). The 100 to 190 m long and 20 to 45 m wide cigar-shaped ore bodies at Dawn Lake are different from the traditional eastern Athabasca Basin ore bodies, which are controlled by NE-SE reverse faults, as they are associated with a steeply west-dipping strike-slip fault system (Chan et al., 2000).

2.4.3 Epp Lake and Read Lake

Both Epp Lake and Read Lake are considered significant uranium prospects with prospective geological features analogous to current uranium deposits. Original exploration of Epp Lake from 1986 to 2000 was conducted by Uranerz and Cameco Corp, and uranium mineralization was discovered in an area adjacent to an E/NE-trending Archean granite dome flanked by metasedimentary rocks and overlain by 800 to 950 m sandstone. Currently this

region is under operation by Denison Mines (http://www.denisonmines.com/i/pdf/Projects/Canada/Epp-Lake-Fact-Sheet.pdf). The basement rock in the Epp Lake region was subjected to metamorphic conditions with temperatures reaching between 700 and 800^{o}C and high to moderate pressure up to 70 kPa (Annesley et al., 1996).

Read Lake is currently operated by Cameco Corp and is located west of the P2 trend that hosts McArthur River Deposit but on the same conductor trend as the Millennium deposit. During the 2007/2008 exploration campaign Cameco discovered significant mineralization 90 to 150 m above the unconformity (www.cameco.com/exploration/majorprojects/athabascabasin/read_lake).

2.4.4 McArthur River

The McArthur River deposit is the largest high-grade U deposit in the world. The average grade is 14.36 % U_3O_8 with total reserves of 416.5 Mlbs U_3O_8 in a group of pods hosted in both the sandstone and the basement (McGill et al., 1993). This major deposit is hosted in the hanging wall of the P2 fault, with varying abundances of cordierite-bearing pelitic rock, and graphite-bearing pelitic gneiss, whereas the footwall is composed of metaquartzite and silicified metarkose (McGill et al., 1993). Alteration for the basement mineralization transitions very abruptly from unaltered host rocks to intense chloritic alteration and then into high grade monometallic U mineralization (Cuney and Kyser, 2008).

CHAPTER 3
SAMPLES AND ANALYTICAL METHODS

3.1 Sample Selection and Description

The samples used in this study were originally collected from within two areas on the eastern margin of the Athabasca Basin, namely the 2500 km^2 NEA/IAEA Athabasca Test Area approximately 300 km north of La Ronge (Cameron, 1983) and a 7500 km^2 area 250 km north of La Ronge (Fig. 1-3). Core logging of both drill holes contributed by Cameco, Cogema Resources Inc., PNC Exploration (Canada) Co. Ltd., and Uranerz was performed by the geological technical team at the Saskatchewan Research Council as part of the Wollaston EAGLE (Eastern Athabasca Geotransect/Lithoprobe Extension) project initiated in 1994. The sites of interest for this study included fresh and altered basement rocks adjacent to known deposits including Dawn Lake, Epp Lake, McClean Lake, McArthur River and Read Lake.

After careful review of historical data, the author Millar and co-supervisor Dr. Annesley selected a suite of samples that displayed anomalous concentrations of Li, B, Th, Pb and U. This suite of samples was made up of potential uranium source rocks including granitic pegmatites, pelitic gneisses and graphitic pelitic gneisses. The samples chosen are listed in Table 3-1.

Pelitic gneiss vary in colour and grain size (Fig. 3-1a), and are often interlayered with graphitic pelitic gneiss, psammopelitic, calc-pelitic and calc-silicate gneiss throughout the eastern Athabasca. These metasedimentary rocks are typically highly deformed, and often migmatitic with up to 60 % leucosomes. Typical mineralogy includes quartz, plagioclase, K-feldspar, biotite with minor garnet, cordierite, sillimanite, tourmaline, chalcopyrite, pyrrhotite and ilmenite. Common accessory minerals are zircon, monazite and apatite, and post-peak metamorphic minerals include chlorite, muscovite, titanite, rutile and sericite.

Sample Number	Deposit Area	Depth m	Rock Type	Comments
A94-040D	Eagle Point	Outcrop	Outcrop	Magnetite bearing Pegmatite
I57 114.5	McClean Lake	114.5	Pegmatite	Paleoweathered
Q6-66 131.2	Dawn Lake	131.2	Pelitic Gneiss	Corderite; Paleoweatherd
Q6-66 149.7	Dawn Lake	149.7	Graphitic Pelitic Gneiss	Bleached; Sulphides
Q6-66 164.2	Dawn Lake	164.2	Pegmatite	Altered Radioactive
Q6-66 170.9	Dawn Lake	170.9	Graphitic Pelitic Gneiss	Bleached
Q6-67 104.4	Dawn Lake	104.4	Pelitic Gneiss	Migmatitic; Paleoweatherd
Q6-72 108.7	Dawn Lake	108.7	Pelitic Gneiss	Paleoweathered
Q6-72 114.5	Dawn Lake	114.5	Pegmatite	Tourmaline
Q6-72 117.2	Dawn Lake	117.2	Graphitic Pelitic Gneiss	Sulphides
Q7-16 266.8	Dawn Lake	266.8	Pegmatite	Tourmaline
Q9-16 183.6	Dawn Lake	183.6	Pelitic Gneiss	Garnet-Corderite; Paleoweathered
Q9-16 191.3	Dawn Lake	191.3	Pelitic Gneiss	Paleoweathered; Corderite
Q9-16 199.6	Dawn Lake	199.6	Graphitic Pelitic Gneiss	Sulphides; Corderite
Q9-16 214.6	Dawn Lake	214.6	Pelitic Gneiss	Garnet-Corderite
Q9-16 217.2	Dawn Lake	217.2	Pelitic Gneiss	Garnet-Corderite
EL 09-797.7	Epp Lake	797.7	Pegmatite	Clay Altered Proximal U
EL-09-823.7	Epp Lake	823.7	Pegmatite	Clay Altered Proximal U
RL-46-570.1	Read Lake	570.1	Pegmatite	Paleoweathed
RL-80-454.5	Read Lake	454.5	Tourmalinite	
MAC 207.511.1	McArthur River	511.1	Graphitic Pelitic Gneiss	
MAC 207.664.8	McArthur River	664.8	Psammitic Gneiss	

Table 3-1. Project sample summary all sample numbers indicate the drill hole then the sample depth.

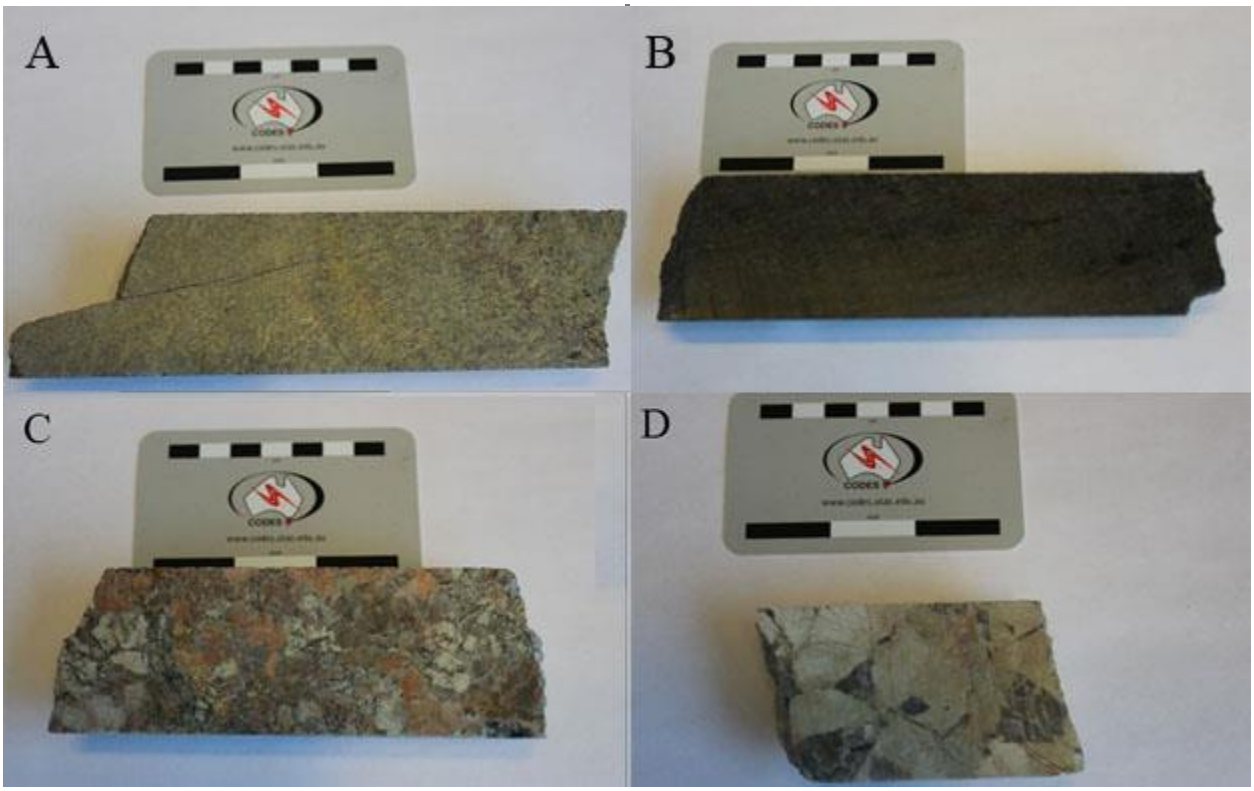

Figure 3-1. Representative samples from the basement beneath the Athabasca Basin in the Dawn Lake area a) cordierite pelitic gneiss, b) sulphide-rich graphitic pelitic gneiss, c) radioactive altered pegmatite and d) tourmaline-rich pegmatite.

Graphitic pelitic gneiss (Fig. 3-1b) are similar to the pelitic gneiss in terms of major minerals (Fig. 3-1a), although the presence of graphite results in dull dark brown to dark grey rocks. Accessory minerals include cordierite, sillimanite, garnet, tourmaline, pyrite, chalcopyrite, ilmenite, apatite, monazite and zircon. Alteration intensity is variable in these compositionally layered gneisses, and includes chlorite, illite, dickite, hematite and dravite.

Granitic pegmatites occur as dykes and sills intruding the Archean basement and Wollaston group metasedimentary rocks, and vary in size from individual veins to up to 25 m thick intrusions. The larger granitic pegmatites typically intrude between the Archean and Paleoproterozoic rocks and commonly along shear zones. These rocks are peraluminous and vary in colour from pink to pinkish grey to greyish white. They can be very coarse grained (Fig.

3-1c, d) to fine grained microgranite and aplite. Major mineralogy in order of typical abundance is K-feldspar, plagioclase, quartz and biotite, and accessory minerals include tourmaline, uraninite, monazite and zircon.

3.2 Sample Preparation

Rock samples were dried at a temperature of 65°C and then jaw crushed to >80% -2 mm material using mild steel plates. A subsample of the crushed material was split out using a sample riffle splitter. The subsample was pulverized with an agate mill to >90% -106 μm powder following the procedures set out by the SRC Geoanalytical C/S/A pulverization method and were stored in plastic snap top vials at SRC's sample storage facility. Stored agate pulverized powder was retrieved for sample analysis throughout this project.

3.3 Bulk Chemical Analysis

All bulk chemical analyses were performed at the SRC Geoanalytical laboratory, Saskatoon. Multiple digestions were used to obtain the data needed to geochemically assess the samples. The partial digestion was used to determine the volatile elements As, Bi, Hg, Se, Sb and Te and the geochemically mobile elements which included Ag, Co, Cu, Mo, Ni, Pb, U, V and Zn. Pulverized material was weighed into digestion tubes and a combination of ultrapure concentrated acids (HNO_3:HCl) outlined by the SRC Geoanalytical ICPMS2 partial digestion method was added before agitation and heating in a hot water bath. A total digestion was used for analysis of the other 38 trace elements including base metals and REE's. An aliquot of pulverized sample was dissolved using a 3:1 mixture of ultrapure HF:HNO_3 acid in Savillex screw-top vials overnight on a hotblock (< 160°C) outlined by the SRC Geoanalytical ICPMS2 total digestion method. Concentrated HNO_3 was added to the dried samples the next morning

which produced a clear solution for analysis. Whole rock analysis (WRA) is used to determine major elemental concentrations, to prepare the samples for WRA the sample pulp and lithium metaborate/tetraborate flux was weighed into platinum crucibles. The platinum crucibles and sample were placed in the sample holder on the Claisse Ox electric fusion instrument. Fusion on the Ox is automated; the instrument adds the samples to the furnace region following the SRC modified Claisse Oxide fusion method and heats the sample until it is melted. The molten material is then removed from the furnace and the platinum crucibles are inverted, the sample is dropped into a solution of 5 % HNO_3 acid solution in Teflon beakers. After the sample solution has been stirred and cooled it is transferred to a 100 mL Class A volumetric flask. Both the partial and total digestions were diluted appropriately and analyzed on a Perkin Elmer NEXION Q-ICP-MS. The Perkin Elmer 5300 dual view inductively coupled plasma optical emission spectrometer (DV-ICP-OES) was used to measure Cr, La, Li and Sr in the total digestion and the major elements and Zr from the WRA. To mass balance the major elements and assess the percent of sample lost on ignition (LOI), the sample was weighed into ceramic crucibles and placed in a muffle oven set at 1000°C overnight. Samples were removed from the muffle oven the next morning, set aside to cool and then reweighed to determine percent LOI. Carbon, sulfur and graphite are the most common elements included within LOI, and thus a LECO instrument with infrared detector was used to differentiate between carbon, inorganic carbon, sulfur and graphite. To determine graphite, the sample was treated with acid and heated in a muffle oven to remove all organic carbon then heated in a LECO C/S analyzer and measured for % C.

3.4 Lead Isotopic Composition

3.4.1 Sample Dissolution

Pb-Pb isotopic ratios were measured at the SRC Geoanalytical laboratory. Sample dissolution was performed using both the SRC Partial and Total Digestion techniques, as outlined in section 3.3 with ultrapure acid and brought up with 18 MΩ/cm deionized water. The partial digestion is an effective tool for dissolution of sulphides and loosely bound elements providing the Pb-Pb ratios of the mobile Pb whereas the total digestion provides Pb-Pb ratios from all lead in the samples including the refractory phases.

3.4.2 Mass Spectrometry

Both the Q-ICPMS Perkin Elmer Elan DRC II and the HR-ICPMS Nu Attom were used to measure the Pb-Pb ratios. The isotopes of interest were ^{204}Pb, ^{206}Pb, ^{207}Pb and ^{208}Pb measured by electron multiplier, the Pb-Pb ratios were calculated using signal intensities (counts/s) and corrections were made for ^{204}Hg interference. For all isotopic measurement NBS 981 and NBS 983 were used to bracket all sample analysis, determine instrumental drift, analytical error and evaluate quality control. SRC commonly analyzes NBS 981 for QC purposes, and all results were within 2σ relative to the accepted values (Fig. 3-2).

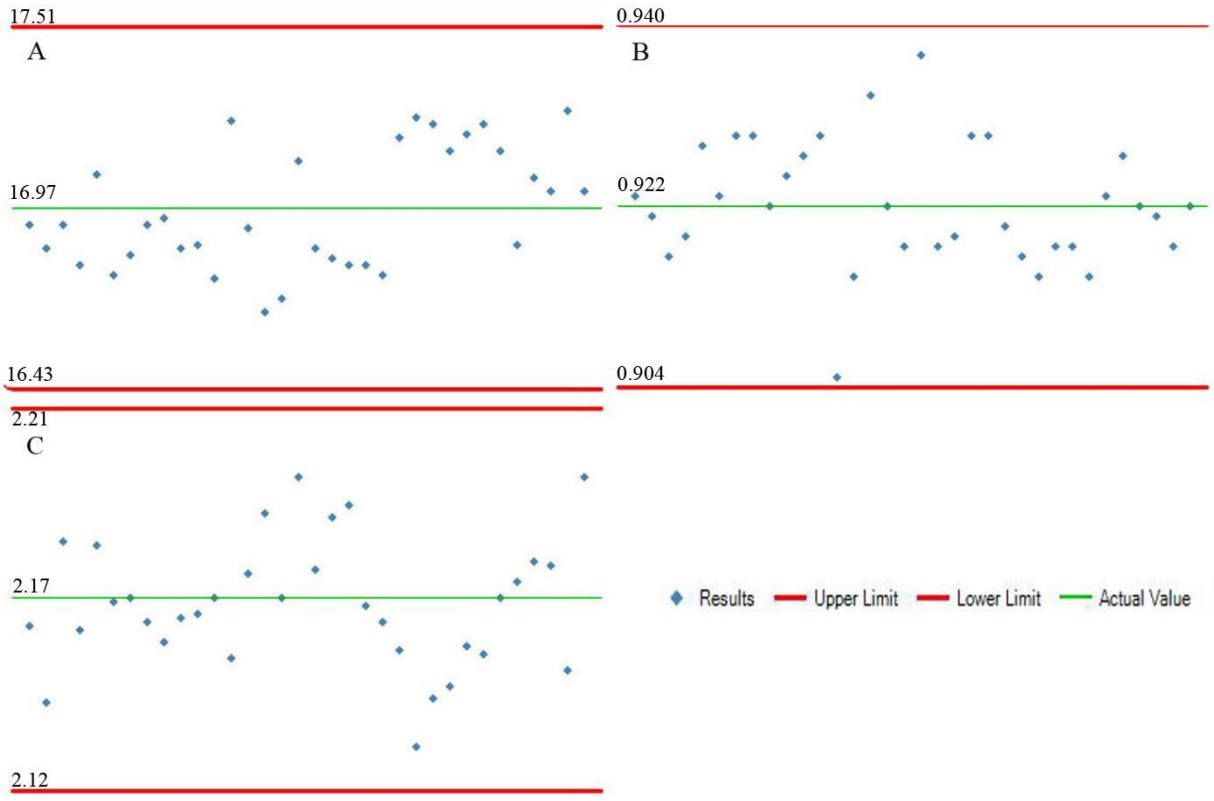

Figure 3-2. Performance of Pb isotopic reference material NBS 981 at the Saskatchewan Research Council Geoanlaytical Laboratory over a 5 year period, fom left to right Pb isotopic ratios from 2008 through 2013, A) Pb^{206}/Pb^{204} B) Pb^{207}/Pb^{206} and C) Pb^{208}/Pb^{206}.

3.5 Lithium Isotopic Composition

3.5.1 Sample Dissolution

All sample dissolution for Li isotopic composition was performed at the University of Maryland (College Park, Maryland), following methods outlined in Rudnick et al., (2004) and Teng et al., (2004). Approximately 7 mg of pulverized rock was dissolved using a 3:1 mixture of ultrapure HF:HNO_3 acid in Savillex screw-top beakers overnight on a hotplate (<90°C). Concentrated HNO_3 was added to the dried samples the next morning which were again heated overnight to dryness, the remaining precipitate was retreated with concentrated HNO_3 on a hotplate until a clear solution was produced. The samples were dried once more and the

precipitate was taken up with 1 mL of 4 M HCl in preparation for chromatographic separation. Approximately 100 ng of Li will be contained in the 1 mL of solution for chromatography.

3.5.2 Column Chemistry

Lithium purification required four sets of column separations based on the procedures set out by Moriguti and Nakamura (1998) and Teng et al. (2004). Each column contains 1 mL of cation resin (BioRad AG50W-x12) with a different sample solution matrix for each step. The fourth column is a repeat of the third to further ensure complete separation of Na and Li (Fig. 3-3). This purification procedure can separate Li from the other elements with >95% efficiency (Marks et al., 2007).

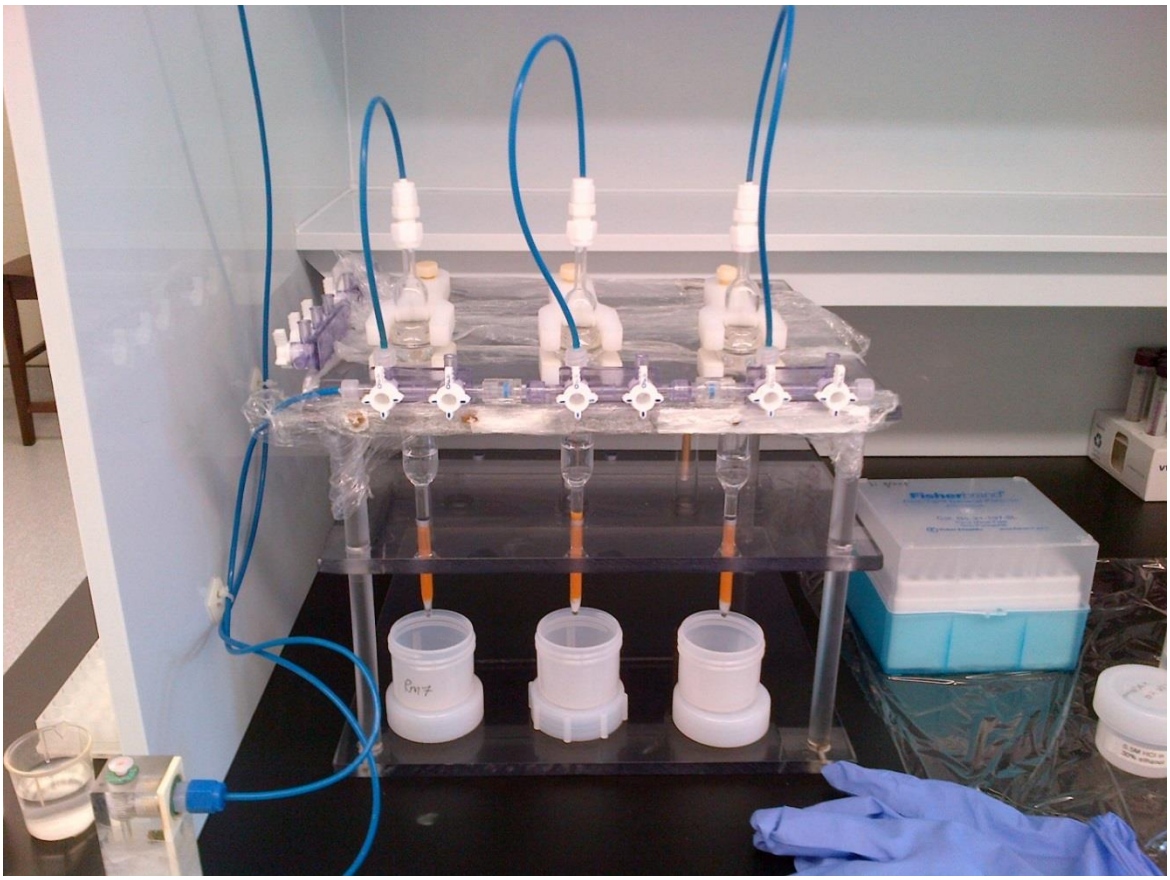

Figure 3-3. All column separations at the University of Maryland were performed in clean laboratory setting. The setup shown is used to process three samples at one time, and is used for both the third and fourth column procedure. Nitrogen gas was used to accelerate the third and fourth column.

The first column removes the major elements from the sample matrix using 12 mL polypropylene Bio-Rad columns filled with 1 mL of Bio-Rad AG50W-x12 resin. Dried precipitate is brought into solution with 1 mL of 4 M HCl, and all the sample must be dissolved to ensure that the Li isotopic fractionation was not influenced by the separation. The first column was equilibrated with 1 mL of 4 M HCl before starting separation. Next, all of the sample solution was loaded onto a polypropylene column (ID 8 mm) followed by 9 mL of 2.5 M HCl. All 9 mL of solution was collected in a 60 mL Teflon beaker and dried overnight on a hotplate. The second column separates Li and Na from all other elements and the setup is the same as the first set of columns, the only difference between the two columns is that on the second column the sample was dissolved in 1.5 mL of 0.15 M HCl. Before loading 1.5 mL of sample onto the column, the column was equilibrated with 1 mL of Milli-Q H_2O. Next 30 mL of 0.15 M HCl was introduced to the column, and all of the 30 mL of solution produced was collected in a 60 mL Teflon beaker and dried overnight. After completing each of the first two column separations, the columns were cleaned first with 10 mL of 6 M HCl and then 10 mL of Milli-Q H_2O. The third column and the fourth columns separate Li from Na. Dried residue was dissolved in 1 mL of 0.15 M HCl and the column was equilibrated with 1 mL Milli-Q H_2O. After equilibration 1 mL of sample was loaded onto the quartz column (ID 3.8 mm). Next 16 mL of 30 % vol. ethanol 0.5 M HCl was added to these much thinner but longer columns. Because of the change in ID the column was pressurized with Nitrogen gas (2-4 mL/min) to reduce the time required for separation (Fig. 3-3). The fourth column is a repeat of the third column used to ensure that Li is completely separated from all other major and trace elements in solution

3.5.3 Mass Spectrometry

Before measuring lithium isotopic composition the Na/Li ratio was determined by MC-ICPMS, and if the Na/Li ratio was > 5 then the samples were passed through the 4th column separation again. The ratios were measured to minimize interference of Na on Li during isotopic measurement, and all samples from this project were <5 when measured. Next the samples were diluted with 2 % v/v HNO_3 to approximately 100 ppb Li. All lithium isotopic measurements were performed on the Nu Plasma multi collector at the University of Maryland with "dry" plasma conditions. The diluted samples were nebulized and dried with a Cetac Airdus desolvating nebulizer to obtain "dry" plasma conditions. ^{7}Li and ^{6}Li measurements were measured simultaneously using the high mass H6 faraday cup and the low mass L5 faraday cup, respectively. For all analysis LSVEC was used to bracket all sample analysis to determine instrumental drift, analytical error and $\delta^{7}Li$ (Flesch et al., 1973). The lithium carbonate reference material prepared by H. Svec in 1973 is the basis for all lithium fractionation measurements, and all Li isotopic compositions from this project were reported as $\delta^{7}Li$.

$$\delta^{7}Li_{sample} = \left(\frac{(^{7}Li/^{6}Li)_{sample}}{(^{7}Li/^{6}Li)_{LSVEC}} - 1\right) \text{x } 1000 \qquad (3.1)$$

Quality control procedures included the analysis of in-house reference materials IRMM-016 (Qi et al., 1997) and UMD-1 ($\delta^{7}Li$ = 54.1 ‰) (Qiu, 2011; Liu, 2013) to measure instrument performance. External USGS rock reference materials G2 ($\delta^{7}Li$ = 0.3 ‰) and BHVO-1 ($\delta^{7}Li$ = 4.2 ‰) (GeoReM database: http://georem.mpch-mainz.gwdg.de/) were used to measure sample dissolution and column chemistry performance. The long term precision of the Li isotopic measurements over 10 years at the University of Maryland Plasma lab is $\leq$ 1.0 ‰ and $\pm$ 10 % (Qiu et al., 2009; Qiu et al., 2011; Teng et al., 2006)

3.6 Boron Isotopic Composition

3.6.1 Sample Dissolution

Boron isotopic analysis was performed at ALS laboratories in Lulea, Sweden by Dr. Ilia Rodushkin, using techniques outlined in Aggarwal et al., (2009) and Gonfiantini et al., (2003). Silicate sample dissolution was performed using a Na_2O/Na_2CO_3 fusion, and the boron was brought into solution using deionized water with a resistivity of 18 MΩ/cm. The fusion is a more effective process compared with the low blank acid digestion mixture of HNO_3, HF and mannitol. Mannitol helps suppress boron volatization during HF digestion (Nakamura et al., 1992). The acid matrix is very effective for sedimentary and biological samples, but can be ineffective for digesting some refractory phases, such as tourmaline (Dr. Ilia Rodushkin, personal communication).

3.6.2 Column Chemistry

The first set of samples and a subset of the second set submitted to ALS were purified using column separation. The initial analysis request sent to ALS requested samples that had both column separated analysis and non-column separated solutions analyzed. After examining the first dataset with RSD of <1‰ for both purified and unpurified solutions the author did not request column separation for the second set of samples because of the excellent results received from the first round of analysis. After receiving the second set of data there was a significant difference in RSD between the first and second sets of data. After further investigation it was determined that the entire first dataset was put through the chemical separation procedure which therefore provided RSD values an order of magnitude better than the second dataset.

Before column separation the samples were neutralized to a pH of 7-8 with a 10 % HNO_3 solution. Next the sample was loaded onto a column containing boron specific Amberlite IRA-743 resin. Boron was eluted off the column with 5 % HCl and the solution was then ready for

ICP-MS isotopic analysis. The ‰ RSD after column separation for boron isotopic analysis was an order of magnitude better then unpurified HR-ICPMS analysis.

3.6.3 Mass Spectrometry

The unpurified fusion cakes were diluted appropriately in 10 % HNO_3 before performing boron isotopic measurements to ensure that the solution matrix is a highly acidic matrix for analysis. All boron isotopic measurement were performed on the Thermo Scientific Element XR SF-ICPMS and a subset of samples were also analyzed on the Thermo Scientific multi collector at ALS laboratories is Lulea, Sweden. For all isotopic measurement NBS 951 (NIST: http://www.nist.gov/srm/upload/SP260-17.PDF) was used to bracket all sample analysis to determine instrumental drift, analytical error and $\delta^{11}B$ (Appendix A). All boron isotopic compositions were reported as $\delta^{11}B$.

$$\delta^{11}B_{sample} = \left(\frac{(^{11}B/^{10}B)_{sample}}{(^{11}B/^{10}B)_{LSVEC}} - 1\right) \text{x } 1000 \quad (3.2)$$

The long term precision of ALS laboratories B isotopic measurements is < 1.0 % RSD for SF-ICPMS and < 0.1 % RSD for MC-ICPMS (ALS Life Sciences, Analytical Packages, Isotopes, 2014).

CHAPTER 4
GEOCHEMICAL RESULTS

4.1 Major and Trace Elements

Major element and selected trace element whole rock data for the metasedimentary and granitic pegmatite samples is presented in Table 4-1 and 4-2. The complete analytical dataset is found in Appendix A. Major element Harker diagrams (Fig. 4-1) show the variation in chemical composition of both metasedimentary and granitic pegmatite samples, which emphasize the heterogeneity of the basement rock types. Granitic pegmatites of this study are typically peraluminous ($Al_2O_3/Na_2O+K_2O+CaO>1$) with the following elemental concentration ranges; high SiO_2 (60-75 wt%), Al_2O_3 (12-20 wt%) and K_2O (1-9 wt %) with variable but typically low TiO_2 (0.05-0.9 wt %). The major elemental concentrations of the metasedimentary rocks are equally as variable, typical major elemental geochemistry is as follows; SiO_2 (55-73 wt%), Al_2O_3 (12-18 wt %), Fe_2O_3 (1-10 wt%), MgO (3-11 wt%), K_2O (0.1-4 wt %) and high TiO_2 (0.5-0.9 wt %) (Table 4-1). The SiO_2 content for the two rock types are relatively similar although the granitic pegmatites tend to have higher values (Fig. 4-1). However, the highest SiO_2 value is from a psammitic gneiss which is expected given the high quartz content of this sample. In granitic pegmatite samples elevated Na_2O concentrations are associated with the presence of tourmaline, and these rocks have the lowest TiO_2 concentrations. The sample with the lowest concentration of SiO_2 is a tourmalinite which has elevated elemental concentrations typical for tourmaline composition; Na_2O, TiO_2, Al_2O_3, CaO and Fe_2O_3.

The relationship between selected trace elements, which are common pathfinder elements and components of either ore or alteration minerals, and U are presented in Figure 4-2. The majority of altered pegmatite samples in the study display enriched U concentrations and depleted trace elements concentrations. Typically, the concentrations of Zn, B, Li and Pb are

Sample Number	Deposit Area	Depth m	Rock Type	Comments	SiO_2 wt %	TiO_2 wt %	Al_2O_3 wt %	Fe_2O_3 wt %	MnO wt %	MgO wt %	CaO wt %	Na_2O wt %	P_2O_5 wt %	K_2O wt %	LOI wt %	SUM
A94-040D	Eagle Point	Outcrop	Pegmatite	Magnetite bearing	71.1	0.72	12.3	4.72	0.05	1.04	0.59	1.64	0.16	7.68	0.50	100.5
I57 114.5	McClean Lake	114.5	Pegmatite	Paleoweathered	71.5	0.41	17.7	4.21	0.01	2.25	0.28	0.77	<0.01	1.11	2.00	100.2
Q6-66 131.2	Dawn Lake	131.2	Pelitic Gneiss	Corderite bearing	64.7	0.90	19.0	1.51	<0.01	4.50	0.46	0.07	0.34	3.41	5.30	100.2
Q6-66 149.7	Dawn Lake	149.7	Graphitic Pelitic Gneiss	Bleached, sulphides	62.0	0.63	17.7	5.44	0.03	3.76	0.20	0.09	0.10	4.44	5.70	100.1
Q6-66 164.2	Dawn Lake	164.2	Pegmatite	Altered radioactive	73.6	0.03	14.0	0.87	<0.01	3.00	0.08	0.18	0.05	4.50	3.50	99.8
Q6-66 170.9	Dawn Lake	170.9	Graphitic Pelitic Gneiss	Bleached	61.9	0.85	16.3	4.65	<0.01	5.62	0.27	0.06	0.10	3.03	6.90	99.7
Q6 67 104.4	Dawn Lake	104.4	Pelitic Gneiss	Migmatitic	57.0	0.67	14.1	10.3	0.04	11.4	0.23	0.04	0.04	0.16	6.50	100.5
Q6-72 108.7	Dawn Lake	108.7	Pelitic Gneiss	Paleoweathered	62.7	0.68	17.2	5.47	0.02	4.79	0.16	0.10	0.06	3.91	4.70	99.8
Q6-72 114.5	Dawn Lake	114.5	Pegmatite	Tourmaline	74.6	0.13	14.7	0.35	<0.01	3.36	0.48	0.09	0.29	2.16	4.00	100.2
Q6-72 117.2	Dawn Lake	117.2	Graphitic Pelitic Gneiss	Sulphides	62.5	0.76	17.7	1.86	<0.01	6.74	0.26	0.07	0.12	2.22	7.50	99.7
Q7-16 266.8	Dawn Lake	266.8	Pegmatite	Tourmaline	63.0	0.05	18.6	2.92	0.05	2.50	0.10	0.50	0.07	9.67	2.70	100.2
Q9-16 183.6	Dawn Lake	183.6	Pelitic Gneiss	Garnet, corderite	57.4	0.80	16.6	4.46	0.02	12.00	0.09	0.06	<0.01	0.91	7.80	100.1
Q9-16 191.3	Dawn Lake	191.3	Pelitic Gneiss	Paleoweathered	69.3	0.59	14.7	1.76	<0.01	5.67	0.10	0.12	<0.01	2.86	4.90	100.0
Q9-16 199.6	Dawn Lake	199.6	Graphitic Pelitic Gneiss	Sulfphides, Corderite	55.2	0.49	12.9	9.83	0.03	8.42	0.07	0.14	0.01	2.86	10.4	100.4
Q9-16 214.6	Dawn Lake	214.6	Pelitic Gneiss	Garnet, corderite	69.2	0.56	12.3	4.55	0.06	6.28	0.09	0.15	0.03	3.31	3.60	100.1
Q9-16 217.2	Dawn Lake	217.2	Pelitic Gneiss	Garnet, corderite	62.7	0.65	15.2	6.48	0.20	5.32	0.34	0.20	0.09	4.64	4.00	99.8
EL 09-797.7	Epp Lake	797.7	Pegmatite	Clay Altered Proximal U	67.6	0.21	18.0	2.32	<0.01	4.48	0.62	0.43	0.37	1.44	4.20	99.7
EL-09-823.7	Epp Lake	823.7	Pegmatite	Clay Altered Proximal U	68.0	0.87	14.5	6.10	0.03	3.14	0.14	0.48	0.02	3.86	2.60	99.7
RI-46-570.1	Read Lake	570.1	Pegmatite		68.6	0.25	20.2	1.10	<0.01	1.57	0.14	0.22	<0.01	4.64	3.20	99.9
RI-80-454.5	Read Lake	454.5	Tourmalinite		38.4	2.40	21.9	23.5	0.04	6.06	1.28	0.51	0.18	1.89	4.20	100.4
MAC 207.511.1	McArthur River	511.1	Graphitic Pelitic Gneiss		62.8	0.86	18.7	1.01	0.01	6.32	0.18	0.09	0.08	1.72	8.20	100.0
MAC 207.664.8	McArthur River	664.8	Psammitic Gneiss		88.3	0.16	7.32	0.29	<0.01	0.18	0.02	0.06	<0.01	2.05	1.40	99.8

Table 4-1. Whole Rock chemical compositions for graphitic pelitic gneiss, pelitic gneiss and pegmatites of the eastern Athabasca Basin.

Sample Number	Deposit Area	Depth	Rock Type	As	B	Co	Cr	Cu	Li	Nd	Ni	Pb_{SUM}	Th	U	Y	Zn
		m		ppm	ppm	ppm	ppm	ppm	ppm	ppm	ppm	ppm	ppm	ppm	ppm	ppm
A94-040D	Eagle Point	Outcrop	Pegmatite	0.48	25	5.8	20	9.9	63	35.7	3	65.6	36.5	156	26.0	76
I57 114.5	McClean Lake	114.5	Pegmatite	2.05	10700	11.5	77	4.8	29	19.0	11	3.67	44.1	28.9	68.8	185
Q6-66 131.2	Dawn Lake	131.2	Pelitic Gneiss	1.87	161	7.1	117	4.9	84	28.8	49	2.76	20.7	7.66	20.2	<1
Q6-66 149.7	Dawn Lake	149.7	Graphitic Pelitic Gneiss	30.4	124	17.2	93	11.7	105	21.8	32	7.65	21.4	17.2	15.4	37
Q6-66 164.2	Dawn Lake	164.2	Pegmatite	0.68	248	1.0	7	106	105	31.2	3	47.8	60.8	154	13.6	62
Q6-66 170.9	Dawn Lake	170.9	Graphitic Pelitic Gneiss	4.74	251	30.8	98	16.3	161	46.5	58	9.31	60.0	17.0	21.6	12
Q6 67 104.4	Dawn Lake	104.4	Pelitic Gneiss	3.58	53	41.7	45	10.3	684	50.4	51	4.48	19.0	5.21	25.3	37
Q6-72 108.7	Dawn Lake	108.7	Pelitic Gneiss	0.71	168	13.2	89	5.8	80	29.5	66	5.49	18.8	5.11	27.7	108
Q6-72 114.5	Dawn Lake	114.5	Pegmatite	2.91	913	2.7	13	8.4	169	9.7	12	4.43	16.2	15.9	18.0	9
Q6-72 117.2	Dawn Lake	117.2	Graphitic Pelitic Gneiss	153	647	94.3	96	22.8	178	24.0	103	9.21	27.2	15.3	24.3	7
Q7-16 266.8	Dawn Lake	266.8	Pegmatite	1.17	198	5.0	140	56.1	105	73.4	8	53.2	96.4	23.2	80.3	10
Q9-16 183.6	Dawn Lake	183.6	Pelitic Gneiss	8.58	98	21.4	95	9.3	309	35.9	77	3.03	18.5	11.4	14.6	34
Q9-16 191.3	Dawn Lake	191.3	Pelitic Gneiss	7.12	167	26.1	64	67.7	135	15.2	34	20.0	11.0	66.0	33.0	25
Q9-16 199.6	Dawn Lake	199.6	Graphitic Pelitic Gneiss	5.34	72	131	58	287	416	27.8	76	24.1	15.2	17.2	20.4	34
Q9-16 214.6	Dawn Lake	214.6	Pelitic Gneiss	0.45	103	11.8	50	11.4	232	31.9	17	10.3	48.0	6.92	9.52	73
Q9-16 217.2	Dawn Lake	217.2	Pelitic Gneiss	0.53	97	17.4	81	5.6	162	21.2	24	9.36	9.96	3.09	17.4	28
EL 09-797.7	Epp Lake	797.7	Pegmatite	2.56	6320	8.0	32	17.2	127	51.8	35	13.0	11.6	205	22.5	104
EL-09-823.7	Epp Lake	823.7	Pegmatite	4.46	4010	15.8	102	53	81	35.1	113	11.2	17.7	9.71	18.4	78
RI-46-570.1	Read Lake	570.1	Pegmatite	0.34	2890	4.4	9	5.5	34	8.1	14	2.04	5.55	4.27	4.71	27
RI-80-454.5	Read Lake	454.5	Tourmalinite	0.66	10000	50.1	54	76.3	74	12.2	112	14.1	2.43	6.03	31.7	18
MAC 207.511.1	McArthur River	511.1	Graphitic Pelitic Gneiss	3.78	1150	13.8	112	23.6	152	14.7	115	8.53	19.2	25.0	32.2	<1
MAC 207.664.8	McArthur River	664.8	Psammitic Gneiss	0.55	99	2.9	26	33.6	25	35.3	9	2.85	69.8	12.3	5.7	1

Table 4-2. Selected trace element compositions for graphitic pelitic gneiss, pelitic gneiss and pegmatites of the eastern Athabasca Basin.

elevated in the samples with higher U concentrations. Elevated U concentrations could be the product of residual U left after alteration of radioactive pegmatites. Metasedimentary rocks display greater variability in trace elements especially As, Co, Ni and Li (Fig. 4-2) which is representative of a heterogeneous basement. Altered metasedimentary samples have depleted concentrations of both U and other trace elements relative to the fresh metasedimentary rocks, which could be an indication of leaching of elements from a metasedimentary source. As expected the higher LOI values are associated with the more carbonaceous graphitic pelitic gneiss and altered samples.

A selection of immobile elements (Nd, Cr, Y, Th and Al_2O_3) plotted on bivariate diagrams versus both B and Li (Fig. 4-3) are used to determine the mobility of B and Li. There is a positive correlation between B and Al_2O_3 for both rock types, and B and Cr for metasedimentary rocks. Altered samples have elevated Nd concentrations relative to fresh rocks suggesting that either Nd was residually concentrated during alteration, or was introduced by fluids. Positive correlation between immobile Al_2O_3 and B is mostly likely due to the influence of tourmaline as the major source of B in the basement rocks. There is a negative correlation between immobile Y, Al_2O_3, Cr and fluid mobile Li in metasedimentary rocks. Generally the concentrations for Cr and Th in the altered metasedimentary rocks are higher than the majority of fresh metasedimentary rocks in this study. The negative correlation between immobile elements and Li along with the elevated concentrations of Cr and Th in altered metasedimentary samples could suggest that alteration fluids were either mobilizing Li and upgrading immobile elements or carrying significant concentrations of Li from another source. Relationships between B, Li and immobile elements in the granitic pegmatites are not as clear possibly due to heterogeneity between the different pegmatites.

The variation in concentrations of K_2O, MgO, Na_2O, CaO, Rb, Ba and Sr can be used to differentiate between the rock types present. Figure 4-4 is a selection of ternary diagrams including both metasedimentary and granitic pegmatite samples. All samples plotted on the CNK ternary diagram (Fig. 4-4a) follow the normal calc-alkaline trend outlined by Barker and Arth (1976) suggesting a similar K-rich source for both the metasedimentary rocks and the granitic pegmaties. All metasedimentary samples on the NKM ternary diagram lie near the MgO- K_2O tie line classifying all as pelitic rocks. (Fig. 4-4b). Metasedimentary rocks appear to be enriched in Ba and Sr relative to the granitic pegmatite rocks (Fig. 4-4c). The majority of altered samples in this study show removal of Sr or enrichment of Ba or Rb relative to the fresh rock.

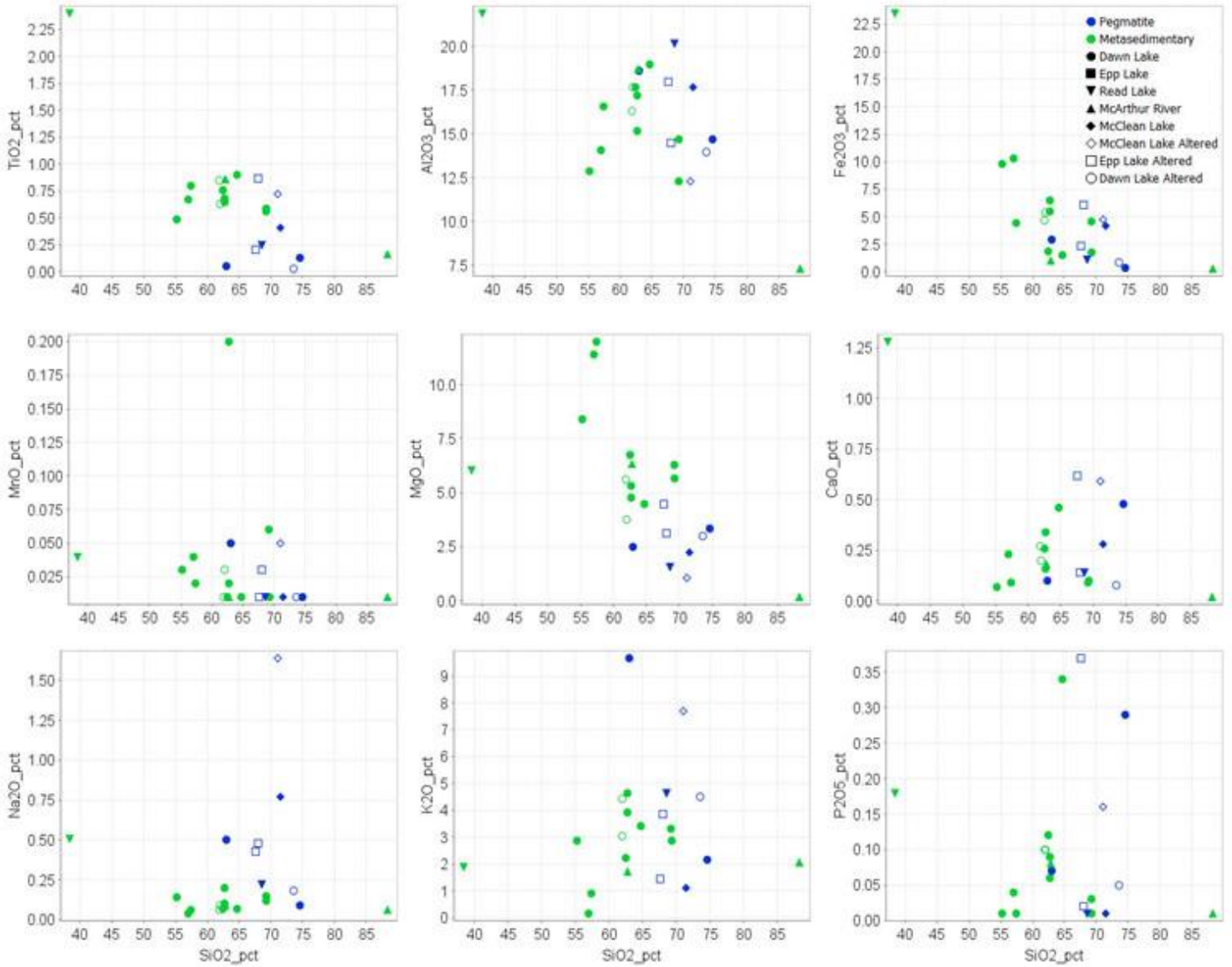

Figure 4-1. Harker diagrams for granitic pegmatite and metasedimentary rocks of the eastern Athabasca Basin. pct – wt%

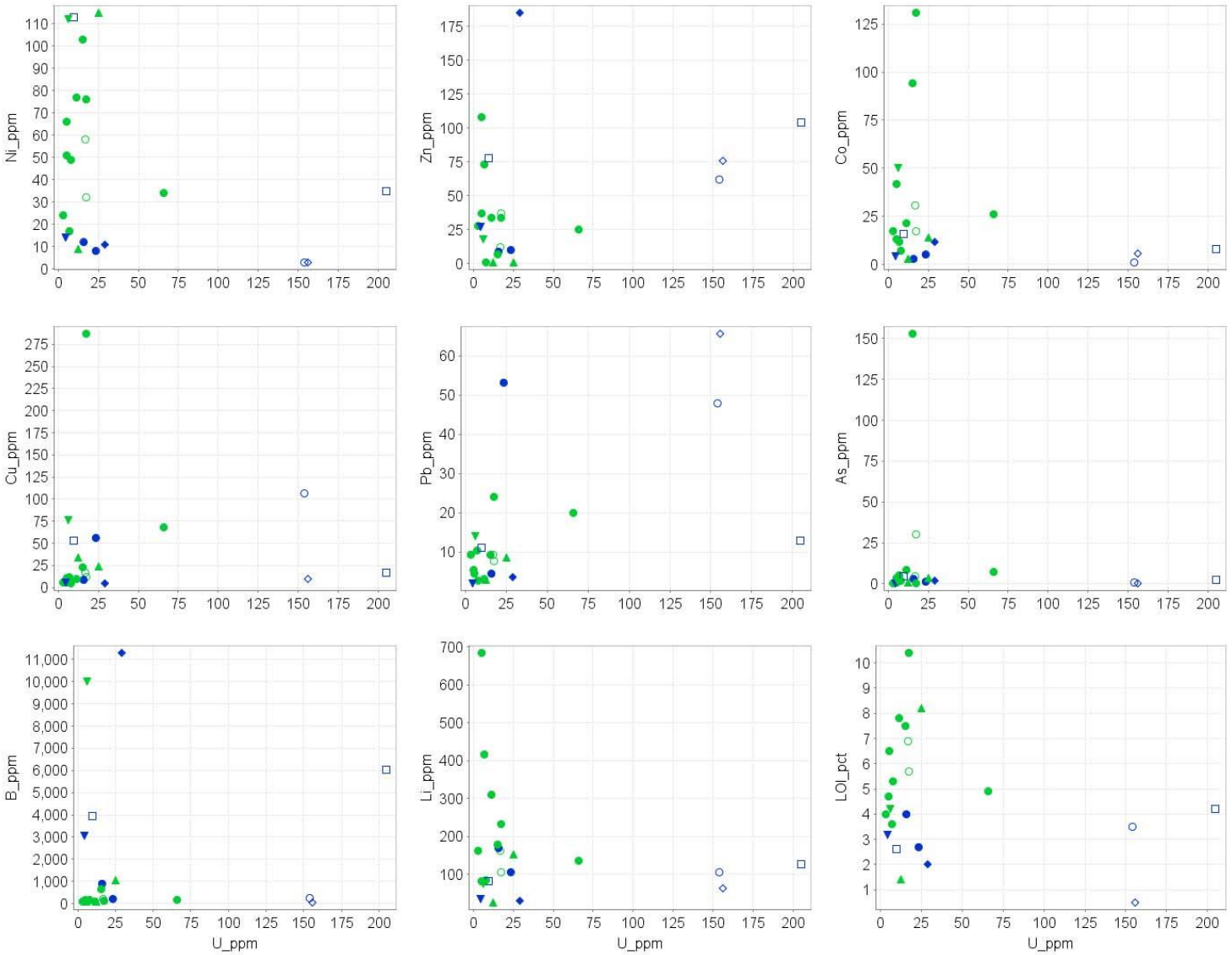

Figure 4-2. Bivariate trace element plots of both metasedimentary (green) and granitic pegmatites (blue) relative to U concentrations. Symbols are the same as Figure 4-1.

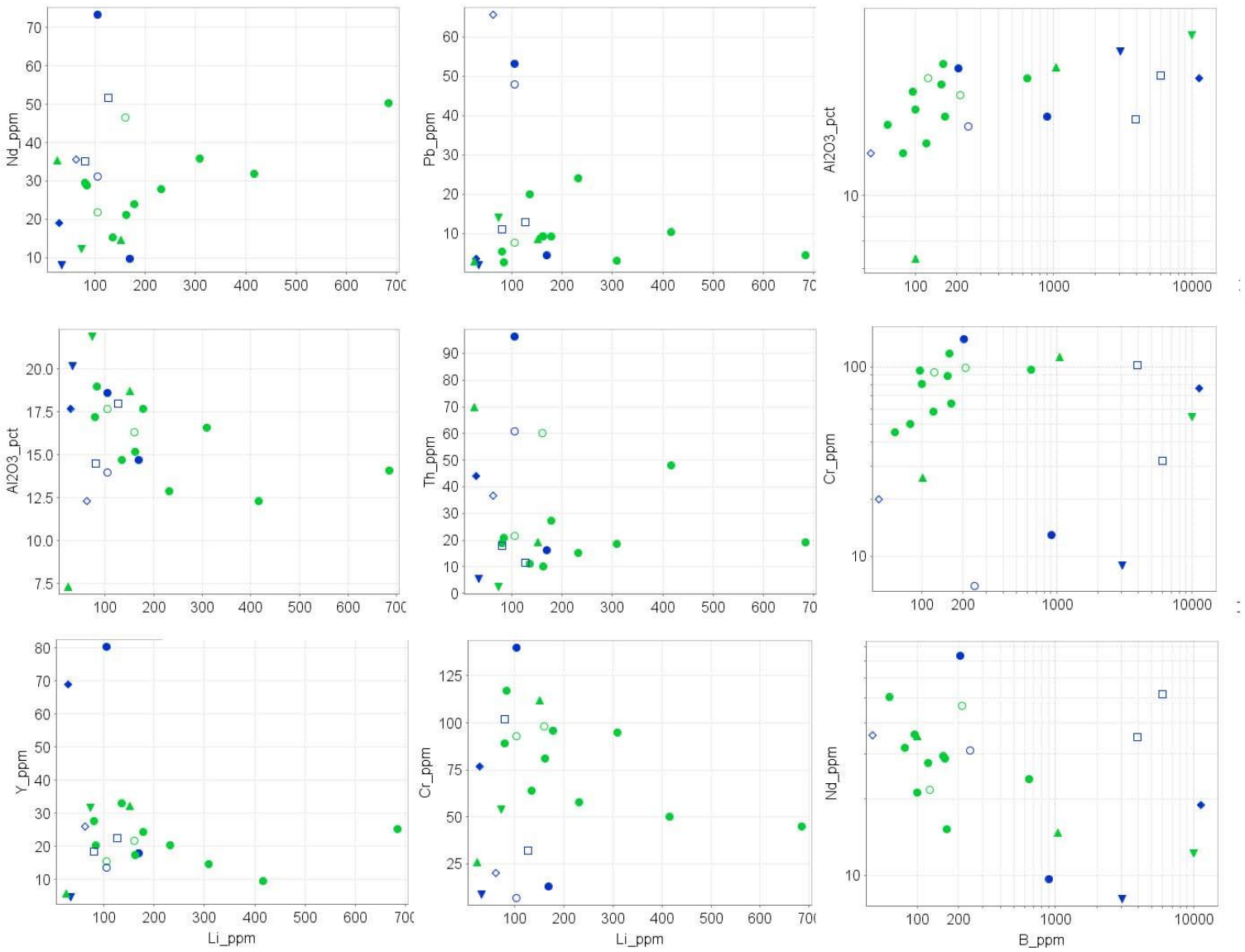

Figure 4-3. Bivariate trace element plots of immobile elements relative to Li and B for eastern Athabasca Basin basement rocks. Symbols are the same as Figure 4-1.

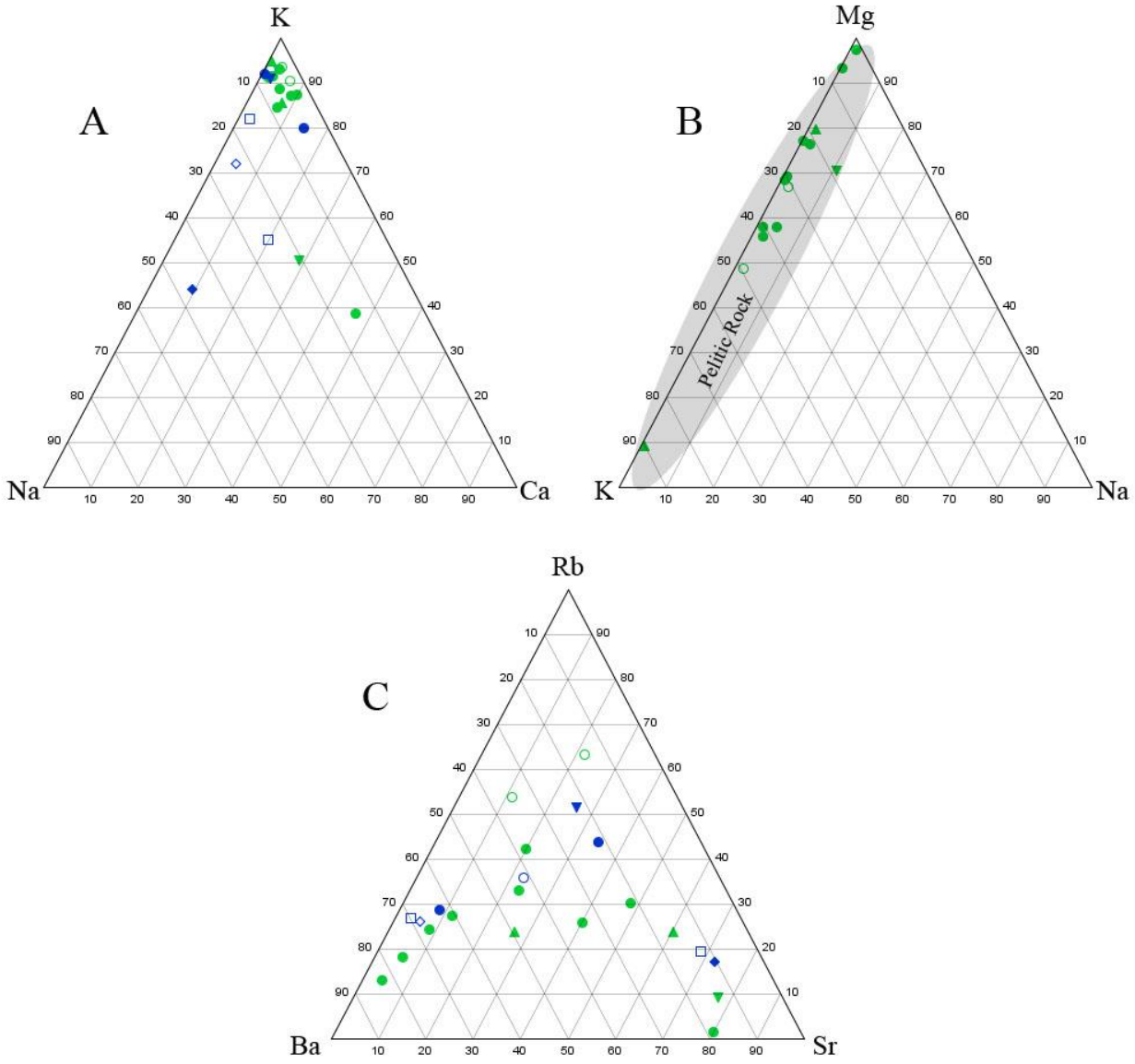

Figure 4-4. A) Ca -Na-K (CNK), B) Na -K-Mg (NKM) and C) Sr-Ba-Rb (ppm) ternary diagrams representative of both metasedimentary and granitic pegmatite samples.

4.2 Lead Isotopes

Granitic pegmatites from this study showed the greatest variation in U, Th, and Pb concentrations relative to the metasedimentary rocks (Table 4-3), although there is no relationship to geographical location. The concentration of uranium and thorium in the granitic

pegmatites of this study varied from 4 to 205 ppm and 2 to 96 ppm, respectively, compared with 3 to 66 ppm and 9 to 69 ppm, respectively, for metasedimentary samples. In addition, the pegmatite samples yielded the largest variation in Th/U ratios from 0.057 to 6.936. Lead concentrations for the pegmatitic samples varies from 3 to 111 ppm whereas the metasedimentary samples yield concentrations ranging from 2 to 36 ppm. Although the different metasedimentary rock types have similar elemental concentrations, the pelitic gneiss samples tend to exhibit greater variation compared to the graphitic pelitic gneiss.

Analysis of the outcrop sample (A94-040d) yielded the largest radiogenic $^{206}Pb/^{204}Pb$ ratio of 192 with a high concentration of uranium (156 ppm). For graphitic pelitic gneiss the higher uranium concentrations (up to 66 ppm) are correlated with the higher total $^{206}Pb/^{204}Pb$ ratios (up to 118) (Fig. 4-5). No correlation between uranium concentrations and $^{206}Pb/^{204}Pb$ ratios was observed for pelitic gneiss. Typically uranium concentrations for the pelitic gneiss are in the range of 3 to 11 ppm, except for an anomalous sample (Q9-16-191.3) from the Dawn Lake region which has a uranium concentration of 66 ppm. The Dawn Lake sample with high uranium content has a relatively low $^{206}Pb/^{204}Pb$ ratio of 30. $^{206}Pb/^{204}Pb$ ratios > 30 (Holk et al., 2003) are considered to be radiogenic, but the anomalous Dawn Lake sample has a ratio that is very close to the lower limit for radiogenic Pb. It would be anticipated that the samples with the highest concentration of uranium should have the largest $^{206}Pb/^{204}Pb$ ratios unless the U is a recent addition to the sample. Figure 4-6 is the combination of two separate bivariate plots looking at the Pb isotopic composition from partial digestion (Fig. 4-6 a) and total digestion analyses (Fig. 4-6 b). Partial $^{207}Pb/^{206}Pb$ ratios versus U shows that the more common Pb component ratios ($^{207}Pb/^{206}Pb$ - 0.7) have lower U concentrations and the altered granitic pegmatite samples enriched in radiogenic Pb also has a higher U concentration. The radiogenic

Pb input is from an uranogenic source which could be either residual U from the pegmatite or U introduced into the samples that yield mobile Pb which is leached during partial dissolution. Total $^{208}Pb/^{204}Pb$ vs $^{206}Pb/^{204}Pb$ (Fig. 4-6b) display the difference between the more thorogenic and uranogenic Pb sources in the samples studied. The altered pegmatites have a high uranogenic component and lower thorogenic component suggesting that the uranium had been precipitated from hydrothermal fluids. In contrast, the metasedimentary samples appear to have a higher thorogenic Pb input.

Sample number	Rock Type	Pb	Th	U	Th/U	$^{207}Pb/^{206}Pb$	$^{208}Pb/^{206}Pb$	$^{206}Pb/^{204}Pb$	Pb^{207} / Pb^{206}	Pb^{208} / Pb^{206}
		ppm	ppm	ppm						
A94-040d	Outcrop	65.6	36.5	156	0.234	0.196	0.263	192.3	0.196	0.263
157 114.5	Pegmatite	3.67	44.1	28.9	1.526	0.594	2.748	29.5	0.594	2.748
Q6-66 131.2	Pelitic Gneiss	2.76	20.7	7.66	2.702	0.306	1.279	71.9	0.306	1.279
Q6-66 149.7	Graphitic Pelitic Gneiss	7.65	21.4	17.2	1.244	0.358	1.141	54.2	0.358	1.141
Q6-66 164.2	Pegmatite	47.8	60.8	154	0.395	0.428	1.485	44.0	0.428	1.485
Q6-66 170.9	Graphitic Pelitic Gneiss	9.31	60.0	17.0	3.529	0.345	1.204	55.6	0.345	1.204
Q6-67 104.4	Pelitic Gneiss	4.48	19.0	5.21	3.647	0.585	2.272	29.3	0.585	2.272
Q6-72 108.7	Pelitic Gneiss	5.49	18.8	5.11	3.679	0.684	2.185	25.0	0.684	2.185
Q6-72 114.5	Pegmatite	4.43	16.2	15.9	1.019	0.164	0.472	189.7	0.164	0.472
Q6-72 117.2	Graphitic Pelitic Gneiss	9.21	27.2	15.3	1.778	0.352	1.133	52.5	0.352	1.133
Q7-16 266.8	Pegmatite	53.2	96.4	23.2	4.155	0.979	3.133	16.4	0.979	3.133
Q9-16 183.6	Pelitic Gneiss	3.03	18.5	11.4	1.623	0.190	0.907	102.4	0.190	0.907
Q9-16 191.3	Pelitic Gneiss	20.0	11.0	66.0	0.167	0.590	1.758	30.0	0.590	1.758
Q9-16 199.6	Graphitic Pelitic Gneiss	24.1	15.2	17.2	0.884	0.655	1.986	26.5	0.655	1.986
Q9-16 214.6	Pelitic Gneiss	10.3	48.0	6.92	6.936	0.926	2.510	17.6	0.926	2.510
Q9-16 217.2	Pelitic Gneiss	9.36	9.96	3.09	3.223	0.950	2.525	17.0	0.950	2.525
EL 09-797.7	Pegmatite	13.0	11.6	205	0.057	0.187	0.363	149.7	0.187	0.363
EL-09-823.7	Pegmatite	11.2	17.7	9.71	1.823	0.806	2.242	20.6	0.806	2.242
RL-46-570.1	Pegmatite	2.04	5.55	4.27	1.300	0.714	1.876	23.0	0.714	1.876
RL-80-454.5	Tourmalinite	14.1	2.43	6.03	0.403	1.043	2.430	15.3	1.043	2.430
MAC 207.511.1	Graphitic Pelitic Gneiss	8.53	19.2	25.0	0.768	0.171	0.514	118.6	0.171	0.514
MAC 207.664.8	Psammitic Gneiss	2.85	69.8	12.3	5.675	0.361	1.491	52.4	0.361	1.491

Table 4-3. Analytical data for U-Th-Pb isotopic analysis of graphitic/non graphitic metasediments and granitic pegmatites from the eastern Athabasca Basin.

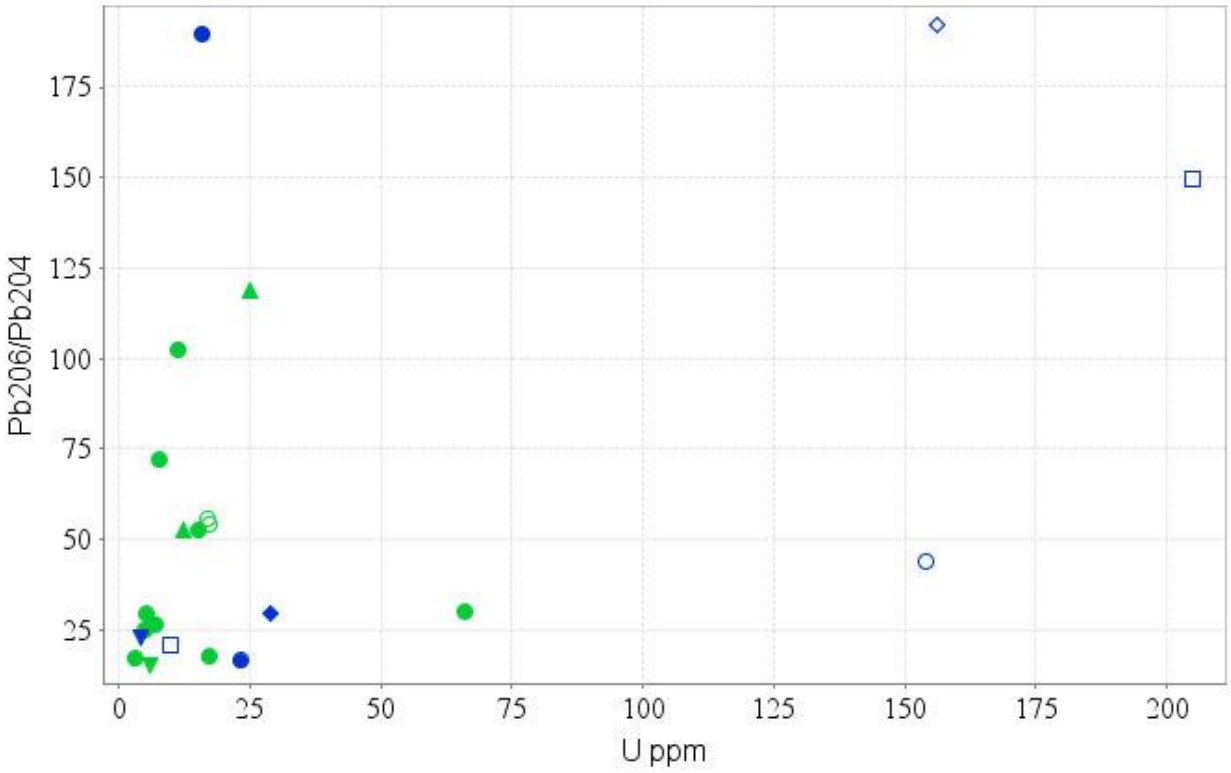

Figure 4-5. Total digestion Pb^{206}/Pb^{204} vs U, varying degrees of increasing Pb^{206}/Pb^{204} ratios with increases in U concentrations. Symbols as in Figure 4-1.

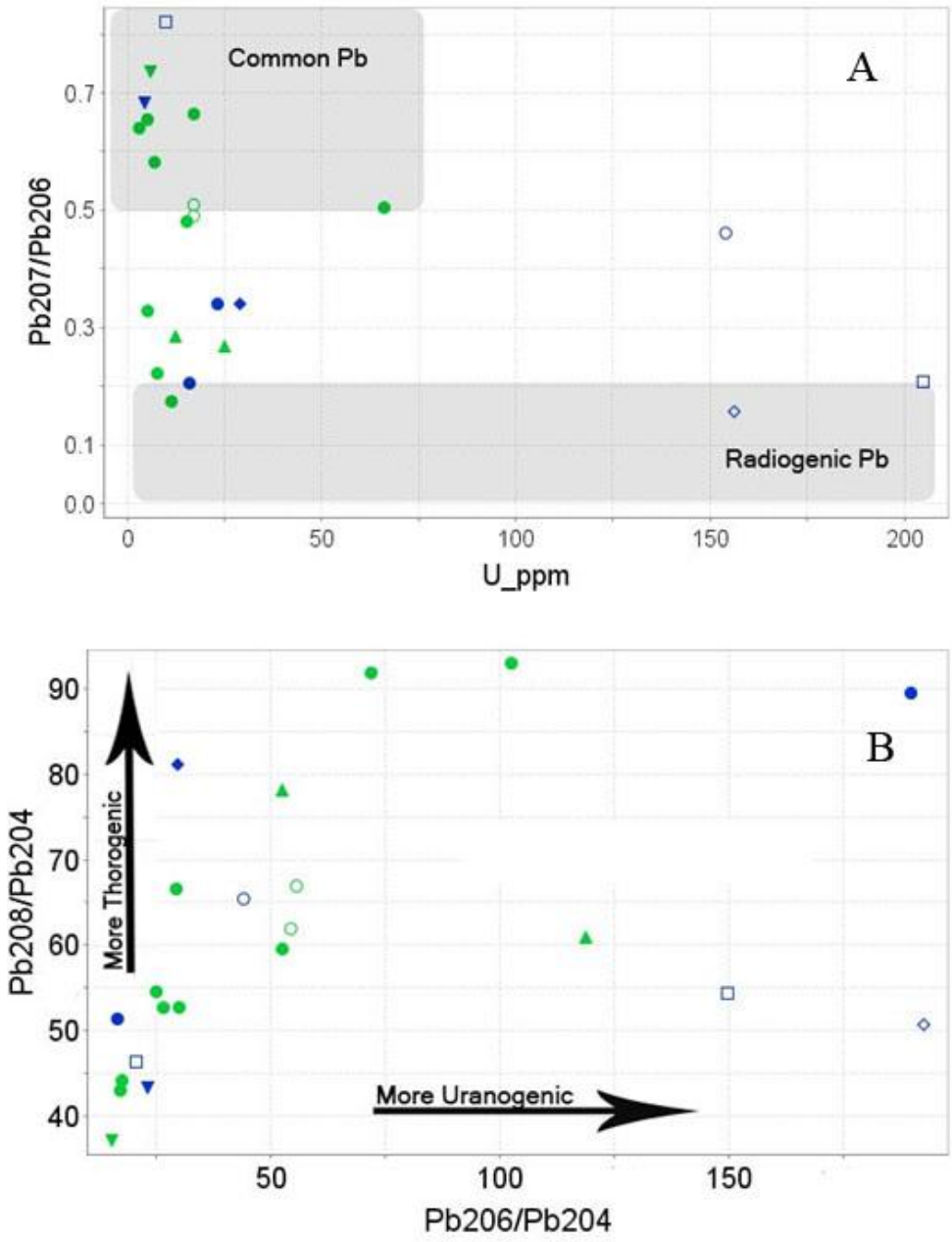

Figure 4-6. A) Partial digestion Pb^{207}/Pb^{206} vs U show partial Pb isotope ratios decreasing towards a radiogenic source. B) Total digestion Pb^{208}/Pb^{204} vs Pb^{206}/Pb^{204}displays the variation in thorogenic and uranogenic Pb in selected samples. Symbols as in Figure 4-1.

4.3 Lithium Isotopes

Lithium concentrations range from 25 to 684 ppm (Table 4-2, 4-4), and the greatest variability is in the metasedimentary samples and particularly the pelitic gneisses. The concentration range for granitic pegmatites is smaller and varies from 29 to 169 ppm, although significant variation was expected as the granitic pegmatites are typically heterogeneous. The bivariate plots of LOI vs Li (Fig. 4-7a) and MgO vs Li (Fig. 4-8a) exhibit positive correlations. An increase of both Li concentration and LOI are potentially representative of addition of Li during hydrothermal alteration whereas decreases in Li and LOI could be related to increasing metamorphic grade (Teng, 2005). Positive correlation between MgO and Li occur because of their similar ionic radii, these two elements substitute for each other but require a charge balance and thus the correlation is related to the coupled substitution.

In contrast δ^7Li does not show any correlation with both LOI (Fig. 4-7b) and MgO, which might suggest that δ^7Li is not affected by metamorphism. Furthermore δ^7Li shows no correlation to bulk Li concentrations (Fig. 4-8b). Regionally δ^7Li does show slight variation between the different sample localities; MacArthur River (4 to 6 ‰), Dawn Lake (4 to 12‰), Read Lake (10 to 14‰), Epp Lake (8 to 10‰) and McClean Lake (-0.4 to 3.4‰) (Fig. 4-9). Altered samples within the different sample locations are some of the lower δ^7Li values for the individual regions, although additional sample analyses are required to confirm these observations.

Sample number	Rock Type	$\delta^{11}B$	$\delta^{7}Li$	B	Li	MgO	LOI
		‰	‰	ppm	ppm	wt %	wt%
A94-040d	Outcrop	4.3	-0.4	25	63	1.04	0.50
157 114.5	Pegmatite	16.1	3.9	10700	29	2.25	2.00
Q6-66 131.2	Pelitic Gneiss	-0.51	4.3	161	84	4.50	5.30
Q6-66 149.7	Graphitic Pelitic Gneiss	0.27	8.0	124	105	3.76	5.70
Q6-66 164.2	Pegmatite	-5.32	6.2	248	105	3.00	3.50
Q6-66 170.9	Graphitic Pelitic Gneiss	0.78	8.1	251	161	5.62	6.90
Q6-67 104.4	Pelitic Gneiss	-5.6	11.9	53	684	11.4	6.50
Q6-72 108.7	Pelitic Gneiss	1.32	12.7	168	80	4.79	4.70
Q6-72 114.5	Pegmatite	-2.39	18.6	913	169	3.36	4.00
Q6-72 117.2	Graphitic Pelitic Gneiss	2.35	8.4	647	178	6.74	7.50
Q7-16 266.8	Pegmatite	1.6	9.7	198	105	2.50	2.70
Q9-16 183.6	Pelitic Gneiss	1.4	7.5	98	309	12.00	7.80
Q9-16 191.3	Pelitic Gneiss	3.54	8.5	167	135	5.67	4.90
Q9-16 199.6	Graphitic Pelitic Gneiss	2.8	11.8	72	416	8.42	10.4
Q9-16 214.6	Pelitic Gneiss	-0.81	8.5	103	232	6.28	3.60
Q9-16 217.2	Pelitic Gneiss	1.7	11.3	97	162	5.32	4.00
EL 09-797.7	Pegmatite	17	8.3	6320	127	4.48	4.20
EL-09-823.7	Pegmatite	17.1	10.4	4010	81	3.14	2.60
RL-46-570.1	Pegmatite	11	14.6	2890	34	1.57	3.20
RL-80-454.5	Tourmalinite	12.1	10.3	10000	74	6.06	4.20
MAC 207.511.1	Graphitic Pelitic Gneiss	-16.3	5.9	1150	152	6.32	8.20
MAC 207.664.8	Psammitic Gneiss	-9.7	9.5	99	25	0.18	1.40

Table 4-4. Analytical data for Li and B isotopic analysis of graphitic/non graphitic metasediments and pegmatites from the eastern Athabasca Basin.

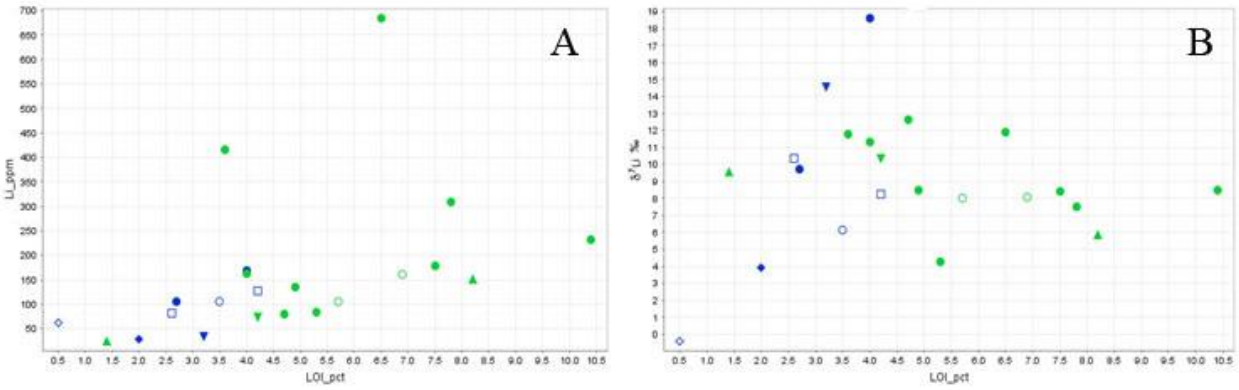

Figure 4-7. Bivariate plots of A) Li vs LOI and B) $\delta^{7}Li$ vs LOI for bulk chemical analysis of eastern Athabasca Basin metasedimentary (green) and granitic pegmatite (blue) samples. Data found in Table 4-3. Sample legend found in Figure 4-1.

4.4 Boron Isotopes

The boron concentrations for granitic pegmatite samples are extremely varied with a range from 25 ppm to 1.10 wt % (Table 4-2, 4-4). In the Epp Lake region both samples had the highest $\delta^{11}B$ result from the entire project area with the pegmatite (EL-09-797.7) yielding the highest $\delta^{11}B$ result of 17.1‰. Quirt (1997) noted in the EAGLE 2 project notes that there is known U mineralization in the EL-09 drill hole within a few meters of both samples. The lowest $\delta^{11}B$ for pegmatite samples of -5.3‰ was obtained from the altered radioactive Dawn Lake sample Q6-66-164.2.

The boron concentrations in metasedimentary rocks are not as variable but do display a significant range in data from 53 ppm to 1150 ppm (Table 4-2, 4-4). The highest boron concentration for metasedimentary samples comes from a graphitic pelitic gneiss sample (MAC 207-511.1), and is more than double the next highest value. Furthermore MAC 207 511.1 yielded the lowest $\delta^{11}B$ of all samples at -16.3‰. In fact, both of the samples from the MacArthur Lake region have the lowest $\delta^{11}B$ possibly suggesting similar sources of boron.

For all rock types there appears to be a positive correlation between Na_2O and B (Fig. 4-10a), which is to be expected as the major reservoir for B in all samples is tourmaline. Also there is a slight correlation between B concentrations and $\delta^{11}B$ (Fig. 4-10b) but there may be other factors influencing these two parameters as there is significant data scatter. Since tourmaline is a major mineral species of interest and it can contain both Li and B, there is no correlation between Li and B therefore there appears to be no relationship between the two elements during crystallization of tourmaline (Fig. 4-11).

A bivariate plot of $\delta^{7}Li$ and $\delta^{11}B$ show that there are differences based on the location of the samples, and especially for B (Fig. 4-9). However, it is important to note that this dataset is not extensive enough to actually measure regional variability in detail and further research is needed for clarification. The differences in $\delta^{11}B$ between regions are as follows; MacArthur River (-16.3 to -9.7 ‰), Dawn Lake (-5.3 to 3.5‰), Read Lake (11.0 to 12.1‰), Epp Lake (17.0 to 17.1‰) and McClean Lake (-2.3 to 16.1 ‰).

.

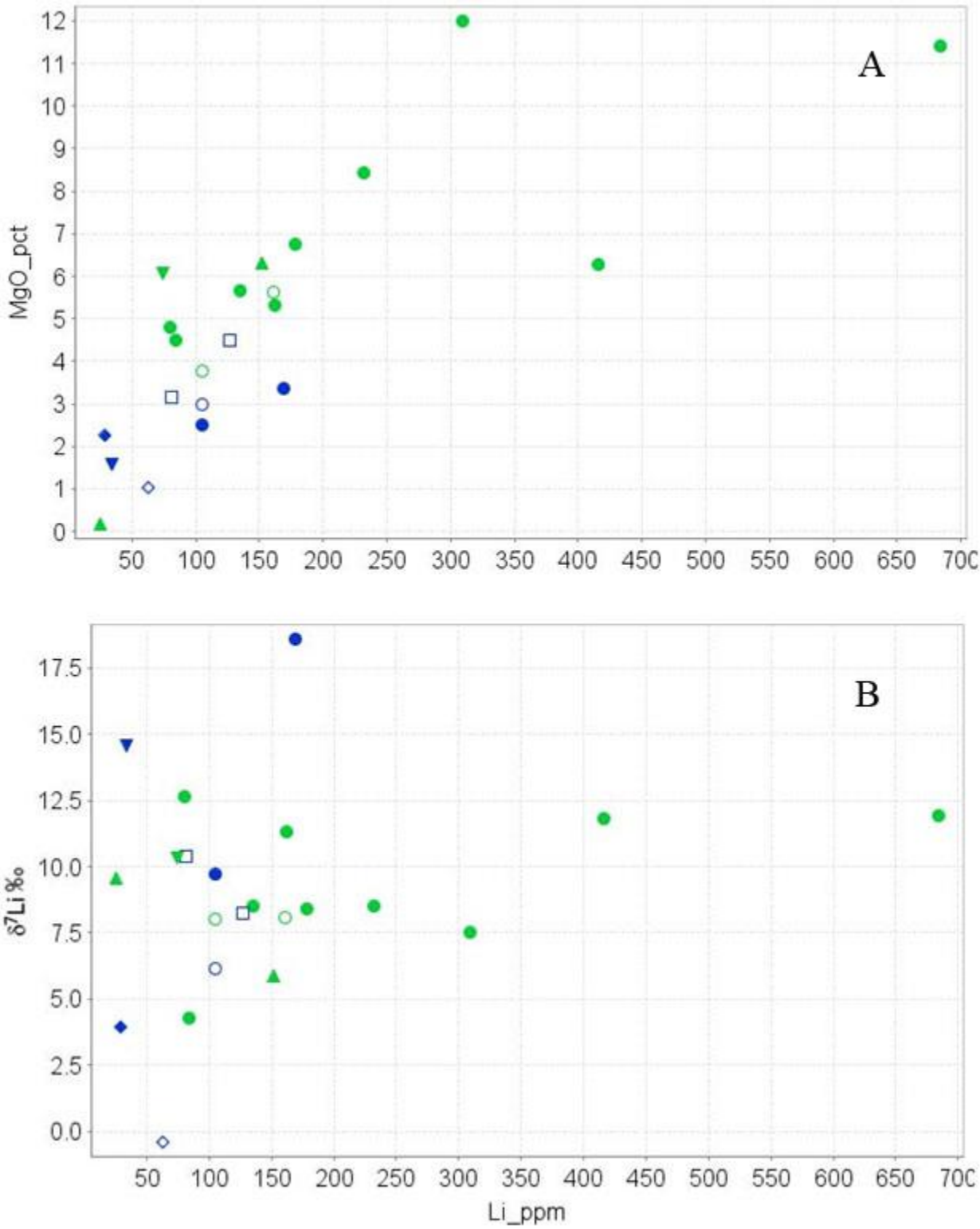

Figure 4-8. A) Bivariate plot of MgO vs Li and B) δ^7Li vs Li for bulk chemical analysis of eastern Athabasca Basin metasedimentary (green) and granitic pegmatite (blue) samples. Data found in Table 4-3. Sample legend found in Figure 4-1.

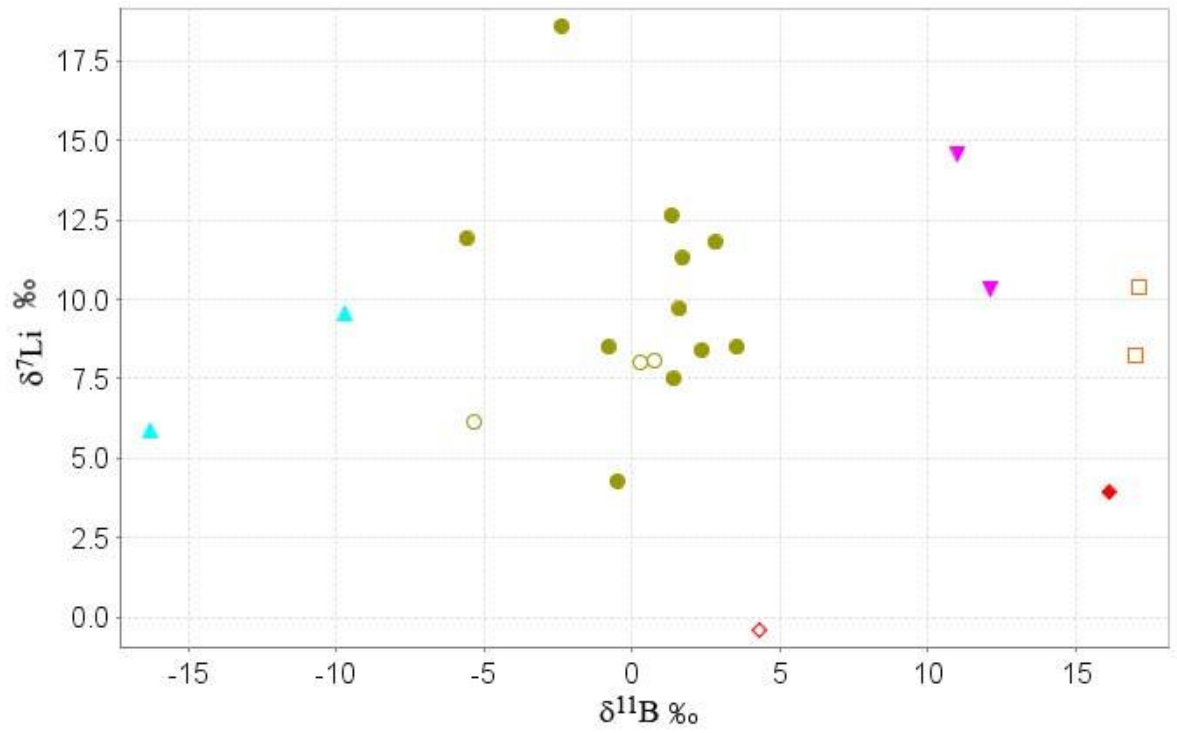

Figure 4-9. Plot of δ^{7}Li vs δ^{11}B for bulk chemical analysis of eastern Athabasca Basin metasedimentary and granitic pegmatite samples displaying the differences in δ^{11}B between regions. Data found in Table 4-3. Blue triangles represent MacArthur River, circular green represent Dawn Lake, red diamonds represent McClean Lake, purple triangles represent Read Lake and the orange squares represent Epp Lake.

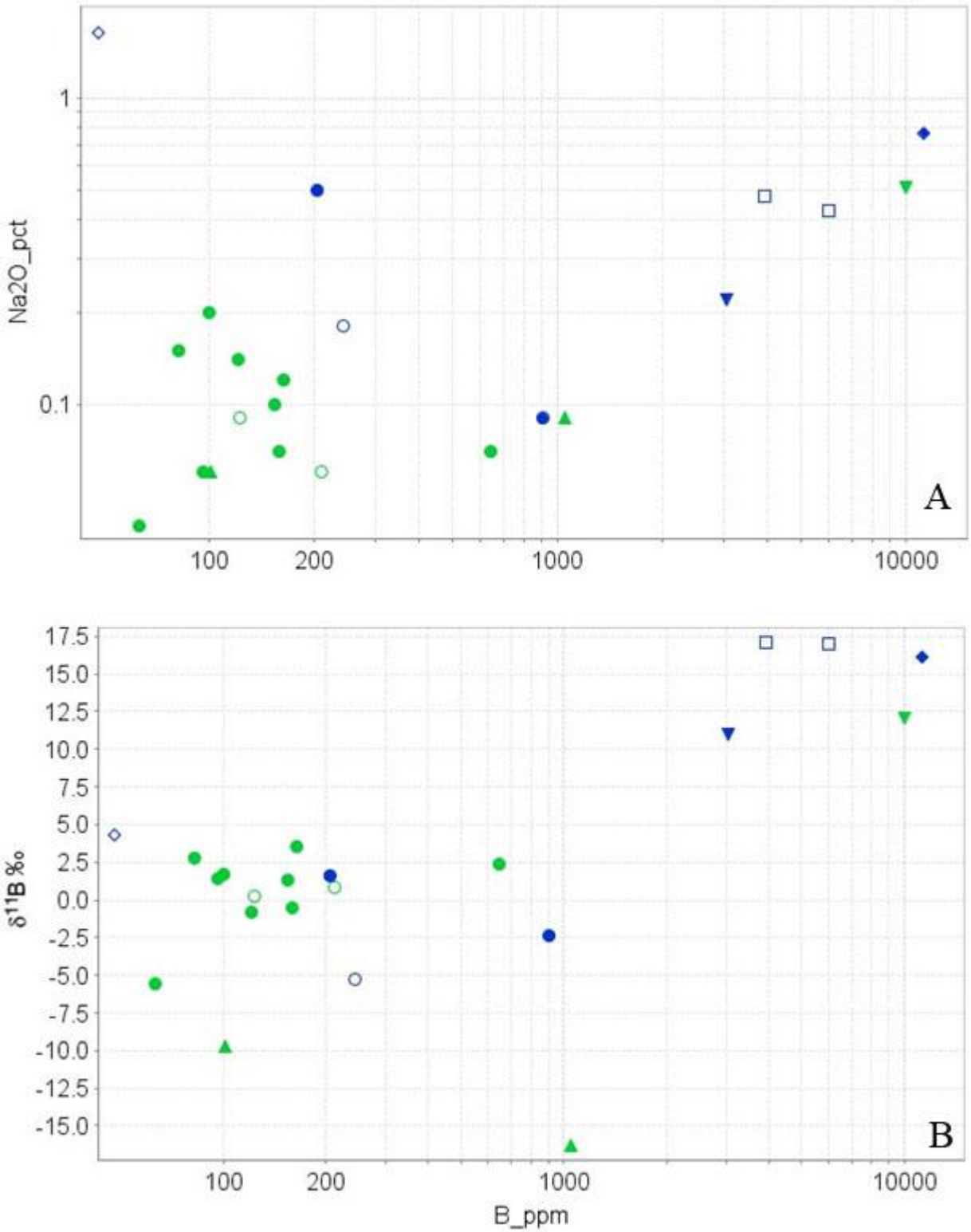

Figure 4-10. Bivariate plot of A) Na_2O vs B and B) $\delta^{11}B$ vs B for bulk chemical analysis of eastern Athabasca Basin metasedimentary (green) and granitic pegmatite (blue) samples. Data found in Table 4-3. Sample legend found in Figure 4-1.

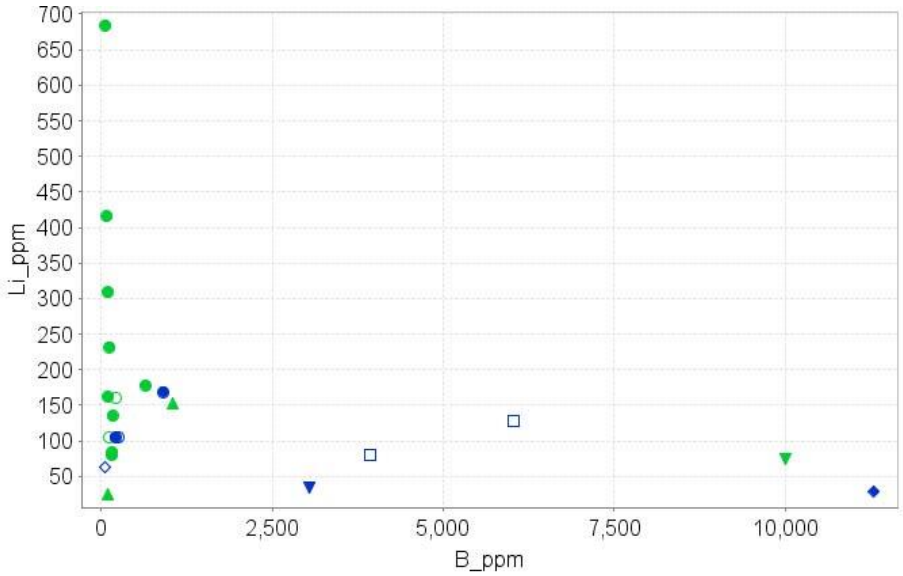

Figure 4-11. Bivariate plot of Li vs B for bulk chemical analysis of eastern Athabasca Basin metasedimentary (green) and granitic pegmatite (blue) samples, there appears to be a mutually exclusive relationship between the concentrations of B and Li. Data found in Table 4-3. Sample legend found in Figure 4-1.

CHAPTER 5
COMPUTATIONAL MODEL OF LITHIUM AND BORON ISOTOPIC SYSTEMS

5.1 Introduction

The effects of water-rock exchange within a geochemical system are important for determining whether any isotopic system can be used as a useful fluid tracer. Many isotope systems with an atomic number greater than 45 are unaffected by physio-chemical fractionation and are commonly referred to as "non-fractionating" isotopes (Sr, Nd, Pb, etc…). Lighter "fractionating" isotopes (H, Li, B, C, O and S) are affected by physio-chemical fractionation, these lighter "fractionating" isotopes reflect many different physio-chemical influences including the composition of the parent fluids at the time of mineral precipitation which can be modified by temperature-dependent fractionation (Eglington, 2014). The lighter "fractionating isotopes are affected in space and time by the composition of the fluids involved in water/rock reactions whereas the heavier isotopes dissolved into the fluid are influenced by the rocks with which they interact.

Permeation of a brine into a relatively porous rock mass will lead to isotopic exchange between the fluid and rock. During this process the initial rock will eventually equilibrate with the fluid whereas further downstream the fluid will equilibrate with the rock. The extent of the reaction front from this advective-diffusive transport can be modelled in mathematical transport equations and is represented by Peclet (P_e) and Damkohler (N_D) numbers. The Peclet number represents the rate of advection to the rate of diffusion with the rock by the flow, whereas the Damkohler number represents the rate to which the fluid equilibrates with the rock over time. The Peclet and Damkohler numbers are calculated using the equation below, the Damkohler number is affected by changes in fluid flow, rock porosity and elemental concentrations (Eglington, 2014).

$$N_D = \frac{IMR_d c_s}{v c_f} \qquad P_e = \frac{vl}{D} \tag{5.1}$$

Parameters used for determining N_D can be found in Table 5-1 but it is important to note that the behavior of the isotopes of interest and the N_D are most affected by variance in the elemental concentrations in the solids and fluids. Very small N_D values are correlated with high concentrations of the element of interest in the fluid and are considered good tracer isotopes that are recharged in specific regions to provide a signature for tracing fluid flow pathways. In contrast, larger N_D values are indicative of higher elemental concentrations in the solid which means the isotope ratio of the fluids will equilibrate with the host rock very quickly, and thus the isotopic composition of the fluids will not be preserved (Fig. 5-1). Intermediate N_D values are excellent for determining water/rock interactions as this fluid will characterize the recharge signature for a period of time but will eventually equilibrate with the country rock. In Figure 5-1 the rock is represented by the three solid lines displaying the differences of N_D of three different isotopic systems when exposed to a fluid flux (dotted line). The highest N_D ($N_D = 10$) represents an isotopic system similar to Pb which would equilibrate with the fluid rapidly compared to a low N_D ($N_D = 0.1$) "non-fractionating" isotopic systems such as H or O which would not be affected significantly by the host rock or fluid flux providing an excellent fluid tracer. Intermediate N_D ($N_D = 1$) isotopic systems possibly including B, Li and potentially Sr require a greater distance for equilibration to occur (Johnson and DePaolo, 1994, 1996).

Significant changes in P_e suggest significant changes in the rock type affecting the dispersion of migrating fluids. Often when modelling advective systems similar to this exercise, P_e tends to not be as important relative to N_D. In modeling advective systems the assumption is made that the fluid dispersion characteristics of large regions with similar litholiges such as the basement rocks beneath the Athabasca Basin will not provide significant changes in P_e thus not

greatly affecting the outcome of the modelled system. Greater consideration is reserved for modelling N_D in an advective system because N_D measures the equilibration reaction between the fluid and rock to advection over distance (Johnson and DePaolo, 1994, 1996).

Symbols	Parameter	Units
phi	Porosity	vol %
rhe_s	Solid density	g/cm^3
rhe_l	Fluid density	g/cm^3
S_w	Saturation ratio	vol %
M	Solid-to-fluid mass ratio	dimensionless
l	Charac. length of system	m
v	Fluid velocity	m/yr
P_e	Peclet number	dimensionless
c_s	Concentration in solid	ppm
c_f	Concentration in liquid	ppb
J_{tot}	Flux of isotope diffusing into liquid phase from dissolution	dimensionless
D	Longitudinal dispersion coefficient	dimensionless
R_D	Average reaction rate for rock-fluid interaction for the isotope of interest	dimensionless
N_D	Damkohler number	dimensionless

Table 5-1. Parameters for determining N_D and their units.

Computational numerical modelling for this project of advective-diffusive Li and B transport through a porous medium, Wollaston metasediments and Hudsonian granitic pegmatites, were calculated using the mathematical equations of Johnson and De Paolo (1994, 1996,1997a,1997b), Bowman et al. (1994) and Alart and Sperb (1997). To verify that the

modelling of the isotopic systems for B and Li is a representative result two non- fractionating (Pb and Sr) and two fractionating (H and O) isotopic systems were modelled for comparison of computed results.

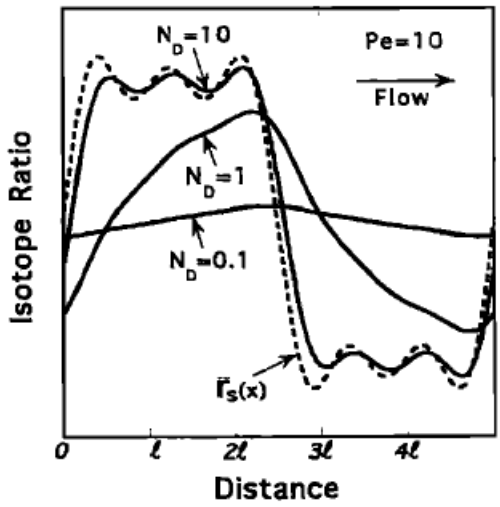

Figure 5-1. The dashed line represents the reacting fluid flux and three hypothetical N_D representing a low N_D (0.1), intermediate N_D (1) and high N_D (10) displaying that the highest N_D is most affected by the fluid flux front. From Johnson and De Paolo (1994).

5.2 Assumptions and Constants

The computational modelling of N_D will aid in determining the validity of using B and Li isotopes as a possible vectoring tool for mineralization. The fluid interacting with the pre-ore, ore and post-ore basement used for the three scenarios had the composition of evaporated seawater as it moved through a representative Athabasca Basin U/C-related uranium deposit based on previously published studies (Annesley et al., 1996, Cloutier et al., 2009, Fayek and Kyser, 1997, Fontes and Matray 1993, Mercadier et al., 2012, Richard et al., 2009, Viezer, 1989) and data from this project. The following assumptions were applied during calculations.

Assumptions:

- Porosity of country rocks is constant
- Permeability is constant in the country rock
- Bulk rock isotopic composition was used, assuming that all minerals react at different rates and we are measuring the net change in the rock (Bullen and Kendall, 1993).
- Steady state has been reached in country rock
- Pressure is constant

In this simple model, we assume constant pressure, porosity and permeability in the basement rocks in the region, even though fractures and shear zones, which are important for transporting fluids in the basement, will be zones with varying fluid pressures and permeability. Modelling the steady state system will also provide the simplest perspective on isotopic fractionation. Pe for this system will remain constant as the rate of advection to diffusion was not as significant for determining changes in the fluid as N_D. If we were measuring the effects of pegmatite emplacement the differences of Pe for different host rocks would be an important factor to model but because we are assuming constant pressure and porosity there will be no change in Pe for the different modelling scenarios (Liu, 2009). Lithium will be a trace element in many minerals including mica, quartz, feldspar, staurolite, cordierite, garnet, tourmaline and clays. The key mineral for boron is tourmaline which is found in many different forms within the basement ranging from disseminated tourmaline to elevated amounts of tourmaline within granitic pegmatites and in proximity to mineralization (Annesley et al. 1995, 1996, 1998, 1999). However, for this simple model we use the bulk isotopic composition and assume the reaction rate (r) to remain constant and is representative of the entire rock body.

Six different isotopic systems H, O, Li, B, Sr and Pb were modelled in this study, and the constants that were used are listed in Table 5-2. Other isotopic systems including H, O and Sr were not measured in this study but were used to verify that the modelling of Li, B and Pb isotopic systems were behaving in a realistic manner. The data from multiple studies (Annesley et al., 1996, Cloutier et al., 2009, Fayek and Kyser, 1997, Fontes and Matray 1993, Mercadier et al., 2012, Richard et al., 2009, Viezer, 1989) was applied to verify that our assumptions were correct and that the calculations for the modelling system were functioning properly. The density of the brine and solids were determined from laboratory measurements of many brines and solids at the Saskatchewan Research Council.

Constants	Value	Units
Phi	20	%
rhe (s)	2.5	g/cm3
rhe (f)	1.1	g/cm3
S (w)	100	%
M	9.091	NU
L	100	m
V	20	m/yr
P(e)	10	NU
R_D	0.000005	NU

Table 5-2. Constants used during computational modelling of B and Li isotopic systems.

Concentrations and isotopic ratios for both the solids and fluids for all elements were sourced from other relevant studies of the Athabasca Basin or whole rock geochemical data from this study. As mentioned above the concentration difference between the fluid and the solid has the greatest effect on the N_D for the system, whereas the choice of isotopic values has limited affect. The concentrations of both H and O were estimated from the expected mineralogy and fluid composition. The δD (Basement = -50‰, Ore Zone = -10‰) and $\delta^{18}O$ (Basement = - 8‰, Ore Zone = -4‰) from Cloutier et al, (2009) were used for the solid and the δD (-100‰) and

$\delta^{18}O$ (5‰) from Richard et al., (2009) were considered representative of the fluids present. Concentrations of Sr, Pb, B and Li in the solid were extracted from the data of Annesley et al., (1996) and this project (Table 4-2).

Isotopic System	*cs*	*cf*
	ppm	ppb
Unaltered Basement		
Lead	10	0.5
Strontium	200	7850
Lithium	100	5400
Boron	100	10800
Oxygen	900002	9000000000
Hydrogen	55	110000000
Ore Zone		
Lead	1000	0.5
Strontium	1930	7850
Lithium	600	5400
Boron	14000	108000
Oxygen	900002	9000000000
Hydrogen	55	110000000
Post Mineralization		
Lead	10	10
Strontium	200	7890
Lithium	10	3300
Boron	100	64000
Oxygen	900002	9000000000
Hydrogen	55	110000000

Table 5-3. Summary of the calculated ND values and concentrations of both the solids and fluids used for calculations.

For the concentration of Li and B in the fluid the assumption was made that the fluids were an evolved seawater or brine, similar to Mercadier et al., (2012). The estimated B and Li concentrations in the brine were based on the values of Fontes and Matray (1993). The Sr

isotopic ratio of the brine was from Viezer (1989) ($^{87}Sr/^{86}Sr = 0.706$) and the Sr isotopic ratio of solids (Basement $^{87}Sr/^{86}Sr = 0.769$, Ore deposit $^{87}Sr/^{86}Sr = 0.710$) was from Fayek and Kyser (1997) (Table 5-3).

5.3 Results

Table 5-4 summarizes the range in N_D values calculated after inputting all factors for the multiple isotopic systems (Table 5-2 and 5-3) into the equations for the calculation of N_D. The N_D values for B and Li are intermediate to the N_D values of the fractionating and non-fractionating isotopes (Fig. 5-2). The importance of this is three fold. Firstly, this means that both isotopic systems have the potential to carry information on the rock reservoir if the concentration in the reservoir is significant. Secondly, because of the properties of B and Li they will effectively carry this reservoir signature for a longer path then non-fractionating isotopes, although they will eventually equilibrate with the host rock potentially providing vectoring towards mineralization. Therefore the isotopic signature of the fluid during mineralization or pre-mineralization could be significantly different from the original reservoir depending on the concentration in the fluid. Exchange in the ore zone may affect the fluids depending on the concentration in the rock. A very high concentration for the B and Li was used for modelling the ore zone and proximal alteration, the high concentrations in the rock caused the N_D to increase by a factor of 10 compared to pre and post-ore models. Suggesting that alteration in close proximity to the ore zone would have a significant effect on the fluid isotopic signature for B and Li if the concentrations are high in that region. Finally as B typically had a lower N_D compared with Li during modelling this suggests that the B isotopic system may be better for providing information on the source whereas the Li isotopes will provide more vectoring information towards mineralization.

Isotopic System	N_D From Model
Unaltered Basement	
Lead	113
Strontium	0.14
Lithium	0.105
Boron	0.053
Oxygen	0.006
Hydrogen	0.00003
Ore Zone	
Lead	11363
Strontium	1.40
Lithium	0.631
Boron	0.737
Oxygen	0.006
Hydrogen	0.00003
Post Mineralization	
Lead	6
Strontium	0.14
Lithium	0.017
Boron	0.009
Oxygen	0.006
Hydrogen	0.00003

Table 5-4. Summary of calculated N_D values

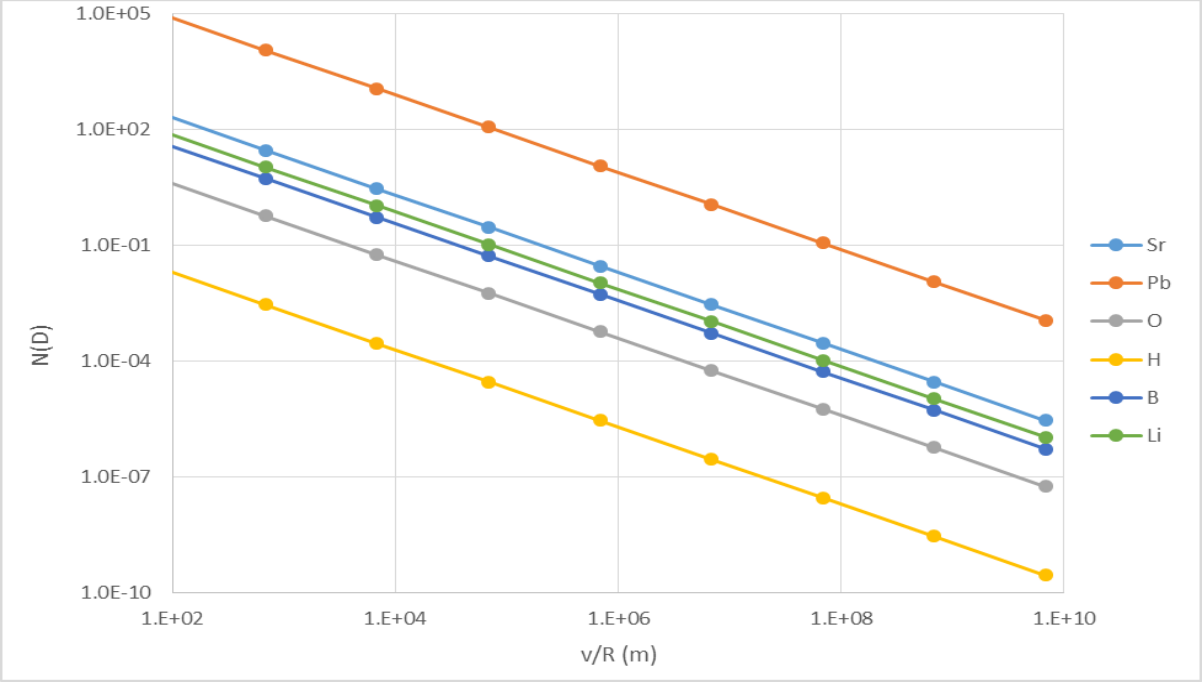

Figure 5-2. N_D vs the ratio of fluid velocity over reaction rate determined using the calculations of DePaula and Johnson (1994). The values are calculated from modelling the fluids reacting with the ore forming system, there are significant differences for N_D up to several orders of magnitude between the different isotopic systems.

5.4 Summary

The focus of the modelling exercise was to determine the kinetic fractionation behaviour of B and Li isotopes in basement rocks beneath the Athabasca Basin. This exercise was simplistic in comparison to natural systems in that there were no constraints placed on the fluid flow system, and many physio-chemical processes including fluid/rock ratios, temperature, pH, fluid chemistry, mineral dissolution rates and equilibrium fractionation effects were not considered. Nevertheless, the modelling indicates that the two isotopic systems behave between fractionating (e.g. H) and non-fractionating (e.g. Pb) isotopes suggest that they could be representative of the reservoir rock signature and fractionation is influenced by physio-chemical processes, but that these systems could demonstrate potential to record fluid flow and act as a possible vectoring tool.

CHAPTER 6
DISCUSSION

The bulk chemical δ^{7}Li and δ^{11}B isotopic signatures measured by both HR-ICPMS and MC-ICPMS on fresh and altered basement rocks beneath the eastern Athabasca Basin display significant ranges. Fractionation of these isotopic systems is influenced by many factors, and this chapter examines the behavior of the two stable isotopic systems in relation to hydrothermal fluid interaction, metamorphism, and partial melting. Ultimately we want to determine whether the isotopic fractionation is observed locally or on a regional scale and if there is any potential relationship to uranium mineralization from the multiple sites sampled throughout the basement beneath the eastern Athabasca Basin. In closing we will discuss the potential of the basement as a possible source of uranium for the U/C-related uranium deposits, and the feasibility of developing routine Li and B isotopic analysis using single collector HR-ICPMS.

6.1 Factors Controlling Lithium and Boron Isotopic Variability

6.1.1 The Effects of Mineralogy and Fluid Compositional on Isotopic Fractionation

Both the concentration and isotopic fractionation of boron and lithium are controlled by multiple factors including mineralogy, fluids, temperature and grain size (Berger et al. 1998; Chen et al., 1991, 2005; William and Hervig, 2005). Lithium can be incorporated into a greater variety of minerals whereas boron preferentially partitions into tourmaline. For example metamorphic minerals in pelitic rocks preferentially partition lithium into the crystal structure in the following order staurolite>cordierite>biotite> muscovite> garnet (Duttrow et al. 1986). Other common minerals that incorporate lithium and boron include quartz, feldspars, and a variety of clay minerals. In regards to lithium the heavier isotope ^{7}Li tends to prefer the liquid

phase during fractional crystallization and prefers smaller coordination sites with stronger bonds, whereas ^{6}Li tends to prefer weaker bond sites and higher coordination in fluids and minerals, such as mica (Wunder et al. 2007). The extent of partitioning of the different isotopes depends on mineral and fluid specific fractionation factors. For example, the Li partition coefficient (K_{Li}) for both minerals and fluids increases with temperature (Seyfried et al., 1984; Berger et al., 1988; Brennan et al. 1998; Seyfried et al., 1998). At temperatures below 300^{o}C lithium isotopic fractionation can occur between lithium-bearing fluids and clay minerals. When precipitating clays ^{6}Li is preferentially incorporated into the crystal structure at lower temperatures (Vigier et al., 2008). As the temperature increases more ^{7}Li is incorporated into the crystal structure until the clay minerals become more unstable at high temperatures, causing the clay to breakdown and thus release Li into the fluid (Chan et al., 1994, 2002; You et al., 1995; Chan and Kastner, 2000). Therefore when investigating lithium isotopic systems in none refractory minerals it is likely that the effects of the last fluid event is the one preserved. Understanding the preservation and recrystallization of the minerals is key to understanding and extracting information from the Li isotopic system (Romer, 2013).

In comparison, the main control for boron concentrations in rock is tourmaline, although boron can be incorporated into many different minerals, including clay minerals and mica, albeit at concentrations 10^{3}-10^{4} times lower than in tourmaline (Henry and Dutrow, 1996). Concentration and fractionation of boron in relation to mineralogy is controlled by temperature of fluids or melts present. When precipitating tourmaline, as temperature increases the boron isotopic fractionation between tourmaline and fluid decreases (Palmer et al, 1992). Depending on pressure, the typical range for δ^{11}B at 450^{o}C between fluid and tourmaline is 5 to 8‰,

whereas when the temperature increases to 750ºC the effect on $\delta^{11}B$ between tourmaline and fluid decreases to 2‰ (Palmer et al., 1992).

The mineral assemblage for the metasedimentary rocks of this project include quartz, plagioclase, K-feldspar and biotite, with minor mineral phases including sillimanite, titanite, chlorite, muscovite and sulphides. Similar to metasedimentary samples, the major mineralogy of the granitic pegmatite samples of this study includes quartz, plagioclase, K-feldspar and tourmaline. The mineralogy of the granitic pegmatites is less variable then the metasedimentary rocks, with tourmaline found as both a minor and major mineral along with biotite and sillimanite in the granitic pegmatites. The alteration mineralogy for both rock types often includes chlorite, illite, dickite, hematite and dravite. Many of the above mentioned minerals incorporate both boron and lithium especially tourmaline, mica and clay minerals. Because of the significant boron concentration differences between tourmaline and other minerals ($10^3 – 10^4$ times greater) it was determined that significant concentrations of boron in the study is typically associated with tourmaline-rich rocks and therefore would be mostly refractory. Thus, the boron isotopic signature should be representative of the boron isotopic signature of the tourmaline preserved in the rocks studied. Unfortunately, if there are multiple generations of tourmaline present in the rock, there could be mixing of boron isotopic signatures if they have different source fluids or have interacted with different fluids.

The mineralogical uptake for lithium is not as clear, as lithium could be found in many minerals including mica, quartz, feldspar, staurolite, cordierite, garnet, tourmaline and clays. When investigating possible mineralogy there is no correlation between the concentrations of lithium and boron in relation to changes in δ^7Li (Fig. 4-8) and $\delta^{11}B$ (Fig. 4-10) respectively in the dataset. Therefore the major mineralogical lithium input from the Athabasca Basin is most

likely not associated with tourmaline due to the dissociation of both the elemental concentrations together with δ^{7}Li and δ^{11}B. As mentioned above lithium would be more affected by low temperature fluids when precipitated in less refractory minerals such as mica, feldspars and clays. From the dataset, correlation between the fluid mobile elements, magnesium and lithium (Fig. 4-8), suggest that lithium is associated to magnesium-bearing minerals. A common source of magnesium in basement fluids occurs from the decomposition of biotite or alteration minerals such as chlorite or dravite. Temperatures in the Athabasca Basin during mineralization were approximately between 130^{o}C and 250^{o}C based on fluid inclusion studies (Derome et al, 2005). Mercadier et al. (2012) suggested, based on the boron isotopic data from the basement beneath the Athabasca Basin that the fluids from which the large U/C-related uranium deposits formed was likely a marine-derived brine. When comparing the δ^{7}Li values of metasedimentary rocks from this project with the δ^{7}Li of different rock and fluid reservoirs, it appears that they fall within the same range as saline water or brines (Fig. 6-2), but this classification is wide ranging and is inclusive of many different rock types.

6.1.2 Lithium and Boron Isotopic Variability in Metasedimentary Rocks

The δ^{7}Li and δ^{11}B of metamorphic rocks, such as pelitic gneiss and graphitic pelitic gneiss, should be representative of the of the original sedimentary rock signature. Marschall et al. (2007) suggested that between 5 and 40 % of lithium is lost during metamorphic dehydration of metapelites, and Teng (2007) confirmed that up to 50 % of lithium is lost during metamorphic dehydration. Although there is a loss of lithium during metamorphism there appears to be no relationship between metamorphic grade and isotopic composition (Romer, 2014; Teng, 2007; Qiu et al., 2009) (Fig. 6-1).

In this study lower LOI and higher metamorphic grade are correlated to decreasing concentrations of lithium and boron. Figure 6-1 displays differences between metasedimentary samples and alteration in relation to the relatively immobile TiO_2 during metamorphism of sedimentary rocks, loss of boron or lithium shift the results towards the origin. Altered metasedimentary samples show a loss of both lithium and boron in relation to TiO_2. Average boron concentrations in shales is 70 to 250 ppm (Pierra and Shaw, 1997) which plot within the metasedimentary samples of this study. Some of the fresh metasedimentary samples have gained boron and lithium relative to TiO_2 in comparison to typical shale, and this is especially obvious in the tourmalinite sample in which the majority of the sample is tourmaline. In altered metasedimentary rocks the δ^7Li and $\delta^{11}B$ values are representative of the original sedimentary rock, and thus the variance in δ^7Li and $\delta^{11}B$ is most likely representative of heterogeneous source material in different parts of the eastern sub-Athabasca basement. Unlike the variation in Li and B concentration with metamorphic grade, δ^7Li and $\delta^{11}B$ are not related to metamorphic grade and therefore any fractionation observed is likely due to other factors such as alteration fluids, mineralogy or partial melting.

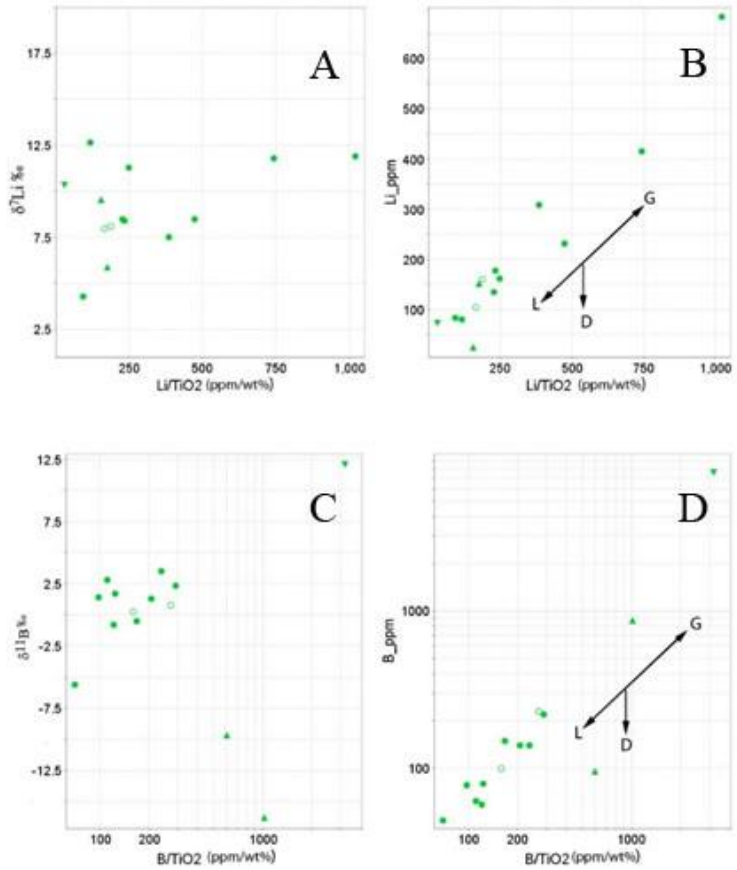

Figure 6-1. Bivariate plot of metasedimentary rocks, A) δ^7Li vs Li/TiO_2, B) [Li] vs Li/TiO_2, C) δ^{11}B vs B/TiO_2 and D) [B] vs B/TiO_2 concentrations of elements vary relative to TiO_2 which is commonly undisturbed during metamorphism. There appears to be no trend for unaltered/altered metasedimentary metasedimentary δ^7Li and δ^{11}B relative to TiO_2 suggesting that most likely the isotopic signatures are reflective of their origin and unaffected by metamorphism. L- Loss, D- Depleted and G – Gain.

6.1.3 Lithium and Boron Isotopic Variability During Partial Melting and the Formation of Granitic Pegmatites

Annesley et al. (2005) determined that partial melting of metasedimentary rocks occurred in the Wollaston Domain ca 1815 Ma. Melt was generated in a fluid absent environment at peak metamorphic conditions of 850ºC and 9 kbar. Over the next 20 to 35 Ma isothermal decompression occurred providing the perfect conditions for biotite dehydration reactions until pressures stabilized around 4 to 5 kbar. From 1775 to 1720 Ma significant extension and tectonic extrusion resulted in orogenic collapse and the formation of the Athabasca Basin 1750 to 1680 Ma (Annesley et al., 2005). McKechnie et al. (2013) suggested that the source for granitic pegmatites in the Fraser Lake region of the Wollaston Domain must ultimately have been the metasediments due to the lack of appropriate age granitic plutons in the basement rocks beneath the Athabasca Basin.

During partial melting lithium is fluid mobile in the initial stages whereas boron is dependent on mineralogy. At high metamorphic grade lithium is easily released from the crystal structure for all mineral phases, although the type of fluid mobilizing lithium has a greater effect on isotopic fractionation. If the fluid is aqueous there is little to no change in δ^7Li relative to the source, but if a magma is created then Li isotopic fractionation can occur (Maloney, 2008). The destabilization of boron in tourmaline can be controlled by factors including undersaturation of boron in the melt (Wolf and London, 1997; London, 1999) and solubility of tourmaline in the melt (Romer, 2007). The high temperatures and pressures suggested by Annesley et al. (2005) would be sufficient enough to melt all minerals present in the metasedimentary rocks including tourmalines. The tourmalinites found throughout the basement lithologies would have been an important source of boron for granitic pegmatites (Jiang-Shao et al. 1999). Similar to lithium,

the heavier isotope ^{11}B preferentially partitions into the melt during partial melting which causes fractionation to occur. Fractionation modifies both the isotopic composition of the source rock and the pegmatite or leucogranite formed from partial melting (Kawakami 2001)

Elevated δ^7Li and $\delta^{11}B$ occur because of the peraluminous melts, as adding aluminum to the silicate melt increases ^7Li in the melt because of the preferential association of ^7Li with higher coordination. Figure 6-2 displays the range of δ^7Li and $\delta^{11}B$ values for granitic pegmatites in comparison to metasedimentary samples of this study. The former are heavier than the latter. Similarly, Teng et al., 2006 determined similar variability between pegmatites and metasedimentary samples from the Black Hills, South Dakota. This offset in fractionation between pegmatites and metasedimentary rocks is due to the partial melting of metasedimentary samples. Large variations in the δ^7Li values for granitic pegmatites could be indicative of the hetereogeneity of metasedimentary rocks in the region. It is also important to note that when the granitic pegmatites intrude the host rock there may be exchange of Li with the wall rock, the effects of this diffusion with the wall rocks depends on the concentration of lithium in the wall rock and the Li the pegmatite (Liu, 2009; Teng et al., 2006; Maloney, 2008). Teng et al. (2006) revealed significant changes to the wall rock δ^7Li due to the intrusion of pegmatite bodies in the Black Hills (South Dakota), whereas the effects of intrusion of the Florence County pegmatites, Wisconsin, was not as significant (Liu et al., 2009).

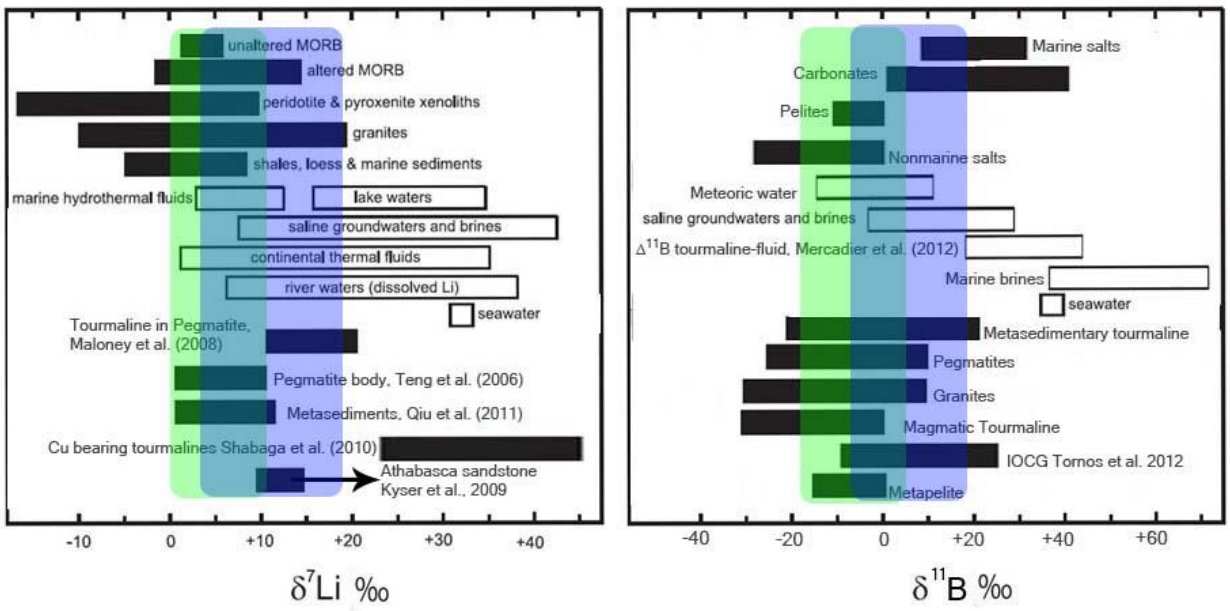

Figure 6-2. Summary of a) lithium and b) boron isotopic compositions including pelitic gneiss, graphitic pelitic gneiss and U-rich pegmatites from the eastern Athabasca Basin. Filled bars are for solid samples and open bars are for fluids. Summary data from Table 1., a) Qiu et al., 2011 and Teng et al., 2006 and b) Mercadier et al., 2012 and Tornos et al., 2012. The blue highlighting represents pegmatite data from this project and the green highlighting represents the metasedimentary samples from this project.

6.1.4 Modelling

Hot, acidic, oxidizing saline brines are considered one of the important transporting fluids for uranium. As the hot, acidic saline brines move through the basement lithologies they scavenge uranium and other elements associated with the accessory minerals (Derome et al., 2005; Derome et al., 2007; Mercadier et al., 2009; Richard et al., 2011). Partitioning of both Li and B into partial melts or fluids can be variable. Lithium is highly soluble in Cl-rich brines at high temperature (Webster et al, 1989) but lithium can also be transported by less saline and cooler fluids if loosely bound to micas and clays. Boron can be mobilized at low temperature by hydrothermal fluids when contained in micas and clay minerals, but is typically immobile when

contained in tourmaline until melting takes place at higher temperature. Temperatures and pressures in the Athabasca Basin and underlying basement during uranium deposition are low enough that tourmaline would be stable (Annesley et al., 2005) meaning that boron from magmatic tourmaline would not be as mobile as uranium and lithium. The distance that boron and lithium travel from their source can differ greatly as boron is often not as mobile due to interaction with biotite which causes tourmalization (Duke, 1985).

Kinetic modelling of the boron and lithium isotopic system in relation to uranium deposition provided good insight into the potential of these isotopic systems. In general the boron isotopic systems is going to be more conservative of the original fluid source compared to lithium which will be more representative of the fluids and the geological processes occurring (Figure 5-2). But the most important factor for both isotopic systems is the concentration in the fluid relative to the elemental concentration in the rock. Boron concentrations in the rocks are significantly higher than lithium concentrations and therefore would most likely preserve the original boron isotopic signature of the source rock. As the majority of boron is locked in the crystal structure of tourmaline and therefore, as mentioned above and modelled, the $\delta^{11}B$ in the rock should not be affected as much as lithium isotopic composition. Mineral chemistry is important and if there are significant amounts of clay present the $\delta^{11}B$ could be more affected by the low temperatures fluids moving through the basement. Modelling also suggests that eventually through extended periods of fluid flow or significant differences in concentrations there may be fractionation changes. Diffusion of boron in minerals or under saturation of boron in the fluids may aid in causing changes in $\delta^{11}B$.

For example, on a regional scale $\delta^{7}Li$ does show slight variation between the different sample localities but in general they are overlapping in $\delta^{7}Li$ values; MacArthur River (4 to 6 ‰),

Dawn Lake (4 to 12‰), Read Lake (10 to 14‰), Epp Lake (8 to 10‰) and McClean Lake (-0.4 to 3.4‰) (Fig. 4-9). Also the altered samples within the different sample regions are some of the lower δ^7Li values for the individual regions although the difference is not distinct. In comparison δ^{11}B does show that there are differences based on the sample region for boron isotopes (Fig. 4-9), although it is important to note that this dataset is not extensive enough to actually measure regional variability and further research is needed for clarification. The differences in δ^{11}B between regions are as follows; MacArthur River (-16.3 to -9.7 ‰), Dawn Lake (-5.3 to 3.5‰), Read Lake (11.0 to 12.1‰), Epp Lake (17.0 to 17.1‰) and McClean Lake (-2.3 to 16.1 ‰). The more distinct divisions in δ^{11}B compared with δ^7Li between regions displays what was expected from the outcome of the modelling exercise. Lithium isotopes will be more prevalent in non-refractory minerals compared to boron which is found primarily in refractory tourmaline. From the modelling we expect that with increased fluid flow on a regional scale we would see equilibrium occur between the different regions as the N_D is higher for lithium compared to boron. δ^{11}B from the formation of the tourmaline should be maintained unless the rock is altered and the boron is precipitated in more non-refractory minerals such as clays.

If we investigate this a little further and look more specifically at δ^7Li within a specific drill hole (Dawn Lake drill hole Q6-66) bleached, altered samples (8.0 and 8.1‰) are slightly heavier compared to fresh rock types (4.3 and 6.6‰). This should be expected as when a rock is altered by hydrothermal fluids ^{7}Li is more favorable by the hydrothermal fluid. As the hydrothermal fluid continues to collect more ^{7}Li this will continue to develop a heavier δ^7Li in the fluid and thus leave behind a heavier δ^7Li signature as it interacts with non-refractory minerals. In regards to δ^{11}B the bleached samples have slightly heavier δ^{11}B values (0.27 and 0.78 ‰) compared to

the fresh rock samples (-0.52 and -5.72 ‰). ^{11}B is preferentially concentrated in the hydrothermal fluid, and thus the $\delta^{11}B$ is heavier for the bleached samples due to the interaction with a hydrothermal fluid, similar to the lithium isotopic variations. . The range between altered and fresh $\delta^{11}B$ may be slightly less because of the preference of boron to be incorporated into tourmaline. But for both $\delta^{7}Li$ and $\delta^{11}B$ the bleached samples appear to be have obtained their isotopic signatures most likely due to interaction with a fluid with a more homogenous isotopic signature.

6.2 Potential of Basement as a Metal Source for U/C-Related Uranium Deposits

To form the world class uranium ore bodies explored for in the Athabasca Basin the initial quantity of uranium required is significant, as the total amount of uranium discovered to date in the Athabasca Basin is greater than 587 063 tonnes (t) U at an average grade of 1.97% U (Sask. Ministry of Economy, 2014). Not only are these deposits rich in uranium but some of the U/C-related uranium deposits have significant concentrations of other metals, including Co, Cu, Ni, Au and As (Jefferson, 2007). The polymetallic source for U/C-related uranium mineralization is an ongoing debate, as to whether the uranium was derived from detrital minerals in the sandstone basin (Hoeve and Sibbald, 1978; Hoeve and Quirt, 1984; Kotzer and Kyser, 1995; Fayek and Kyser, 1997;) or from the U-rich minerals in the basement (Annesley and Madore, 1999; Madore et al. 2000; Hecht and Cuney, 2000; Cuney et al. 2003; Richard et al., 2010; McKechnie et al., 2012a, 2012b; Mercadier et al., 2013).

Across the Athabasca Basin, typical uranium concentrations in the basement are variable and >5 ppm, Madore et al. (2000) suggested the average basin wide basement uranium concentration was 12.6 ppm determined from multiple studies. Unaltered pelitic gneiss can have

U concentrations upwards of 40 ppm, typical granitic pegmatites have concentrations as high as 2400ppm U (McKechnie et al., 2013). This study has wide ranging uranium concentrations with an average of 16 ppm for the metasedimentary rocks and 75 ppm for granitic pegmatites. In comparison to the basement lithologies typical basin uranium concentrations are low, <3ppm (Jefferson et al., 2007). Basement samples from this study have variable U, Co, Cu, Ni and As concentrations (Table 4-2) with uranium concentrations up to 23 ppm and 12 ppm for unaltered granitic pegmatites and unaltered metasedimentary rocks, respectively. Typically the concentrations are significantly greater than average crustal abundances in both altered and unaltered samples. A good indicator of the uranium potential for both the altered and unaltered rocks is examining the Th/U ratios. Crustal Th/U ratios are approximately 4 (Cuney and Kyser, 2008) whereas Th/U ratios for uranium deposits can be well below 0.1 (Mercadier, 2013). Both unaltered and altered samples of this study have Th/U values that range from 1 to 0.1 (Fig. 6-3). Higher Th/U ratios suggest that the uranium is locked up in the crystal structure of refractory minerals, such as zircon and monazite, whereas the lower Th/U suggest the uranium is precipitated in minerals such as uraninite and coffinite. Higher Th/U ratios can also signify the loss of uranium from minerals such as monazite yielding Th-rich, U-poor minerals, such as huttonite or thorite. Altered pegmatites in this study have the lowest Th/U ratios (Table 4-3), which suggests that the pegmatites are a possible U-rich source of uranium for the high-grade deposits U/C-related uranium deposits.

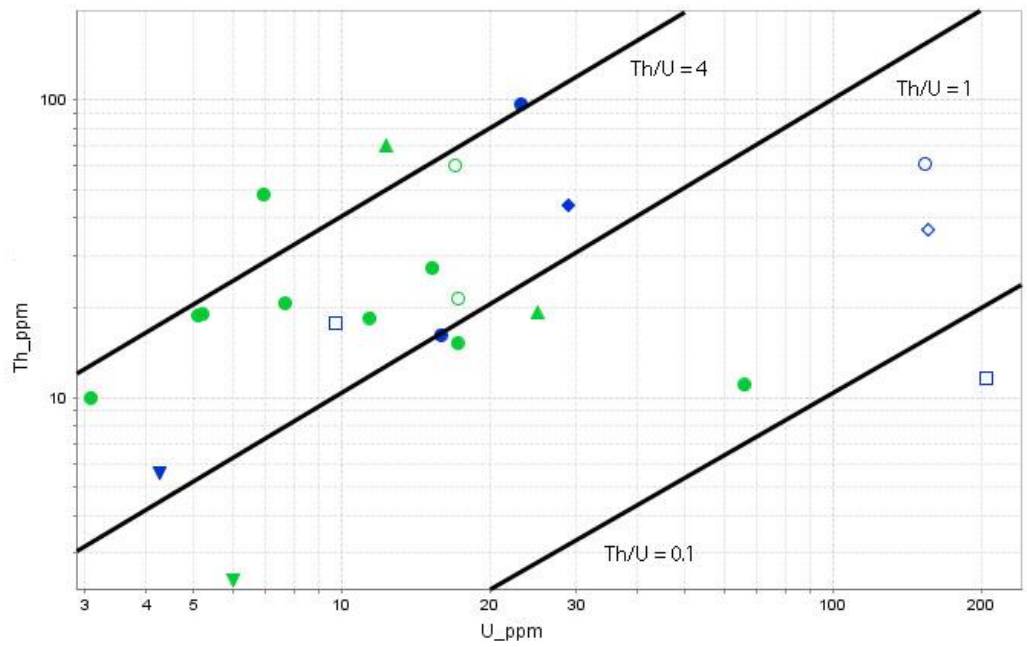

Figure 6-3. Bulk chemical Th vs U from the eastern Athabasca Basin. Sample legend found in Figure 4-1.

Accessory minerals in both the metasedimentary rocks and granitic pegmatites include zircon, monazite and uraninite (Annesley et al. 1995, 1996, 1998, 1999). As mentioned above uranium concentrations for the granitic pegmatites are the highest, monazites in the granitic pegmatites can have UO_2 concentrations >1.0wt% (Annesley and Madore, 2000) which is atypical for monazite. The crystallization of the high uranium monazite is considered to result from the generation of pegmatitic melts from a uranium-rich metasedimentary source, within the Wollaston-Mudjatik Transition Zone which is a high heat production zone. Higher UO_2 concentrations would provide lower than normal Th/U signifying a good potential uranium source.

Also noted in Table 4-2 was that the metasedimentary samples have higher concentrations for all other metals, excluding uranium, when compared to the pegmatites of this study. The presence of As, Co, Cu, Ni and Zn associated with some U/C-related uranium mineralization

requires polymetallic sources and a combination of a metasedimentary and granitic pegmatite source would provide these elements.

To determine whether the basement can provide enough uranium for forming the U/C-related uranium deposits Madore et al. (2000) calculated the potential uranium input from leucogranites and granitic pegmatites of the Wollaston Domain. The study determined that based on basin wide geochemical data a hypothetical basement shear zone 25km long, 1 km wide and 5 km deep could have an average bulk uranium concentration of 12.6 ppm U. For simplicity if this hypothetical shear zone had a bulk uranium concentration of 10 ppm and 25 % of this uranium was mobilized during fluid flow events there would be enough uranium to form the McArthur River uranium deposit. The hypothetical concentrations could be considered conservative compared to the rocks of this study, with metasedimentary and granitic pegmatite samples averaging 16 ppm and 75 ppm U respectively. Ineffective uranium mobilization at the concentrations observed could still provide enough uranium for many of the deposits in the Athabasca Basin. As well this estimation excludes the potential metal sources from metasedimentary rocks. The high concentrations of both uranium and other metals in large structural corridors inundated with high fluid flow could provide enough uranium to form many of the deposits on the eastern Athabasca Basin.

Even though the elemental concentrations are significantly higher than the sandstone extensive fluid migration through the comparatively impermeable basement would be needed. The largest permeability in the basement occurs within fault and shear zones but most likely further disruption of the basement lithologies would be required for the large volumes of fluid to leach uranium. Microfaulting in the basement (Mercadier et al., 2010) is a potential method of fluid infiltration, and very fine fractures are common and are reactivated over time and seal after

brines have passed through them (Boiron et al., 2010). Altered monazites have been observed 200m below the unconformity, and the majority of this altered monazite had no uranium left in the crystal structure (Hecht and Cuney, 2000). For successful infiltration low viscosity hydrothermal fluid would be advantageous for manoeuvring through this complicated set of fine fractures. The often fluoride-rich peraluminous basement lithologies are good source rock for low viscous melts. Furthermore it has been determined that the combination of F and Li with silicate melts generates a low viscosity fluid increasing the mobility of uranium (Cuney, 2014).

Unaltered and altered basement rocks have $^{207}Pb/^{206}Pb$ ratios (Table 4-3), extracted using the SRC partial leach technique, similar to the radiogenic 0.1 ratio observed in uranium deposits of the Athabasca Basin. There appears to be mixing in some of the unaltered samples (Fig. 4-7a), as the $^{207}Pb/^{206}Pb$ isotopic signature suggests common Pb and radiogenic Pb, which could be explained by the interaction of Pb rich fluids mobilized from uranium mineralization coming in contact with unaltered basement samples. The residual radiogenic $^{207}Pb/^{206}Pb$ signatures are either representative of resetting during fluid migration in the rocks, a fluid carrying uranium or late fluids that have interacted with a uranium deposit and then passed through the basement leaving the radiogenic $^{207}Pb/^{206}Pb$ isotopic signature.

6.3 HR-ICP-MS and MC-ICP-MS Analysis Discussion

If new analytical techniques are to be used for the exploration for U/C-type uranium deposits they must be rapid and cost effective processes. Data from Table 4-4 displays a significant range in both $\delta^{7}Li$ and $\delta^{11}B$, and thus there is the potential for using less precise bulk chemical analysis to extract information for exploration. It is well known that the MC-ICPMS method is rapid, and the precision for both lithium and boron isotopes compared to single collector instruments is

excellent but the disadvantage of this method is that it is considerably more expensive (Tomascak et al., 1999). MC-ICPMS provides greater precision due to the simultaneous detection of isotopes and differences in the ion beam, the shape of the ion beam and the ability of the MC-ICPMS to distribute energy more evenly leads to more stable flat-top isotope peaks. Kosler et al (2001) suggested that single collector Q-ICPMS can provide fast and effective isotopic measurement for lithium with acceptable δ^7Li values if proper sample preparation techniques are used. Single collector instruments, including both Q-ICPMS and HR-ICPMS, can provide greater sensitivity and therefore require less sample for analysis because of the use of electron multiplier detectors over faraday detectors commonly used by MC-ICPMS (Kosler et al., 2001). Difficulties for single collector instruments is accounting for isobaric interferences and plasma instability issues. The single collector HR-ICPMS is the perfect mix of both systems, as isotopes can be measured using either the electron multiplier detector or faraday detector. With HR-ICPMS the majority of isotopic measurements will be analyzed using the electron multiplier because of the greater sensitivity but the option of having a faraday for higher lithium concentrations or to compare measurements with MC-ICPMS is a significant advantage over Q-ICPMS. Plasma instability can be resolved by using fast switching mode between isotopes on the HR-ICPMS but this reduces precision. Compared to Q-ICPMS, HR-ICPMS has greater stability and focusing power, it can also produce the more precise flat-top peak also produced by MC-ICPMS. The higher resolving power of HR-ICPMS mitigates the influence of isobaric interferences (N^{2+}, C^{2+} and $^6LiH^+$) better then Q-ICPMS and most importantly, the precision for HR-ICPMS is better.

For comparison of all methods used for analysis in this project 2σ is plotted in Figure 6-4. The 2σ for HR-ICPMS is approximately an order of magnitude larger then MC-ICPMS. Figure

6-4 also highlights the importance of column separation for both boron and lithium isotopes. The matrix separated MC-ICPMS measurements for both lithium and boron have a 2σ well below 1‰ and thus provide very precise isotopic ratios. HR-ICPMS measurements of column separated solutions for boron isotopic analysis 2σ mean is 2.5‰ which is suitable for measuring geological differences for $\delta^{7}Li$ or $\delta^{11}B$ compared to the 2σ mean for samples not separated from the sample matrix which was approximately 5‰. The difference does not seem significant but the 2σ without separation is quite variable and can vary up to 25 ‰. Data obtained without separation did not provide confidence in the researchers that valuable geological information could be extracted. Lithium isotopic analysis should behave in a similar manner when analyzed by HR-ICPMS. Preliminary work on lithium isotopes on LSVEC at the SRC Mining and Minerals Division aspirated with a Nu Instruments DSN100 desolvating nebulizer provided 2σ variance of approximately 3 to 5‰ for LSVEC. This preliminary range in 2σ was approximately an order of magnitude greater then MC-ICPMS work performed at the University of Maryland. More work is needed to refine the method in regards to data acquisition time, replicates and developing chemical separation techniques for samples.

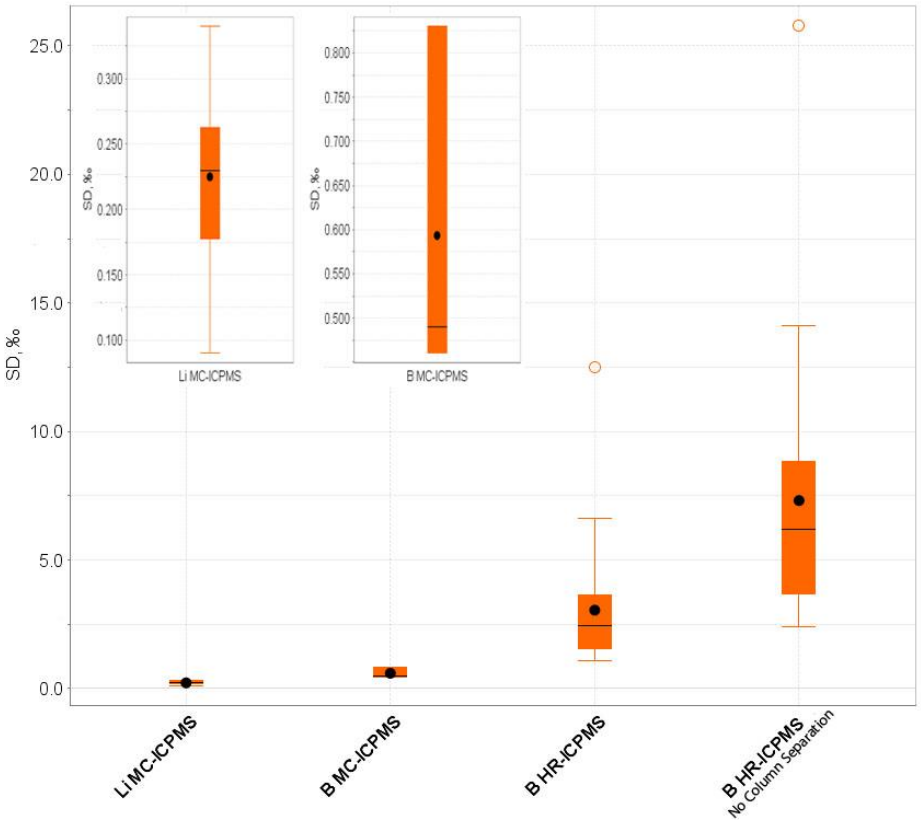

Figure 6-4. Plot of standard deviation (SD) for different analytical procedures used in this project.

As shown in figure 6-4 all B isotopic analysis are affected by matrix interferences and need column separation to purify the sample for analysis (Tomascak et al., 1999). The necessity for column separation using traditional chromatographic techniques would require a clean lab to perform these tasks. Traditional column separation processes are often time consuming and labour intensive, and so to potentially reduce costs but maintain the quality of data some form of automation would be required. When performing chemical separations all samples must be carefully prepared and eluted through the columns to ensure that all of the isotopes of interest are collected, and studies have shown that up to 60‰ mass fractionation can occur due to improper column separation of lithium (Choi, 2013). While reliable commercially available automated

systems for column separations are relatively new there are a few potential systems such as the ESI Prepfast or HPIC. All automated systems reduce the workload by loading the sample on the column, eluting the isotopes of interest, wash the column and condition the system for the next sample. This can reduce the time required for column separation from purifying a handful of samples over a few days to up to 50 samples in 24 hrs. The automation of the chemical purification requires less space as the equipment would require clean workspace but not necessarily a new clean lab. Combining the HR-ICPMS with automated matrix separation could provide the cost effective and rapid turn-around time needed by the uranium exploration industry to make boron and lithium a viable analysis tool.

CHAPTER 7
SUMMARY AND FUTURE WORK

7.1 Summary

The objectives of this study were to measure the baseline whole rock B and Li isotopic signatures of the basement rocks beneath the eastern Athabasca Basin to determine if there is any relationship to uranium mineralization, and to determine the feasibility of performing these measurements as a routine analysis by single collector HR-ICPMS.

The major source of boron in the basement rocks is tourmaline, whereas lithium can be derived from several minor and major minerals, including mica, quartz, feldspars and alteration minerals. Metamorphism can cause changes in the concentration of elemental lithium and boron but does not affect the δ^7Li and δ^{11}B signatures. During partial melting of sedimentary rocks during high-grade metamorphism there should be fractionation leading to the formation of magmas with heavier isotopic signatures. This relationship is seen in the metasedimentary and granitic pegmatites in this study, thus providing further support for a metasedimentary source for the granitic pegmatites intruding the basement both beneath and outside the Athabasca Basin.

Elevated Co, Cu, Ni and U concentrations determined in both the metasedimentary rocks and granitic pegmatites would be sufficient for producing the world class U/C-related uranium deposits in the Athabasca Basin. Partial leach $^{207}Pb/^{206}Pb$ ratios range from 0.7 to 0.1 which is the common lead $^{207}Pb/^{206}Pb$ ratio compared to the radiogenic $^{207}Pb/^{206}Pb$ ratio respectively. This range in Pb-Pb ratios suggests that there is a possible mixing of uranium-bearing fluids which are the same age as the U/C-related uranium deposits of the Athabasca Basin in both fresh and altered rocks. The residual radiogenic $^{207}Pb/^{206}Pb$ signatures are either representative of resetting in the residual material during fluid migration in the rocks or fluids carrying uranium passed through the basement leaving the radiogenic $^{207}Pb/^{206}Pb$ isotopic signature.

Investigating the accuracy, precision, and reproducibility of HR-ICPMS and MC-ICPMS in comparison with the natural ranges of δ^7Li and δ^{11}B suggest that both Li and B isotopic measurements could become routine analyses by single collector HR-ICPMS. To achieve this all solutions would need to be column separated from the sample matrix to ensure the low 2σ required to obtain applicable results.

7.2 Future Research

- Results display great potential for measurement of B and Li isotopes by HR-ICPMS, and the goal is to continue developing these isotopic methods at SRC. Method development would include research into column separation, which could be considered the most time consuming and labor intensive process for isotopic analysis. As well investigating the practical application of automation for purification of elements of interest. Automating this step in isotopic analysis could reduce error in sample processing by minimizing human interaction and reducing labor costs, thus providing a more cost effective analysis.

- To fully understand the baseline bulk chemical isotopic signatures further microscopic isotopic study would be needed. Recent developments in SIMS analysis can provide in-situ measurements of individual minerals for δ^7Li and δ^{11}B.

- This project is the first step towards developing a larger database for both δ^7Li and δ^{11}B in the Athabasca Basin, which will provide a further understanding of how these two isotopic systems behave in relation to uranium deposits. Measurement of both isotopic systems in the basement and overlying sandstone will provide more potential for unravelling the relationship between the rock units and implications for fluid flow.

- Further work to determine the B and Li isotopic systematics related to uranium deposits, might include investigating the fractionation during intense clay alteration or measurement of small-scale variability of $\delta^{7}Li$ and $\delta^{11}B$ in a specific location.

REFERENCES

Aggarwal, J., Bohm, F., Foster, G., Halas, S., Honisch, B., Jiang, S., Kosler, J., Liba, A., Rodushkin, I., Sheehan, T., Jiun-San Shen, J., Tonarini, S., Xie, Q., You, C., Zhao, Z., Zuleger, E., 2009. How well do non-traditional stable isotope results compare between different laboratories: results from the interlaboratory comparison of boron isotope measurements. Journal of Analytical Atomic Spectrometry 24 (6), 825-831.

Al-Ammar, A., Reitznerová, E., Barnes, R.M., 2000. Improving boron isotope ratio measurement precision with quadrupole inductively coupled plasma-mass spectrometry. Spectrochimica Acta Part B 55, 1861-1867.

Alexandre, P., Kyser, K., Jiricka, D., 2009. Critical Geochemical and Mineralogical factors for the formation of Unconformity-Related Uranium Deposits: Comparison between Barren and Mineralized Systems in the Athabasca Basin, Canada. Economic Geology 104, 413-435.

Alexandre, P., Kyser, K., Polito, P., Thomas, D., 2005. Alteration Mineralogy and Stable Isotope Geochemistry of Paleoproterozoic Basement-Hosted Unconformity-Type Uranium Deposits in the Athabasca Basin, Canada. Economic Geology 100 (8), 1547-1563.

ALS Life Sciences, Analytical Packages, Isotopes, 2014. Boron isotope ratios. 2014.

Annesley, I.R., Madore, C., Portella, P., 2005. Geology and thermotectonic evolution of the western margin of the Trans-Hudson Orogen: evidence from the eastern sub-Athabasca basement, Saskatchewan. Canadian Journal of Earth Science (42), 573-597.

Annesley, I.R., Madore, C., Portella, P., 2001. Paleoproterozoic structural, metamorphic, and magmatic evolution of the eastern sub-Athabasca basement: Controls on unconformity-type uranium deposits. A hydrothermal odyssey extended conference abstracts, Townsville, Australia, 17-19 May 2001 Edited by P.J. Williams. James Cook University EGRU Contribution 59, 3-4.

Annesley, I.R., Madore, C., Krogh, T.E., Kwok, Y.Y., Kamo, S.L., 1999. New U–Pb zircon and monazite geochronological results for Archean and Paleoproterozoic basement to the southeastern part of the Athabasca Basin, Saskatchewan. In Summary of Investigations 1999 2 (Sask. Geol. Surv., Regina, Saskatchewan), 90-99.

Annesley, I.R., 1999. Interpretive geology of Segment 4 sub-Athabasca basement using geophysics; In Wollaston EAGLE 2 Project: Geodynamic evolution of the Archean/Paleoproterozoic basement in Segment 4 (Annesley, I.R., Madore, C., and Shi, R.), Saskatchewan Research Council Publication No. 10395-1C99, 15 p. (Confidential).

Annesley, I.R., Madore, C., Shi, R., 1999. Regional geology and geodynamic evolution of Segment 4; In Wollaston EAGLE 2 Project: Geodynamic evolution of the Archean/Paleoproterozoic basement in Segment 4 (Annesley, I.R., Madore, C., and Shi, R), Saskatchewan Research Council Publication No. 10395-1C99, 85 p. plus appendices (Confidential).

Annesley, I.R., Reilkoff, B., Hajnal, Z., 1999. Magnetic and gravity modeling across Segment 3; Saskatchewan Research Council Publication No. 10398-1C99, 24 p. (Confidential).

Annesley, I.R. and Reilkoff, B., 1998. Interpretive geology of the sub-Athabasca basement using geophysics; In Geodynamic and Uranium Metallogenic Evolution of the Wollaston EAGLE 2 Project Area (Annesley, I.R., Madore, C., Shi, R., and Quirt, D.H.),

Saskatchewan Research Council Publication No. 10395-1C98, 18 p. plus appendices (Confidential).

Annesley, I.R., Reilkoff, B., and Hajnal, Z., 1998. Magnetic and Gravity Modeling of the Points North Road Transect; Saskatchewan Research Council Publication No. 10398-1C98, 25 p. plus profile (Confidential).

Annesley, I.R., Madore, C., Shi., R., Krogh, T.E., 1997. U-Pb geochronology of thermotectonic events in the Wollaston Lake area. Wollaston Domain: a summary of 1994-1996 results. Summary of Investigations 1997, Saskatchewan Geological Survey, Saskatchewan Energy and Mines, Miscellaneous Report. 97 (4), 162-173.

Annesley, I.R., Madore, C., and Shi, R., 1997. Thermotectonic evolution of the Wollaston EAGLE Project Area; In: Thermotectonic and Uranium Metallogenic Evolution of the Wollaston EAGLE Project Area (Annesley, I.R., Madore, C., Shi, R., Quirt, D.H.), Saskatchewan Research Council Publication No. R-1420-2-C-97, 62 p. plus appendices (Confidential).

Annesley, I.R. and Madore, C., 1996. Laboratory measurements of magnetic susceptibility and density from Archean/Early Proterozoic lithological units within the Wollaston EAGLE Project area; Saskatchewan Research Council, Publication No. R-1420-1-C.96, (in preparation)

Annesley, I.R., Madore, C., and Shi, R., 1996. Wollaston EAGLE Project, Revision Mapping/Integrated Geology (Segment 2); In: Wollaston EAGLE Project: Segment 2 Report (Annesley, I.R., Madore, C., Shi, R., Quirt, D.H., Dyck, J., Hajnal, Z., and Reilkoff, B.), Saskatchewan Research Council Publication No. R-1420-5-C-96, 184 p. (Confidential).

Annesley, I.R., Madore, C., and Shi, R., 1995. Wollaston EAGLE Project, Revision Mapping/Integrated Geology; In: Wollaston EAGLE Project: Segment 1 Report (Annesley, I.R., Madore, C., Quirt, D.H., Shi, R., and Dyck, J.), Saskatchewan Research Council Publication No. R-1230-16-C-95, 132 p.

Annesley, I.R., Madore, C., 1994. A geological study of the Wollaston–Mudjatik domain boundary in the Wollaston Lake area, Hearne Province, Saskatchewan. Sask. Res. Council, Publ. (R–1230–6–C–94).

Annesley, I.R., Madore, C., 1989. The Wollaston Group and its underlying Archean basement in Saskatchewan: 1989 fieldwork and preliminary observations. . Summary of Investigations 1989, Sask. Geol. Surv., Regina, Saskatchewan, 54-60.

Ashton, K.E., Hartlaub, R.P., Heaman, L.M., Morelli, R.M., Card, C.D., Bethune, K., Hunter, R.C., 2009. Post-Talston sedimentary and intrusive history of the southern Rae province, along the northern margin of the Athabasca Basin, Western Canadian Shield. Precambrian Research 175, 16-34.

Barker, F., and Arth, J.G., 1976, Generation of trondjemitic-tonalitic liquids and Archean bimodal trondhjemite-baslat suites; Geology, 4, 596-600.

Berger, G.,Schott, J.,Guy,C., 1988. Behavior of Li, Rb and Cs during basalt glass and olivine dissolution and chlorite, smectite and zeolite precipitation from seawater — experimental

investigations and modelization between 50 °C and 300 °C. Chemical Geology 71, 297–312.
Brisban, D., Cuney, M., 2010, SEG-PDAC 2010 Uranium Geology and Deposit Types Course, PDAC 2010, Toronto, Ont.
Bottomley, D.J., Chan, L.H., Katz, A., Starinsky, A., Clark, I.D., 2003. Lithium Isotope Geochemistry and Origin of Canadian Shield Brines. Ground Water (41), 847-856.
Brenan J. M., Ryerson F. J. and Shaw H. F., 1998. The role of aqueous fluids in the slab-to-mantle transfer of boron, beryllium, and lithium during subduction: experiments and models. Geochim. Cosmochim. Acta 62, 3337–3347.
Boiron, M.C., Cathelineau, M., and Richard, A., 2010. Fluid flows and metal deposition near basement⁄cover unconformity: lessons and analogies from Pb–Zn–F–Ba systems for the understanding of Proterozoic U deposits: Geofluids, v. 10, p. 270–292.
Bullen, T. D., Kendall, C., 1993. The natural variability of weathering input in a sandy silicate aquifer: Evidence from Sr isotopes in groundwaters and experimental extracts (abstract), Eos Trans. AGU, 74 (43), Fall Meeting suppl., 281.
Cameron, E.M., 1983. Uranium Exploration in Athabasca Basin, Saskatchewan, Canada. 82-11.
Campbell, J.E., 2007. Quaternary geology of the eastern Athabasca Basin, Saskatchewan; in EXTECHIV: Geology and Uranium EXploration TECHnology of the Proterozoic Athabasca Basin, Saskatchewan and Alberta, (ed.) C.W. Jefferson and G. Delaney; Geological Survey of Canada, Bulletin 588 , 211-228.
Card, C., Pana, D., Portella, P., Thomas, D., Annesley, I., 2007. Basement rocks the Athabasca Basin, Saskatchewan and Alberta; in EXTECHIV: Geology and Uranium EXploration TECHnology of the Proterozoic Athabasca Basin, Saskatchewan and Alberta, (ed.) C.W. Jefferson and G. Delaney; Geological Survey of Canada, Bulletin 588 , 69-89.
Card, C.D. (2012) A proposed domainal reclassification for Saskatchewan's Hearne and Rae provinces. *In* Summary of Investigations 2012, Saskatchewan Geological Survey, Saskatchewan Energy and Mines, Miscellaneous Report 4(2), p 9.
Card, C., Bethune, K., Davis, W., Rayner, N., Ashton, K., 2014. The case for a distinct Taltson orogeny: Evidence from northwest Saskatchewan, Canada. Precambrian Research, 255, 245-265.
Chacko, T., Cole, D.R., Horita, J., 2001. Equilibrium oxygen, hydrogen and carbon isotope fractionation factors applicable to geological systems. In: Valley, J.W. and Cole, D.R., (Eds.). Stable Isotope Geochemistry. Mineralogical Society of America, Washington, DC.
Chan, D., Jiricka, D., Mainville, A., 2000. Geology and uranium resources of the Dawn Lake deposit. .
Chan L. H. and Kastner M., 2000. Lithium isotopic compositions of pore fluids and sediments in the Costa Rica subduction zone: implications for fluid processes and sediment contribution to the arc volcanoes. Earth Planet. Sci. Lett. 183, 275–290.
Chan L. H., Gieskes J. M., You C. F. and Edmond J. M., 1994. Lithium isotope geochemistry of sediments and hydrothermal fluids of the Guayamas Basin, Gulf of California. Geochim. Cosmochim. Acta 58, 4443–4454.
Chan L. H., Alt J. C. and Teagle D. A. H., 2002. Lithium and lithium isotope profiles through the upper oceanic crust: a study of seawater–basalt exchange at ODP Sites 504B and 896A. Earth Planet. Sci. Lett. 201, 187–201.
Cloutier, J., Kyser, K., Olivo, G., Brisban, D., 2011. Geochemical, isotopic, and geochronlologic constraints on the formation of the Eagle Point basement-hosted uranium deposit,

Athabasca Basin, Saskatchewan, Canada and recent remobilization of primary uraninite in secondary structures. Mineralium Deposita 46 (1), 35-56.
Cloutier, J., Kyser, K., Olivo, G.R., Alexandre, P., 2010. Contrasting Patterns of Alteration at the Wheeler River Area, Athabasca Basin, Saskatchewan, Canada: Insights into the Apparently Uranium-Barren Zone K Alteration System. Economic Geology 105 (2), 303-324.
Cloutier, J., Kyser, K., Olivo, G.R., Alexandre, P., and Halaburda, J., 2009. The Millennium uranium deposit, Athabasca Basin, Saskatchewan, Canada: an atypical basement-hosted unconformity-related uranium deposit. Economic Geology, 104, 815–840.
Cuney, M., 2014. Felsic magmatism and uranium deposits. Bull. Soc. geol. France 185 (2), 75-92.
Cuney, M., Kyser, K. (Eds.), 2008. Recent and Not-so-Recent Developments in Uranium Deposits and Implications for Exploration. Mineralogical Association of Canada, Quebec City, QC.
Cuney, M., Brouand, M., Cathelineau, M., Derome, D., Freiberger, R., Hecht, L., Kister, P., Lobaev, V., Lorilleux, G., Peiffert, C., Bastoul, A.M., 2003. What parameters control the high grade-large tonnage of the Proterozoic unconformity related uranium deposit? In Uranium Geochemistry 2003, International Conference, April 13-16, 2003, Proceedings, (Cuney, M., ed.). Unité Mixte de Recherche CNRS 7566G2R, Université Henri Poincaré, Nancy, France, p. 123-126.
Derome, D., Cathelineau, M., Cuney, M., Fabre, C., Lhomme, T., 2005. Mixing of Sodic and Calci Brines and Uranium Deposition at McArthur River, Saskatchewan, Canada: A Raman and Laser-Induced Breakdown Spectrocopic Study of Fluid Inclusions. Economic Geology 100, 1529-1545.
Derome, D., Cathelineau, M., Fabre, C., Boiron, M., Banks, D., Lhomme, T., Cuney, M., 2007. Paleo-fluid composition determined from individual fluid inclusions by Raman and LIBS: Application to mid-Proterozoic evaporitic Na-Ca brines (Alligator Rivers Uranium Field, northern territories Australia). Chemical Geology 237, 240-254.
Eglington, B., 2014. Isotopes and Fluid-Rock Interaction., Unpublished educational word document.
Duttrow, B.L., Holdaway, M.J., Hinton, R.W., 1986. Lithium in staurolite and its petrologic significance. Contributions to Mineralogy and Petrology 94, 496-506.
Fayek, M., Kyser, T.K., 1997. Characterization of multiple fluid-flow events and rare-earth-element mobility associated with formation of unconformity-type uranium deposits in the Athabasca Basin, Saskatchewan. The Canadian Mineralogist 35 (3), 627-658.
Flesch, G.D., Anderson Jr., A.R., Svec, H.J., 1973. A secondary isotopic standard for 6Li/7Li determinations. International Journal of Mass Spectrometry and Ion Physics 12 (3), 265-272.
Fontes, J.C., Matray, J.M., 1993. Geochemistry and origin of formation brines from the Paris Basin, France 1. Brines associated with Triassic salts. Chemical Geology, 109, 149-175
Galbraith, C.G., Clarke, D.B., Trumbull, R.B., Wiedenbeck, M., 2009. Assessment of Tourmaline Compositions as an Indicator of Emerald Mineralization at the Tsa da Glisza Prospect, Yukon Territory, Canada. Economic Geology 104, 713-731.
Gangjian, W., Jingxian, W., Ying, L., Ting, K., Zhongyuan, R., Jinlong, M., Yigang, X., 2013. Measurement of high-precision boron isotope of silicate materials by a single column purification method and MC-ICP-MS. J. Anal. At. Spectrom. 28, 606-612.

Garda, G.M., Trumbull, R.B., Beljavskis, P., Wiedenbeck, M., 2009. Boron isotope composition of tourmalinite and vein tourmalines associated with gold mineralization, Serra do Itaberaba Group, central Ribeira Belt, SE Brazil. Chemical Geology 264 (1–4), 207-220.

Gonfiantini, R., Tonarini, S., Gröning, M., Adorni-Braccesi, A., Al-Ammar, A.S., Astner, M., Bächler, S., Barnes, R.M., Bassett, R.L., Cocherie, A., Deyhle, A., Dini, A., Ferrara, G., Gaillardet, J., Grimm, J., Guerrot, C., Krähenbühl, U., Layne, G., Lemarchand, D., Meixner, A., Northington, D.J., Pennisi, M., Reitznerová, E., Rodushkin, I., Sugiura, N., Surberg, R., Tonn, S., Wiedenbeck, M., Wunderli, S., Xiao, Y., Zack, T., 2003. Intercomparison of Boron Isotope and Concentration Measurements. Part II: Evaluation of Results Geostandards and Geoanalytical Research 27 (1), 41-57.

Hajnal, Z., White, D.J., Takacs, E., Gyorfi, I., Annesley, I.R., Wood, G., O'Dowd, C., Nimeck, G., 2010. Application of modern 2-D and 3-D seismic reflection techniques for uranium exploration in the Athabasca Basin. Canadian Journal of Earth Science 47, 761-782.

Hecht, L., Cuney, M., 2000. Hydrothermal alteration of monazite in the Precambrian crystalline basement of the Athabasca Basin (Saskatchewan, Canada): implications for the formation of unconformity-related uranium deposits. Mineralium Deposita 35, 791-795.

Henry, D.J., Dutrow, B.L., 1996. Boron: Mineralogy, Petrology, and Geochemistry- Chapter 10 Metamorphic Tourmaline and Its Petrologic Applications. Reviews in Mineralogy 33, 503-558.

Hoeve, J., Quirt, D., 1984. Mineralization and host rock alteration in relation to clay mineral diagenesis and evolution of the middle Proterozoic Athabasca basin, northern Saskatchewan, Canada. Saskatchewan Research Council Technical Report 187, 187 p.

Hoeve, J., Sibbald, T.I., 1978. On the genesis of Rabbit Lake and other unconformity-type uranium deposits in northern Saskatchewan, Canada. Economic Geology 73, 1450-1473.

Hoffman, P.F., 1990. Subdivision of the Churchill Province and extent of the Trans-Hudson orogeny. In The Early Proterozoic Trans-Hudson Orogen of North America (Lewry, J.F. & Stauffer, M.R., eds.). Geological Association of Canada Special Paper 37, 15-39.

Hoffman, P.F., 1988. United plates of America, the birth of a craton: Early Proterozoic assembly and growth of Laurentia. Annual Review of Earth and Planetary Sciences 16, 543-603.

Holk, G.J., Kyser, T.K., Chipley, D., Hiatt, E.E., Marlatt, J., 2003. Mobile Pb-isotopes in Proterozoic sedimentary basins as guides for exploration of uranium deposits. Journal of Geochemical Exploration 80 (2–3), 297-320.

Hore, S., Hill, S., 2011, Palaeo-redox Fronts Exposed within a Key Section at Four Mile West, South Australia, IAGS 2011 Abstract Volume, Roveniemi, Finland.

Jefferson, C.W., Thomas, D.J., Gandhi, S.S., Ramaekers, P., Delaney, G., Brisban, D., Cutts, C., Portella, P., Olson, R.A., 2007. Unconformity-associated uranium deposits of the Athabasca Basin, Saskatchewan and Alberta; in EXTECH IV: Geology and Uranium EXploration TECHnology of the Proterozoic Athabasca Basin, Saskatchewan and Alberta, (ed.) C.W. Jefferson and G. Delaney; Geological Survey of Canada, Bulletin 588, 23-69.

Jiang, S.-Y., Henry, D. J., de Brodtkorb, M. K., Ametrano, S., 1999. Chemistry and boron isotopes of tourmalinites from the Sierras Pampeanas, Argentina. Mineral Deposits: Process to Processing, 539-542.

Jiang, S., Palmer, M.R., 1998. Boron isotope systematics of tourmaline from granites and pegmatites; a synthesis. European Journal of Mineralogy 19 (6), 1253-1265.

Johnson, T.M., DePaolo, D.J., 1994. Interpretation of isotopic data in groundwater systems: Model development and application to Sr isotope data from Yucca Mountain. Water Resources Research, 30, 1571-1587.
Johnson, T.M., DePaolo, D.J., 1996. Reaction-transport models for radiocarbon in groundwater: The effects of longitudinal dispersion and the use of Sr isotope ratios to correct for water-rock interaction. Water Resources Research, 32, 2203-2212.
Johnson, T.M., DePaolo, D.J., 1997a, Rapid exchange effects on isotope ratios in groundwater systems 1. Development of a transport dissolution-exchange model. Water Resources Research, 33, 187-195.
Johnson, T.M., DePaolo, D.J., 1997b, Rapid exchange effects on isotope ratios in groundwater systems 2. Flow investigation using Sr isotope ratios. Water Resources Research, 33, 197-209.
Kawakami, T., 2001. Boron depletion controlled by the breakdown of tourmaline in the migmatite zone of the Aoyama area, Ryoke Metamophic Belt, Southwestern Japan. The Canadian Mineralogist 39 (6), 1529-1546.
King, R.L., Bebout, G.E., Grove, M., Moriguti, T., Nakamura, E., 2007. Boron and lead isotope signatures of subduction-zone melange formation: Hybridization and fractionation along the slab-mantle interface beneath volcanic arcs. Chemical Geology 239, 305-322.
Kosler, J., Kucera, M., Sylvester, P., 2001. Precise measurement of Li isotopes in planktonic foraminiferal tests by quadrupole ICPMS. Chemical Geology 181, 161-179.
Kotzer, T.G., Kyser, T.K., Irving, E., 1992. Paleomagnetism and the evolution of fluids in the Proterozoic Athabasca Basin, Northern Saskatchewan. Canadian Journal of Earth Science 29, 1474-1491.
Kotzer, T.G., & Kyser, T.K., 1995. Petrogenesis of the Proterozoic Athabasca Basin, northern Saskatchewan, Canada, and its relation to diagenesis, hydrothermal uranium mineralization and paleohydrogeology. Chemical Geology 120, 45-89.
Kyser, K., Geagea, M., Chipley, D., Alexandre, P., Raycroft, P., Vuletich, A., Schwartz-Narbonne, R., 2009. Tracing progressive redox gradients and directions of hydrothermal flow using uranium and lithium isotopes. , 255-258.
Liesbscher, A., Meixner, A., Romer, R.L., Heinrich, W., 2007. Experimental calibration of the vapour-liquid phase relations and lithium isotope fractionation in the system H2O-LiCl at 400^{o}C/20-28 MPa. Geofluids 7, 369-375.
Liu, X., 2009. Advection-diffusion controlled lithium isotopic distribution in contact aureoles: A case study from the Florence county pegmatites, Wisconsin. MSc. Thesis, University of Maryland, 87 p.
Liu, X., Rudnick, R.L., 2011. Constraints on continental crustal mass loss via chemical weathering using lithium and its isotopes. Earth, Atmospheric, and Planetary Sciences 108 (52), 20873-20880.
Liu, X., Rudnick, R.L., McDonough, W.F., Cummings, M.L., 2013. Influence of chemical weathering on the composition of the continental crust: Insights from Li and Nd isotopes in bauxite profiles developed on Columbia River Basalts. Geochimica et Cosmochimica Acta 115 (0), 73-91.
Liu, X., Rudnick, R.L., Hier-Majumder, S., Sirbescu, M.C., 2010. Process controlling lithium isotopic distribution in contact aureoles: A case study of the Florence County pegmatites, Wisconsin. Geochemistry Geophysics Geosystems 11 (8).

Macdonald, C., 1980. Mineralogy and geochemistry of a Precambrian regolith in the Athabasca Basin. M.Sc. Thesis: University of Saskatchewan. , 1-151.

Madore, C., Annesley, I.R., Wheatley, K., 2000. Petrogenesis, age, and uranium fertility of peraluminous leucogranites and pegmatites of the McClean Lake/Sue and Key Lake deposit area. Geological Association of Canada-Mineralogical Association of Canada, Program Abstract 25, 1041 (CD-ROM).

Madore, C. and Annesley, I.R., 1996. Wollaston EAGLE Project, Basal Wollaston Group: Facies (Segment 2); In: Wollaston EAGLE Project: Segment 2 Report (Annesley, I.R., Madore, C., Shi, R., Quirt, D.H., Dyck, J., Hajnal, Z., and Reilkoff, B.), Saskatchewan Research Council Publication No. R-1420-5-C-96, 122 p. (Confidential).

Madore, C. and Annesley, I.R., 1995. Wollaston EAGLE Project, Basal Wollaston Group: Facies; In: Wollaston EAGLE Project: Segment 1 Report (Annesley, I.R., Madore, C., Quirt, D.H., Shi, R., and Dyck, J), Saskatchewan Research Council Publication No. R-1230-30-C-95, 69 p.

Magna, T., Wiechert, U.H., Halliday, A.N., 2004. Low-blank isotope ratio measurement of small samples of lithium using multiple-collector ICPMS. International Journal of Mass Spectrometry 239 (1), 67-76.

Maloney, J.S., 2007. Lithium and lithium isotopes in tourmaline as indicators of crystallization processes: A study of San Diego County pegmatites, California. MSc. Thesis, University of Missouri-Columbia, 60 p.

Maloney, J.S., Nabelek, P.I., Sirbescu, M.C., 2008. Lithium and its isotopes in tourmaline as indicators of the crystallization process in the San Diego County pegmatites, California, USA. European Journal of Mineralogy 20 (5), 905-916.

Marks, M.A.W., Rudnick, R.L., McCammon, C., Vennemann, T., Markl, G., 2007. Arrested kinetic Li isotope fractionation at the margin of the Ilímaussaq complex, South Greenland: Evidence for open-system processes during final cooling of peralkaline igneous rocks. Chemical Geology 246 (3-4), 207-230.

Marschall, H.R., Jiang, S., 2011. Tourmaline Isotopes: No Element Left Behind. Elements 7 (5), 313-319.

Marschall, H.R., Pogge von Strandmann, P.A.E., Seitz, H., Elliott, T., Niu, Y., 2007. The lithium isotopic composition of orogenic eclogites and deep subducted slabs. Earth and Planetary Science Letters 262 (3–4), 563-580.

Marschall, H.R., Altherr, R., Ludwig, T., Kalt, A., Gméling, K., Kasztovszky, Z., 2006. Partitioning and budget of Li, Be and B in high-pressure metamorphic rocks. Geochimica et Cosmochimica Acta 70 (18), 4750-4769.

McGill, B.D., Marlatt, J.L., Matthews, R.B., Sopuck, V.J., Homeniuk, L.A., Hubregtse, J.J., 1993. The P2 North uranium deposit, Saskatchewan, Canada. Exploration Mining Geology 2, 321-331.

McKechnie, C.L., Annesley, I.R., Ansdell, K.M., 2012. Geological Setting, Petrology, and Geochemistry of Granitic Pegmatites and Leucogranites Hosting U-Th-REE Mineralization at Fraser Lakes Zone B, Wollaston Domain, Northern Saskatchewan, Canada. Exploration and Mining Geology 21, 1-26.

McKechnie, C.L., Annesley, I.R., Ansdell, K.M., 2012a. Radioactive abyssal granitic pegmatites and leucogranites in the Wollaston Domain, Northern Saskatchewan Canada: mineral

compositions and conditions of emplacement in the Fraser Lakes area. Canadian Mineralogist, 50, 1637-1667.
McKechnie, C.L., Annesley, I.R., Ansdell, K.M., 2012b. Medium- to low pressure pelitic gneisses of Fraser Lakes Zone B, Wollaston Domain, Northern Saskatchewan Canada: mineral compositions, metamorphic P-T-t path, and implications for the genesis of radioactive abyssal granitic pegmatites. Canadian Mineralogist, 50, 1669-1694.
Mercadier, J., Annesley, I.R., McKechnie, C.L., Bogdan, T.S., Creighton, S., 2013. Magmatic and Metamorphic Uraninite Mineralization in the Western Margin of the Trans-Hudson Orogen (Saskatchewan, Canada): A Uranium Source for Unconformity-Related Uranium Deposits? Economic Geology 108 (5), 1037-1065.
Mercadier, J., Richard, A., Boiron, M.-C., Cathelineau, M., & Cuney, M., 2010. Migration of brines in the basement rocks of the Athabasca Basin through microfracture networks (P-Patch U deposit, Canada). Lithos 115, 121–136.
Mercadier, J., Richard, A., Cathelineau, M., 2012. Boron- and magnesium-rich marine brines at the origin of giant unconformity-related uranium deposits: δ11B evidence from Mg-tourmalines. Geology 40 (3), 231-234.
Millot, R., Vigier, N., Gaillardet, J., 2010. Behaviour of lithium and its isotopes during weathering in the Mackenzie Basin, Canada. Geochimica et Cosmochimica Acta 74 (14), 3897-3912.
Moriguti, T., Nakamura, E., 1998. High-yield lithium separation and the precise isotopic analysis for natural rock and aqueous samples. Chemical Geology 145 (1–2), 91-104.
Nakamura, E., Ishikawa, T., Birck, J., Allègre, C.J., 1992. Precise boron isotopic analysis of natural rock samples using a boron-mannitol complex. Chemical Geology 94 (3), 193-204.
Olive, K.A., Schramm, D.N., 1992. Astrophysical Li-7 as a Product of Big-Bang Nucleosyntheis and Galactic Cosmic-Ray Spallation. Nature 360 (6403), 439-442.
Pagel, M., 1975. Determination des conditions physico-chimiques de la silicification diagenetique des gres Athabasca (Canada) au moyen des inclusions fluids. Comptes Rendus Academie Sciences Paris 280. , 2301-2304.
Pal, D.C., Trumbull, R.B., Wiedenbeck, M., 2010. Chemical and boron isotope compositions of tourmaline from the Jaduguda U (–Cu–Fe) deposit, Singhbhum shear zone, India: Implications for the sources and evolution of mineralizing fluids. Chemical Geology 277 (3-4), 245-260.
Palmer, M.R., London, D., Morgan VI, G.B., Babb, H.A., 1992. Experimental determination of fractination of 11B/10B between tourmaline and aqueous vapor: A temperature- and pressure- dependent isotopic system. Chemical Geology: Isotope Geoscience section 101 (1-2), 123-129.
Parslow, G.R., Thomas, D.J., 1982. Uranium occurrences in the Cree Lake Zone. Mineralogical Magazine 46, 163-171.
Pascal, M., 2014. Graphite-Bearing and Graphite-Depleted Basement Rocks in the Dufferin Lake Zone, South-Central Athabasca Basin, Saskatchewan.
Portella, P., Annesley, I.R., 2000. Paleoproterozoic thermotectonic evolution of the eastern sub-Athabasca basement, northern Saskatchewan: Integrated geophysical and geological data. Summary of Investigations 2000, Saskatchewan Geological Survey, Saskatchewan Energy and Mines, Miscellaneous report 2000-4-2 2, 191-200.
Qi, H.P., Taylor, P.D.P., Berglund, M., De Bièvre, P., 1997. Calibrated measurements of the isotopic composition and atomic weight of the natural Li isotopic reference material

IRMM-016. International Journal of Mass Spectrometry and Ion Processes 171 (1–3), 263-268.
Qiu, L., Rudnick, R.L., Ague, J.J., McDonough, W.F., 2011. A lithium isotopic study of sub-greenschist to greenschist facies metamorphism in an accretionary prism, New Zealand. Earth and Planetary Science Letters 301 (1–2), 213-221.
Qiu, L., Rudnick, R.L., McDonough, W.F., Merriman, R.J., 2009. Li and δ7Li in mudrocks from the British Caledonides: Metamorphism and source influences. Geochimica et Cosmochimica Acta 73 (24), 7325-7340.
Quirt, D., 1997. Metallogenetic Model; in Annesley, I.R., Madore, C., Shi, R., and Quirt, D. (eds.), Thermotectonic and Uranium Metallogenetic Evolution of the Wollaston EAGLE Project Area. R-1420-5-C-96.
Ramaekers, P., 1990. Geology of the Athabasca Group (Helikian) in northern Saskatchewan; Saskatchewan Geological Survey, Saskatchewan Energy and Mines, Report 195. , 1-57.
Ramaekers, P., Jefferson, C.W., YEO, G.M., Collier, B., Long, D.G.F., Drever, G., McHardy, S., Jiricka, D., Cutts, C., Wheatly, K., Catuneanu, S., Bernier, S., Kupsch, B., Post, R.T., 2007. Revised geological map and stratigraphy of the Athabasca Group, Saskatchewan and Alberta; in EXTECH IV: Geology and Uranium EXploration TECHnology of the Proterozoic Athabasca Basin, Saskatchewan and Alberta, (ed.) C.W. Jefferson and G. Delaney; Geological Survey of Canada, Bulletin 588 , 155-193.
Reid, K.D., Ansdell, K., Jiricka, D., Witt, G., Card, C., 2014. Regional Setting, Geology, and Paragenesis of the Centennial Unconformity-Related Uranium Deposit, Athabasca Basin, Saskatchewan, Canada. Economic Geology 109 (3), 539-566.
Richard, A., Rozsypal, C., Mercadier, J., Banks, D.A., Cuney, M., Boiron, M.-., Cathelineau, M., 2012. Giant uranium deposits formed from exceptionally uranium-rich acidic brines. Nature Geoscience 5 (2), 142-146.
Richard, A., Pettke, T., Cathelineau, M., Boiron, M., Mercadier, J., Cuney, M., Derome, D., 2010. Brine-rock interaction in the Athabasca basement (McArthur River U deposit, Canada): consequences for fluid chemistry and uranium uptake. Terra Nova 22 (4), 303-308.
Richard, A., 2009. Brine migration at the basement/sedimentary cover unconformity and formation of Proterozoic uranium mineralizations (Athabasca Basin, Canada). Unpublished Ph. D. thesis, Institut National Polytechnique de Lorraine, Nancy, France, 239 p.
Richard, A., Banks, D.A., Mercadier, J., Boiron, M., Cuney, M., Cathelineau, M., 2011. An evaporated seawater origin for the ore-forming brines in unconformity-related uranium deposits (Athabasca Basin, Canada): Cl/Br and δ37Cl analysis of fluid inclusions. Geochimica et Cosmochimica Acta 75 (10), 2792-2810.
Romer, R. L., Meixner, A. and Hahne, K., 2014 a. Lithium and boron isotopic composition of sedimentary rocks – The role of source history and depositional environment: a 250 Ma record from the Cadomian orogeny to the Variscan orogeny. Gondwana Res., 26, 1093-1110.
Romer, R. L., Meixner, A. and Hahne, K., 2014 b. Lithium and boron isotopic fractionation in sedimentary rocks during metamorphism – The role of rock composition and protolith mineralogy. Geochimica et Cosmochimica Acta 128, 158–177.
Rudnick, R.L., Tomascak, P.B., Njo, H.B., Gardner, L.R., 2004. Extreme lithium isotopic fractionation during continental weathering revealed in saprolites from South Carolina. Chemical Geology 212 (1–2), 45-57.

Seydoux-Guillaume, A., Paquette, J., Wiedenbeck, M., Montel, J., Heinrich, W., 2002. Experimental resetting of the U-Th-Pb systems in monazite. Chemical Geology 191, 165-181.

Seyfried, W.E., Chen, X., Chan, L.H., 1998. Trace element mobility and lithium isotope exchange during hydrothermal alteration of seafloor weathered basalt: An experimental study at 350 degrees C, 500 bars. Geochim. Cosmochim. Acta 62, 949-960.

Shabaga, B.M., Fayek, M., Hawthorne, F.C., 2010. Boron and lithium isotopic compositions as provenence indicators of Cu-bearing tourmalines. Mineralogical Magazine 74 (2), 241-255.

Stepanov, A.S., Hermann, J., Rubatto, D., Rapp, R.P., 2012. Experimental study of monazite /melt partitioning with implications for the REE, Th and U geochemistry of crustal rocks. Chemical Geology 300-301, 200-220.

Teng, F., 2005. Lithium isotopic systematics of the continental crust. Ph.D. thesis, University of Maryland, 199p.

Teng, F., McDonough, W.F., Rudnick, R.L., Walker, R.J., Sirbescu, M.C., 2006. Lithium isotopic systematics of granites and pegmatites from the Black Hills, South Dakota. American Mineralogist 91 (10), 1488-1498.

Teng, F.Z., McDonough, W.F., Rudnick, R.L., Dalpé, C., Tomascak, P.B., Chappell, B.W., Gao, S., 2004. Lithium isotopic composition and concentration of the upper continental crust. Geochimica et Cosmochimica Acta 68 (20), 4167-4178.

Teng, F., McDonough, W.F., Rudnick, R.L., Wing, B.A., 2007. Limited lithium isotopic fractionation during progressive metamorphic dehydration in metapelites: A case study from the Onawa contact aureole, Maine. Chemical Geology 239 (1–2), 1-12.

Thomas, D., Matthews, R.B., Sopuck, V., 2000. Athabasca Basin (Canada) unconformity-type uranium deposits: exploration model, current mine developments and exploration directions. In. Geology and Ore Deposits 2000: The Great Basin and Beyond. Geological Society of Nevada Symposium, Reno, Nevada, May 15-18, 2000, Proceedings, 1, 103-126.

Tirez, K., Brusten, W., Widory, D., Petelet, E., Bregnot, A., Xue, D., Boeckx, P., Bronders, J., 2010. Boron isotope ratio ($\delta^{11}B$) measurements in Water Framework Directive monitoring programs: comparison between double focusing sector field ICP and thermal ionization mass spectrometry. Journal of Analytical Atomic Spectrometry 25, 964-974.

Tomascak, P.B., Brown, M., Solar, G.S., Becker, H.J., Centorbi, T.L., Tian, J., 2005. Source contributions to Devonian granite magmatism near the Laurentian border, New Hampshire and Western Maine, USA. Lithos 80, 75-99.

Tomascak, P.B., 2004. Developments in the Understanding and Application of Lithium Isotopes in the Earth and Planetary Sciences. Reviews in Mineralogy and Geochemistry 55 (1), 153-195.

Tomascak, P.B., Carson, R. W., Shirey, S.B., 1999. Accurate and precise determination of Li isotopic compositions by multi-collector sector ICP-MS. Chemical Geology, 158, 145-154.

Tornos, F., Wiedenbeck, M., Velasco, F., 2012. The boron isotope geochemistry of tourmaline-rich alteration in the IOCG systems of northern Chile: implications for a magmatic-hydrothermal origin. Mineralium Deposita 47 (5), 483-499.

Trumbull, R.B., Slack, J.F., Krienitz, M., Belkin, H.E., Wiedenbeck, M., 2011. Fluid sources and metallogenesis in the Blackbird Co–Cu–Au–Bi–Y–REE district, Idaho, U.S.A.: insights from major-element and boron isotopic compositions of tourmaline. The Canadian Mineralogist 49 (1), 225-244.

Trumbull, R. B., Krienitz, M.-S., Grundmann, G., Wiedenbeck, M., 2009. Tourmaline geochemistry and δ11B variations as a guide to fluid-rock interaction in the Habachtal emerald deposit, Tauern Window, Austria. - Contributions to Mineralogy and Petrology, 157, 3, 411-427

van Hinsberg, V.J., 2011. Preliminary experimental data on trace-element partitioning between tourmaline and silicate melt. The Canadian Mineralogist 49 (1), 153-163.

van Hinsberg, V.J., Henry, D.J., Dutrow, B.L., 2011. Tourmaline as a Petrologic Forensic Mineral: A Unique Recorder of Its Geologic Past. Elements 7 (5), 327-332.

van Hinsberg, V.J., Henry, D.J., Marschall, H.R., 2011. Tourmaline: an ideal indicator of its host environment. The Canadian Mineralogist 49 (1), 1-16.

Veizer, J., 1989, Strontium isotopes in seawater through time. Annual Review Earth Planetary Science, 17, 141-167.

Vogl, J., Rosner, M., Pritzkow, W., 2011. Development and validation of a single collector SF-ICPMS procedure for the determination of boron isotope ratios in water and food samples. J. Anal. At. Spectrom 26, 861-869.

Wagani, I., Wagani, I., Janots, É., Gnos, E., 2011. Detrital monazite in the Tim Mersoi Basin, Niger: provenance and contribution to the uranium budget in siliciclastic sediments. The Canadian Mineralogist 49 (2), 487-501.

Wallis, R.H., Saracoglu, N., Brummer, J.J., Golightly, J.P., 1983. Geology of the McClean Uranium Deposits; In Uranium Exploration in Athabasca Basin, Saskatchewan, Canada, ed. E.M. Cameron. Geological Survey of Canada 82 (11), 71-110.

Webster, J.D., Holloway, J.R., Hervig, R.L., 1989. Partitioning of Lithophile trace elements between H2O and H2O+CO2 fluids and topaz rhyolite melt. Economic Geology 84, 116-134.

Wilke, M., Nabelek, P.I., Glascock, M.D., 2002. B and Li in Proterozoic metapelites from the Black Hills, U.S.A.: Implications for the origin of leucogranitic magmas. American Mineralogist 87 (4), 491-500.

Wilson, M.R., Kyser, T.K., 1987. Stable isotope geochemistry of alteration associated with the Key Lake uranium deposit, Canada. Economic Geology 82 (6), 1540-1557.

Williams, L.B., Hervig, R.L., 2005. Lithiumand boron isotopes in illite-smectite: the importance of crystal size. Geochimica et Cosmochimica Acta 69, 5705–5716.

Wunder, B., Meixner, A., Romer, R.L., Feenstra, A., Schettler, G., Heinrich, W., 2007. Lithium isotope fractionation between Li-bearing staurolite, Li-mica and aqueous fluids: An experimental study. Chemical Geology 238 (3–4), 277-290.

Xavier, R.P., Wiedenbeck, M., Trumbull, R.B., Dreher, A.M., Monteiro, L.V.S., Rhede, D., de Araújo, C.E.G., Torresi, I., 2008. Tourmaline B-isotopes fingerprint marine evaporites as the source of high-salinity ore fluids in iron oxide copper-gold deposits, Carajás Mineral Province (Brazil). Geology of Ore Deposits 36 (9), 743-746.

Yeo, G.M., Delaney, G., 2007. The Wollaston Supergroup, stratigraphy and metallogeny of a Paleoproterozoic Wilson cycle in the Trans-Hudson orogen, Saskatchewan. In EXTECH IV: Geology and Uranium Exploration TECHnology of the Proterozoic Athabasca Basin, Saskatchewan and Alberta (C.W. Jefferson & G. Delaney, eds.). Geol. Surv. Can., Bull. (588), 89-117.

You, C.F., Chan, L.H., Spivack, A.J., Gieskes, J.M., 1995. Lithium, boron, and their isotopes in sediments and pore waters of Ocean Drilling Program Site 808, Nankai Trough: implications for fluid expulsion in accretionary prisms. Geology 23, 37–40.

http://www.economy.gov.sk.ca/adx/aspx/adxGetMedia.aspx?DocID=11716,11397,11228,3385,5460,2936,Documents&MediaID=ae4c1616-faf5-43f6-9a07-16232e00af50&Filename=Model+A-1_Athabasca+Basin+Unconformity-associated+Uranium.pdf

APPENDIX A
GEOCHEMICAL DATA

Sample Number	Deposit Area	Depth	Rock Type	Comments	HR-ICPMS		Duplicate		Duplicate		MC-ICPMS	
		m			$\delta^{11}B$ ‰	*SD* ‰	$\delta^{11}B$ ‰	*SD* ‰	$\delta^{11}B$ ‰	*SD* ‰	$\delta^{11}B$ ‰	*SD* ‰
A94-040D	Eagle Point	Outcrop	Pegmatite	Magnetite bearing Pegmatite	4.3	17.9	-2.3	12.5				
I57 114.5	McClean Lake	114.5	Pegmatite	Paleoweathered	16.1	6.6						
Q6-66 131.2	Dawn Lake	131.2	Pelitic Gneiss	Corderite; Paleoweatherd	-0.51	1.93						
Q6-66 149.7	Dawn Lake	149.7	Graphitic Pelitic Gneiss	Bleached; Sulphides	0.27	1.58						
Q6-66 164.2	Dawn Lake	164.2	Pegmatite	Altered Radioactive	-5.32	1.99						
Q6-66 170.9	Dawn Lake	170.9	Graphitic Pelitic Gneiss	Bleached	0.78	1.1						
Q6 67 104.4	Dawn Lake	104.4	Pelitic Gneiss	Migmatitic; Paleoweatherd	-5.6	3.5	-4.9	2.6				
Q6-72 108.7	Dawn Lake	108.7	Pelitic Gneiss	Paleoweathered	1.32	1.5					2.01	0.46
Q6-72 114.5	Dawn Lake	114.5	Pegmatite	Tourmaline	-2.39	1.88			2.1	3.4	-0.87	0.83
Q6-72 117.2	Dawn Lake	117.2	Graphitic Pelitic Gneiss	Sulphides	2.35	2.74			2.23	2.11	3.43	0.49
Q7-16 266.8	Dawn Lake	266.8	Pegmatite	Tourmaline	1.6	1.28						
Q9-16 183.6	Dawn Lake	183.6	Pelitic Gneiss	Garnet-Corderite; Paleoweathered	1.4	1.16						
Q9-16 191.3	Dawn Lake	191.3	Pelitic Gneiss	Paleoweathered; Corderite	3.54	1.44						
Q9-16 199.6	Dawn Lake	199.6	Graphitic Pelitic Gneiss	Sulphides; Corderite	2.8	2.54	-3.9	3.1	-4.1	2.6		
Q9-16 214.6	Dawn Lake	214.6	Pelitic Gneiss	Garnet-Corderite	-0.81	2.52						
Q9-16 217.2	Dawn Lake	217.2	Pelitic Gneiss	Garnet-Corderite	1.7	2.29						
EL 09-797.7	Epp Lake	797.7	Pegmatite	Clay Altered Proximal U	17	3.7						
EL-09-823.7	Epp Lake	823.7	Pegmatite	Clay Altered Proximal U	17.1	2.8						
RI-46-570.1	Read Lake	570.1	Pegmatite		11	3.6						
RI-80-454.5	Read Lake	454.5	Tourmalinite		12.1	2.4						
MAC 207.511.1	McArthur River	511.1	Graphitic Pelitic Gneiss		-16.3	5.2						
MAC 207.664.8	McArthur River	664.8	Psammitic Gneiss		-9.7	3.5	-9.6	3.7				

Sample Number	MC-ICPMS	Duplicate	LECO Instrumental Analysis					SRC Trace Element Lithium Metaborate Fusion Q-ICPMS Finish									
	δ^7Li ‰	δ^7Li ‰	C wt %	S wt %	Graphite wt%	Inorg C wt %	Org C wt %	Ag ppm	As ppm	Ba ppm	Be ppm	Bi ppm	Cd ppm	Ce ppm	Co ppm	Cs ppm	Cu ppm
A94-040D	-0.4		0.07	0.01	0.01	0.01	0.06	0.5	0.3	891	1.2	<0.1	0.4	128	5.8	6.3	9.9
I57 114.5	3.9		0.08	0.01	0.01	0.01	0.07	0.3	3.6	10	2.5	0.4	<0.1	53	11.5	0.2	4.8
Q6-66 131.2	4.3		0.06	0.01	0.01	0.01	0.05	0.4	5.5	109	3.3	<0.1	<0.1	75	7.1	1.3	4.9
Q6-66 149.7	8.0		0.47	1.62	0.33	0.01	0.14	0.4	28.7	162	4	0.8	0.1	53	17.2	2.1	11.7
Q6-66 164.2	6.2		0.07	0.02	0.01	0.01	0.06	0.2	0.7	151	3	<0.1	<0.1	75	1	1.2	106
Q6-66 170.9	8.1		0.67	2.15	0.65	0.01	0.02	0.5	4.7	15	5.3	0.6	0.2	177	30.8	1.1	16.3
Q6 67 104.4	11.9		0.06	0.01	0.01	0.01	0.05	0.8	26.9	24	5.1	0.4	<0.1	125	41.7	0.2	10.3
Q6-72 108.7	12.7		0.28	0.01	0.23	0.01	0.05	0.5	1.9	219	3.5	0.4	<0.1	75	13.2	7.2	5.8
Q6-72 114.5	18.6	15.7	0.08	0.01	0.01	0.01	0.07	1.3	2.7	17	2.6	0.6	0.1	27	2.7	0.8	8.4
Q6-72 117.2	8.4		1.39	0.48	1.25	0.01	0.14	1.3	149	65	6.4	3	0.2	85	94.3	1.2	22.8
Q7-16 266.8	9.7		0.05	0.02	0.02	0.01	0.03	0.2	1.2	712	2.6	0.1	<0.1	175	5	2.5	56.1
Q9-16 183.6	7.5		0.08	0.01	0.03	0.01	0.05	0.3	14.1	27	8.5	<0.1	<0.1	94	21.4	2.3	9.3
Q9-16 191.3	8.5		0.1	0.28	0.02	0.01	0.08	0.5	8.2	151	5.2	2.9	0.1	36	26.1	1.4	67.7
Q9-16 199.6	11.8	10.3	3.22	6.5	2.8	0.08	0.42	0.9	5	330	6	0.8	0.2	70	131	2.9	287
Q9-16 214.6	8.5		0.22	0.04	0.13	0.03	0.09	0.3	0.4	834	4.5	0.2	0.2	227	11.8	3	11.4
Q9-16 217.2	11.3		0.29	0.01	0.28	0.01	0.01	0.2	0.4	486	4.7	<0.1	<0.1	66	17.4	3	5.6
EL 09-797.7	8.3		0.09	0.01	0.01	0.01	0.08	<0.1	3.7	29	8	1.2	0.2	143	8	1.4	17.2
EL-09-823.7	10.4		0.15	1.16	0.09	0.04	0.02	0.5	4.5	601	3.7	0.3	0.2	86	15.8	5.1	53
RI-46-570.1	14.6		0.07	0.01	0.01	0.01	0.06	0.4	0.3	30	2.5	<0.1	<0.1	19	4.4	0.5	5.5
RI-80-454.5	10.3		0.06	0.01	0.02	0.01	0.04	0.3	1.1	22	6.7	0.2	0.1	29	50.1	0.4	76.3
MAC 207.511.1	5.9		1.82	0.03	1.58	0.06	0.24	0.4	4.2	105	4.6	0.4	0.1	42	13.8	0.9	23.6
MAC 207.664.8	9.5		0.06	0.01	0.01	0.01	0.05	0.1	1.2	17	0.4	<0.1	<0.1	233	2.9	0.2	33.6

Sample Number	SRC Trace Element Lithium Metaborate Fusion Q-ICPMS Finish continued																
	Dy ppm	Er ppm	Eu ppm	Ga ppm	Gd ppm	Ge ppm	Hf ppm	Hg ppm	Ho ppm	La ppm	Lu ppm	Mo ppm	Nb ppm	Nd ppm	Ni ppm	Pb^{204} ppm	Pb^{206} ppm
A94-040D	4.74	2.43	1.14	16.9	5.05	1.7	17	<0.1	1.12	51	0.4	19.3	31	35.7	3	0.174	44.9
I57 114.5	10.6	4.55	0.38	44	6.13	2.7	3.3	<0.1	2.21	22	0.6	<0.1	4	19	11	0.013	1.32
Q6-66 131.2	3.52	1.64	1	22.8	4.62	1.1	4.1	0.1	0.76	42	0.2	<0.1	14	28.8	49	0.004	1.36
Q6-66 149.7	2.51	1.23	0.93	27.6	3.31	1.6	4.7	<0.1	0.58	27	0.2	4.5	16	21.8	32	0.034	3.33
Q6-66 164.2	3.24	0.91	0.88	15.6	6.39	1.4	3.7	<0.1	0.55	39	0.1	<0.1	1	31.2	3	0.252	18.2
Q6-66 170.9	4.09	1.77	0.61	21.1	6.11	1.3	5.8	<0.1	0.84	60	0.2	3.6	19	46.5	58	0.029	3.93
Q6 67 104.4	3.48	2.08	1.08	14	4.4	2.2	4.7	<0.1	0.88	75	0.3	<0.1	19	50.4	51	0.027	1.32
Q6-72 108.7	4.41	2.42	0.63	24.2	4.76	1.9	4.7	<0.1	1.05	41	0.4	<0.1	13	29.5	66	0.034	1.77
Q6-72 114.5	2.96	1.39	0.42	14.7	2.32	2	2.4	<0.1	0.65	13	0.2	<0.1	17	9.7	12	0.003	3.33
Q6-72 117.2	3.76	2.19	0.84	23.6	3.55	1.9	5.3	<0.1	0.92	34	0.4	12.2	12	24	103	0.037	4.65
Q7-16 266.8	11.6	7.96	1.48	15.5	11.9	2	1.8	<0.1	3.15	77	1.7	<0.1	2	73.4	8	0.411	12.7
Q9-16 183.6	2.59	1.36	0.56	21.9	3.58	1.7	4.5	0.2	0.56	50	0.2	<0.1	11	35.9	77	0.005	1.74
Q9-16 191.3	4.79	2.54	0.7	17.4	4.09	1.6	4.7	0.4	1.14	18	0.4	3.1	13	15.2	34	0.13	6.84
Q9-16 199.6	3.15	1.83	1.14	12.5	3.82	2	3.9	<0.1	0.78	41	0.3	22	10	27.8	76	0.16	7.59
Q9-16 214.6	2.06	0.87	1.7	13.5	3.99	1.8	7.4	0.4	0.4	39	0.1	0.5	7	31.9	17	0.08	2.67
Q9-16 217.2	2.86	1.61	1.1	12.5	3.23	1.4	3.2	<0.1	0.72	30	0.3	<0.1	7	21.2	24	0.074	2.38
EL 09-797.7	4.18	1.7	1.74	26	6.45	2.6	9.5	0.1	0.83	81	0.3	<0.1	1	51.8	35	0.028	9.15
EL-09-823.7	3.4	1.62	0.94	18.7	4.9	2.4	5.3	<0.1	0.75	51	0.3	19.8	17	35.1	113	0.08	3.28
RI-46-570.1	0.73	0.4	0.66	24.9	1.45	1.1	0.5	<0.1	0.16	11	0.1	<0.1	7	8.1	14	0.013	0.734
RI-80-454.5	5.19	2.8	1.26	27.3	4.47	1.9	4.5	<0.1	1.28	16	0.5	<0.1	7	12.2	112	0.126	3.68
MAC 207.511.1	4.18	2.64	0.82	24.1	2.9	1.4	5.3	0.2	1.1	22	0.5	0.3	13	14.7	115	0.02	5.7
MAC 207.664.8	1.16	0.52	0.46	6.6	3.51	0.5	3.3	<0.1	0.22	51	0.1	<0.1	3	35.3	9	<0.001	0.675

Sample Number	SRC Trace Element Lithium Metaborate Fusion Q-ICPMS Finish continued																
	Pb^{207} ppm	Pb^{208} ppm	Pb_{SUM} ppm	Pr ppm	Rb ppm	Sb ppm	Se ppm	Sm ppm	Sn ppm	Sr ppm	Ta ppm	Tb ppm	Te ppm	Th ppm	Tl ppm	Tm ppm	U ppm
A94-040D	8.74	11.7	65.6	11.3	343	<1	1	5.96	5.3	73	3.27	0.75	<0.1	36.5	<0.01	0.42	156
I57 114.5	0.415	1.92	3.67	6.26	16.6	<1	<1	5.09	8.9	70	1.2	1.46	<0.1	44.1	<0.01	0.8	28.9
Q6-66 131.2	0.219	1.17	2.76	8.99	83.5	<1	2	5.29	3.9	129	1.4	0.63	<0.1	20.7	<0.01	0.27	7.66
Q6-66 149.7	0.973	3.32	7.65	6.36	250	<1	1	4.23	5.4	52	1.66	0.45	<0.1	21.4	<0.01	0.19	17.2
Q6-66 164.2	7.49	21.9	47.8	9.27	130	<1	2	8.04	4.9	82	0.19	0.78	<0.1	60.8	<0.01	0.12	154
Q6-66 170.9	0.919	4.43	9.31	13.8	64.2	<1	<1	8.3	2.5	22	1.53	0.8	<0.1	60	<0.01	0.26	17
Q6 67 104.4	0.742	2.39	4.48	15.2	2	<1	1	6.79	2	104	1.74	0.59	0.3	19	<0.01	0.36	5.21
Q6-72 108.7	0.913	2.77	5.49	9.06	246	<1	1	5.35	5.2	116	1.71	0.73	0.1	18.8	<0.01	0.44	5.11
Q6-72 114.5	0.297	0.796	4.43	3.02	34.3	<1	1	2.55	6.4	27	5.04	0.46	<0.1	16.2	<0.01	0.25	15.9
Q6-72 117.2	1.07	3.46	9.21	7.25	48.9	<1	<1	3.99	1.4	34	1.59	0.57	<0.1	27.2	<0.01	0.41	15.3
Q7-16 266.8	10.6	29.5	53.2	21.5	326	<1	1	14.6	5.5	95	0.56	1.77	<0.1	96.4	<0.01	1.62	23.2
Q9-16 183.6	0.188	1.1	3.03	10.7	37.6	<1	<1	5.8	0.9	60	1.31	0.48	<0.1	18.5	<0.01	0.22	11.4
Q9-16 191.3	3.53	9.52	20	4.38	67.9	<1	<1	3.54	4.6	29	1.86	0.71	<0.1	11	<0.01	0.46	66
Q9-16 199.6	4.35	12	24.1	8.39	120	<1	<1	4.81	5.4	42	1.62	0.54	<0.1	15.2	<0.01	0.32	17.2
Q9-16 214.6	2.08	5.46	10.3	9.42	132	<1	1	5.31	5.4	41	0.8	0.47	<0.1	48	<0.01	0.13	6.92
Q9-16 217.2	1.93	4.98	9.36	6.29	117	<1	<1	3.81	3.7	37	0.85	0.47	0.1	9.96	<0.01	0.3	3.09
EL 09-797.7	1.36	2.46	13	16.7	47.3	<1	1	8.77	4.1	165	0.26	0.83	<0.1	11.6	<0.01	0.28	205
EL-09-823.7	2.09	5.75	11.2	10.5	232	<1	1	6.33	8.4	28	1.22	0.66	<0.1	17.7	<0.01	0.28	9.71
RI-46-570.1	0.32	0.977	2.04	2.29	69.3	<1	<1	1.78	6.5	35	1.42	0.15	<0.1	5.55	<0.01	0.08	4.27
RI-80-454.5	3.21	7.08	14.1	3.26	15	<1	<1	2.77	9.6	126	0.74	0.77	<0.1	2.43	<0.01	0.51	6.03
MAC 207.511.1	0.724	2.08	8.53	4.61	50.8	<1	<1	2.76	5	57	1.46	0.56	<0.1	19.2	<0.01	0.49	25
MAC 207.664.8	0.016	2.16	2.85	10.9	25.6	<1	<1	5.6	0.6	65	0.3	0.34	<0.1	69.8	<0.01	0.08	12.3

Sample Number						Whole Rock Analysis - Lithium Metaborate Fusion ICP-OES Finish											
	W ppm	Y ppm	Yb ppm	Zn ppm	Zr ppm	SiO_2 wt %	TiO_2 wt %	Al_2O_3 wt %	Fe_2O_3 wt %	MnO wt %	MgO wt %	CaO wt %	Na_2O wt %	P_2O_5 wt %	K_2O wt %	LOI wt %	SUM
A94-040D	1	26	2.34	76	452	71.1	0.72	12.3	4.72	0.05	1.04	0.59	1.64	0.16	7.68	0.5	100.5
I57 114.5	1	68.8	4.32	185	64	71.5	0.41	17.7	4.21	0.01	2.25	0.28	0.77	<0.01	1.11	2	100.24
Q6-66 131.2	6	20.2	1.57	<1	99	64.7	0.9	19	1.51	<0.01	4.5	0.46	0.07	0.34	3.41	5.3	100.19
Q6-66 149.7	2	15.4	1.14	37	101	62	0.63	17.7	5.44	0.03	3.76	0.2	0.09	0.1	4.44	5.7	100.09
Q6-66 164.2	<1	13.6	0.6	62	73	73.6	0.03	14	0.87	<0.01	3	0.08	0.18	0.05	4.5	3.5	99.81
Q6-66 170.9	2	21.6	1.54	12	137	61.9	0.85	16.3	4.65	<0.01	5.62	0.27	0.06	0.1	3.03	6.9	99.68
Q6 67 104.4	3	25.3	2.12	37	107	57	0.67	14.1	10.3	0.04	11.4	0.23	0.04	0.04	0.16	6.5	100.48
Q6-72 108.7	4	27.7	2.44	108	102	62.7	0.68	17.2	5.47	0.02	4.79	0.16	0.1	0.06	3.91	4.7	99.79
Q6-72 114.5	1	18	1.54	9	41	74.6	0.13	14.7	0.35	<0.01	3.36	0.48	0.09	0.29	2.16	4	100.16
Q6-72 117.2	2	24.3	2.38	7	122	62.5	0.76	17.7	1.86	<0.01	6.74	0.26	0.07	0.12	2.22	7.5	99.73
Q7-16 266.8	2	80.3	10.9	10	36	63	0.05	18.6	2.92	0.05	2.5	0.1	0.5	0.07	9.67	2.7	100.16
Q9-16 183.6	10	14.6	1.34	34	108	57.4	0.8	16.6	4.46	0.02	12	0.09	0.06	<0.01	0.91	7.8	100.14
Q9-16 191.3	20	33	2.72	25	113	69.3	0.59	14.7	1.76	<0.01	5.67	0.1	0.12	<0.01	2.86	4.9	100
Q9-16 199.6	4	20.4	2.04	34	87	55.2	0.49	12.9	9.83	0.03	8.42	0.07	0.14	0.01	2.86	10.4	100.35
Q9-16 214.6	22	9.52	0.88	73	215	69.2	0.56	12.3	4.55	0.06	6.28	0.09	0.15	0.03	3.31	3.6	100.13
Q9-16 217.2	<1	17.4	1.77	28	74	62.7	0.65	15.2	6.48	0.2	5.32	0.34	0.2	0.09	4.64	4	99.82
EL 09-797.7	5	22.5	1.77	104	183	67.6	0.21	18	2.32	<0.01	4.48	0.62	0.43	0.37	1.44	4.2	99.67
EL-09-823.7	2	18.4	1.67	78	124	68	0.87	14.5	6.1	0.03	3.14	0.14	0.48	0.02	3.86	2.6	99.74
RI-46-570.1	1	4.71	0.5	27	11	68.6	0.25	20.2	1.1	<0.01	1.57	0.14	0.22	<0.01	4.64	3.2	99.92
RI-80-454.5	<1	31.7	3.06	18	115	38.4	2.4	21.9	23.5	0.04	6.06	1.28	0.51	0.18	1.89	4.2	100.36
MAC 207.511.1	10	32.2	2.92	<1	123	62.8	0.86	18.7	1.01	0.01	6.32	0.18	0.09	0.08	1.72	8.2	99.97
MAC 207.664.8	<1	5.7	0.48	1	88	88.3	0.16	7.32	0.29	<0.01	0.18	0.02	0.06	<0.01	2.05	1.4	99.78

Sample Number	WRA continued			SRC Partial Digestion HR-ICPMS Finish					SRC Total Digestion HR-ICPMS Finish	
	Cr ppm	Sc ppm	V ppm	Pb^{206} / Pb^{204}	Pb^{207} / Pb^{204}	Pb^{208} / Pb^{204}	Pb^{207} / Pb^{206}	Pb^{208} / Pb^{206}	Pb^{206} / Pb^{204}	Pb^{207} / Pb^{204}
A94-040D	20	5	34	785.084	123.599	109.193	0.157	0.139	192.277	37.614
I57 114.5	77	37	14	64.454	21.932	195.074	0.340	3.027	29.527	17.548
Q6-66 131.2	117	19	127	136.640	30.248	165.563	0.221	1.212	71.879	21.977
Q6-66 149.7	93	15	156	35.425	18.087	58.289	0.511	1.645	54.157	19.400
Q6-66 164.2	7	<2	<2	44.680	20.565	70.863	0.460	1.586	44.006	18.838
Q6-66 170.9	98	12	125	35.894	17.557	54.147	0.489	1.509	55.557	19.157
Q6 67 104.4	45	12	73	47.027	15.427	88.912	0.328	1.891	29.281	17.141
Q6-72 108.7	89	17	150	26.337	17.263	63.017	0.655	2.393	24.962	17.064
Q6-72 114.5	13	2	25	163.781	33.602	89.878	0.205	0.549	189.712	31.055
Q6-72 117.2	96	17	325	36.780	17.694	55.520	0.481	1.510	52.491	18.464
Q7-16 266.8	140	50	30	66.391	22.552	186.904	0.340	2.815	16.383	16.032
Q9-16 183.6	95	17	115	112.329	19.627	92.228	0.175	0.821	102.422	19.473
Q9-16 191.3	64	8	94	36.141	18.199	66.283	0.504	1.834	29.960	17.665
Q9-16 199.6	58	11	256	30.227	17.569	60.831	0.581	2.012	26.488	17.358
Q9-16 214.6	50	11	74	25.780	17.120	53.842	0.664	2.089	17.565	16.272
Q9-16 217.2	81	13	96	26.925	17.250	51.802	0.641	1.924	17.011	16.156
EL 09-797.7	32	9	61	109.755	22.917	51.655	0.209	0.471	149.695	27.989
EL-09-823.7	102	18	325	20.021	16.449	42.966	0.822	2.146	20.625	16.630
RI-46-570.1	9	5	51	24.430	16.707	57.137	0.684	2.339	23.047	16.451
RI-80-454.5	54	52	377	22.753	16.732	40.695	0.735	1.789	15.287	15.939
MAC 207.511.1	112	19	378	76.059	20.303	60.272	0.267	0.792	118.594	20.305
MAC 207.664.8	26	2	10	74.168	21.125	113.442	0.285	1.530	52.372	18.897

Sample Number	SRC Total Digestion HR-ICPMS Finish continued			Na_2CO_3/Na_2O_2 Fusion ICP-OES	SRC Total Digestion ICP-OES Finish										
	Pb^{208} / Pb^{204}	Pb^{207} / Pb^{206}	Pb^{208} / Pb^{206}	B ppm	Al_2O_3 wt %	Ba ppm	CaO wt %	Ce ppm	Cr ppm	Fe_2O_3 wt %	K_2O wt %	La ppm	Li ppm	MgO wt %	MnO wt %
A94-040D	50.587	0.196	0.263	25	13.4	1030	0.65	103	14	5.32	8.79	50	63	1.12	0.053
I57 114.5	81.153	0.594	2.748	10700	13.5	11	0.19	44	76	3.02	1.04	18	29	1.6	0.009
Q6-66 131.2	91.911	0.306	1.279	161	21.9	141	0.5	92	125	1.78	3.88	51	84	4.93	0.005
Q6-66 149.7	61.800	0.358	1.141	124	20.2	207	0.26	64	93	6.07	5.18	31	105	4.04	0.034
Q6-66 164.2	65.363	0.428	1.485	248	15.6	169	0.1	86	7	1	5.06	45	105	3.37	0.004
Q6-66 170.9	66.893	0.345	1.204	251	19.3	20	0.31	93	120	5.56	3.57	45	161	6.36	0.008
Q6 67 104.4	66.523	0.585	2.272	53	15.7	21	0.16	142	52	11.7	0.077	87	684	12	0.048
Q6-72 108.7	54.547	0.684	2.185	168	19.5	268	0.25	88	115	6.37	4.5	46	80	5.36	0.023
Q6-72 114.5	89.482	0.164	0.472	913	16.1	29	0.65	36	12	0.39	2.32	18	169	3.91	0.006
Q6-72 117.2	59.486	0.352	1.133	647	19.8	75	0.24	71	104	2.18	2.39	37	178	7.38	0.007
Q7-16 266.8	51.335	0.979	3.133	198	21.7	895	0.13	204	160	3.44	11.9	96	105	2.85	0.055
Q9-16 183.6	92.944	0.190	0.907	98	21.5	37	0.14	116	123	5.66	0.996	63	309	14.8	0.021
Q9-16 191.3	52.683	0.590	1.758	167	16.7	170	0.13	48	61	2.02	3.2	23	135	6.36	0.007
Q9-16 199.6	52.598	0.655	1.986	72	15.2	381	0.1	74	66	11.8	3.35	42	416	9.05	0.03
Q9-16 214.6	44.088	0.926	2.510	103	14.3	956	0.09	81	62	5.41	3.61	42	232	6.91	0.046
Q9-16 217.2	42.962	0.950	2.525	97	18.5	719	0.41	118	101	8.17	5.61	53	162	6.3	0.274
EL 09-797.7	54.348	0.187	0.363	6320	15.7	36	0.57	161	20	1.69	1.46	88	127	4.03	0.006
EL-09-823.7	46.236	0.806	2.242	4010	11.8	704	0.11	83	75	5.84	4.24	46	81	2.7	0.028
RI-46-570.1	43.241	0.714	1.876	2890	21.4	39	0.12	18	7	0.94	5.36	11	34	1.49	0.002
RI-80-454.5	37.153	1.043	2.430	10000	21.2	31	1.05	35	51	26.5	2.07	16	74	5.03	0.037
MAC 207.511.1	60.906	0.171	0.514	1150	20.4	120	0.2	46	116	1.17	1.85	24	152	6.94	0.012
MAC 207.664.8	78.101	0.361	1.491	99	7.76	20	0.03	36	27	0.34	2.11	19	25	0.243	<0.001

Sample Number	SRC Total Digestion ICP-OES Finish continued						SRC Partial Digestion Q-ICPMS Finish										
	Na_2O wt %	P_2O_5 wt %	Sr ppm	TiO_2 wt %	V ppm	Zr ppm	Ag ppm	As ppm	Be ppm	Bi ppm	Cd ppm	Co ppm	Cs ppm	Cu ppm	Dy ppm	Er ppm	Eu ppm
A94-040D	1.66	0.254	98	0.755	40.2	732	0.08	0.48	0.19	0.07	0.03	3.85	4.65	3.96	5.34	2.82	0.44
I57 114.5	0.48	0.038	87	0.285	13.7	42	0.02	2.05	0.26	0.25	<0.01	5	0.05	1.29	2.2	0.84	0.06
Q6-66 131.2	0.03	0.389	179	1.03	144	178	0.02	1.87	1.39	0.02	0.01	3.38	0.35	0.77	1.71	0.6	0.64
Q6-66 149.7	0.05	0.204	73	0.688	176	166	0.14	30.4	0.65	0.98	0.02	15.7	0.23	3.38	0.8	0.3	0.4
Q6-66 164.2	0.14	0.082	106	0.028	3	118	0.03	0.68	0.98	0.08	<0.01	0.67	0.2	90.8	2.72	0.67	0.5
Q6-66 170.9	0.02	0.174	32	1.02	155	230	0.32	4.74	2.73	0.75	0.05	31.7	0.3	2.91	1.1	0.48	0.34
Q6 67 104.4	<0.01	0.155	107	0.764	85.7	161	0.02	3.58	3.89	0.05	<0.01	26.6	0.27	0.79	2.13	1.19	0.42
Q6-72 108.7	0.07	0.129	159	0.714	178	164	0.06	0.71	1.69	0.06	0.03	8.62	8.05	1.13	0.99	0.41	0.29
Q6-72 114.5	0.04	0.478	42	0.145	30.9	163	0.1	2.91	0.43	0.84	0.09	2.19	0.28	4.87	2.72	1.1	0.31
Q6-72 117.2	0.04	0.136	44	0.727	376	193	0.99	153	2.29	6.01	0.06	93.5	0.3	19	1.3	0.58	0.66
Q7-16 266.8	0.51	0.116	140	0.061	38.6	50	0.02	1.17	1.49	0.1	<0.01	3.9	0.38	49.2	4.82	2.19	0.3
Q9-16 183.6	0.03	0.054	94	1.1	155	186	0.05	8.58	4.75	0.16	<0.01	18.1	0.98	5.1	0.77	0.39	0.21
Q9-16 191.3	0.09	0.032	37	0.47	86.4	183	0.35	7.12	3	4.28	0.08	25.8	0.51	42.8	2.54	1.2	0.37
Q9-16 199.6	0.1	0.08	61	0.455	284	154	1.63	5.34	4.18	1.05	0.2	133	2.33	230	0.83	0.39	0.34
Q9-16 214.6	0.12	0.077	56	0.667	91	143	0.05	0.45	2.71	0.18	<0.01	5.56	1.61	6.29	0.43	0.16	0.77
Q9-16 217.2	0.17	0.195	66	0.807	124	169	0.02	0.53	4.14	0.09	<0.01	12.3	2.45	2.52	0.66	0.2	0.6
EL 09-797.7	0.23	0.421	217	0.124	46.9	311	0.05	2.56	2.13	1.31	0.05	2	0.51	11.4	2.01	0.77	0.45
EL-09-823.7	0.31	0.062	37	0.856	266	165	0.18	4.46	1.63	0.38	0.06	13.6	3.25	39.4	0.28	0.14	0.18
RI-46-570.1	0.12	0.03	47	0.239	45.4	7	0.01	0.34	0.31	0.02	<0.01	0.39	0.21	1.75	0.16	0.06	0.1
RI-80-454.5	0.31	0.389	123	2.37	390	160	<0.01	0.66	0.74	0.04	<0.01	2.55	0.18	76.8	0.76	0.34	0.38
MAC 207.511.1	0.06	0.105	79	0.698	398	190	0.03	3.78	1.62	0.3	<0.01	11.2	0.39	19.5	1.26	0.58	0.58
MAC 207.664.8	0.02	0.026	76	0.163	13.8	118	0.01	0.55	0.11	0.02	<0.01	2.24	0.11	17.4	0.2	0.07	0.07

Sample Number	SRC Partial Digestion Q-ICPMS Finish continued																
	Ga ppm	Gd ppm	Ge ppm	Hf ppm	Hg ppm	Ho ppm	Mo ppm	Nb ppm	Nd ppm	Ni ppm	Pb^{204} ppm	Pb^{206} ppm	Pb^{207} ppm	Pb^{208} ppm	Pb_{SUM} ppm	Pr ppm	Rb ppm
A94-040D	5.97	7.41	0.1	0.19	0.03	1.01	9.04	0.85	43.5	1.42	0.086	65.9	8.71	7.19	81.9	14.5	95.5
I57 114.5	0.46	2.82	0.01	0.21	0.03	0.34	0.34	0.1	9.32	2.21	0.004	0.519	0.099	1.26	1.88	3.19	0.94
Q6-66 131.2	3.35	3.25	0.01	0.2	<0.01	0.26	0.1	0.02	11.5	15	0.003	0.708	0.111	0.664	1.49	3.47	3.69
Q6-66 149.7	3.83	2.01	0.04	0.32	<0.01	0.13	4.87	<0.01	10.8	23.9	0.097	3.78	1.6	4.75	10.2	2.98	5.6
Q6-66 164.2	2.26	7.7	0.04	0.26	<0.01	0.34	0.13	<0.01	23.5	0.71	0.608	28.1	10.9	34.1	73.7	6.62	2.49
Q6-66 170.9	7	2.3	0.04	0.5	<0.01	0.19	3.57	0.02	11.4	55.1	0.091	3.76	1.48	4.19	9.52	3.45	7.89
Q6 67 104.4	8.28	2.69	0.12	0.08	0.04	0.42	0.14	0.16	10.5	25.7	0.005	0.429	0.104	0.653	1.19	2.76	0.77
Q6-72 108.7	8.01	2.43	0.04	0.32	<0.01	0.16	0.13	0.03	10.9	26.7	0.036	1.06	0.604	1.96	3.66	3.3	161
Q6-72 114.5	1.19	2.75	0.01	0.16	<0.01	0.45	0.15	<0.01	5.34	3.24	0.015	2.84	0.467	1.13	4.45	1.5	2.28
Q6-72 117.2	4.19	2.23	0.04	0.27	<0.01	0.22	8.24	<0.01	13.4	76.3	0.142	5.9	2.34	6.74	15.1	3.92	4.7
Q7-16 266.8	3.91	12.4	0.07	0.04	<0.01	0.76	0.63	0.02	69.3	4.22	0.046	3.4	0.968	8.24	12.6	22.4	12.7
Q9-16 183.6	9.35	1.43	0.03	0.16	<0.01	0.13	0.12	0.01	9.13	44.2	0.008	1.17	0.154	0.717	2.05	2.67	10.3
Q9-16 191.3	4.47	3.04	0.04	0.25	<0.01	0.47	2.03	<0.01	4.9	23.9	0.198	7.55	3.27	10.2	21.2	1.33	4.37
Q9-16 199.6	7.5	1.53	0.13	0.07	<0.01	0.15	25.7	0.02	7.24	71.1	0.249	7.81	3.98	12.1	24.1	2.17	51.8
Q9-16 214.6	5.53	0.8	0.05	0.01	<0.01	0.07	0.52	0.04	3.2	6.88	0.012	0.304	0.176	0.485	0.977	0.97	42.1
Q9-16 217.2	7.25	1.54	0.04	0.04	<0.01	0.09	0.82	0.08	5.56	18	0.027	0.99	0.448	1.29	2.75	1.6	63.8
EL 09-797.7	2.12	2.67	0.02	0.07	0.28	0.32	0.2	0.02	7.22	10.2	0.052	7.81	1.31	2.65	11.8	1.93	3.36
EL-09-823.7	4.22	0.47	0.07	0.05	0.01	0.05	18.1	0.23	2.43	95.4	0.054	1.28	0.829	1.97	4.13	0.76	95.2
RI-46-570.1	0.65	0.4	<0.01	<0.01	<0.01	0.02	0.13	<0.01	1.79	1.67	0.01	0.249	0.136	0.425	0.82	0.56	4.11
RI-80-454.5	1.23	1.55	0.02	0.04	<0.01	0.13	0.12	0.01	5.66	11.7	0.014	0.356	0.22	0.475	1.06	1.43	1.1
MAC 207.511.1	3.19	1.71	0.01	0.27	<0.01	0.22	0.44	<0.01	8.76	43	0.036	3.43	0.696	1.9	6.07	2.69	5.39
MAC 207.664.8	0.23	0.6	<0.01	0.08	<0.01	0.03	0.36	<0.01	3.64	3.89	0.002	0.234	0.041	0.266	0.543	1.2	1.4

Sample Number	SRC Partial Digestion Q-ICPMS Finish continued															
	Sb ppm	Sc ppm	Se ppm	Sm ppm	Sn ppm	Ta ppm	Tb ppm	Te ppm	Th ppm	U ppm	V ppm	W ppm	Y ppm	Yb ppm	Zn ppm	Zr ppm
A94-040D	<0.01	3.8	1.3	7.26	2.58	<0.01	0.89	<0.01	31.8	147	18.2	<0.1	28.2	2.04	69	8.47
I57 114.5	<0.01	0.3	<0.1	2.9	0.68	<0.01	0.41	<0.01	31.9	2.68	1.4	<0.1	10.7	0.66	2.5	5.93
Q6-66 131.2	<0.01	2.9	0.3	2.74	0.18	<0.01	0.37	<0.01	9	4.42	12.2	<0.1	7.08	0.34	5.2	6.72
Q6-66 149.7	<0.01	1.8	0.5	2.32	0.17	<0.01	0.19	0.01	15.8	10.9	24	<0.1	3.41	0.15	25.9	12.2
Q6-66 164.2	<0.01	0.3	1.3	7.8	0.32	<0.01	0.75	<0.01	65.1	170	0.6	<0.1	9.25	0.25	67.8	10.9
Q6-66 170.9	<0.01	3.7	0.6	2.35	0.46	<0.01	0.23	0.03	14.6	11.2	32.6	<0.1	5.48	0.27	34.4	24.5
Q6 67 104.4	<0.01	7.7	0.1	2.16	0.45	<0.01	0.35	0.07	9.55	1.88	41.3	<0.1	13.7	0.95	26.9	3.42
Q6-72 108.7	<0.01	10.5	0.2	2.32	1.1	<0.01	0.24	<0.01	7.73	1.12	72.6	<0.1	4.34	0.27	94.2	11.2
Q6-72 114.5	<0.01	0.5	0.4	2.11	0.37	<0.01	0.5	<0.01	12.5	15.4	2.8	<0.1	13.4	0.94	2.6	5.44
Q6-72 117.2	0.04	3.7	5.3	2.34	0.17	<0.01	0.24	0.04	14.1	10.6	57.9	<0.1	6.3	0.4	19.4	14
Q7-16 266.8	<0.01	19	2	14.2	0.5	<0.01	1.06	<0.01	93	21.5	13.7	<0.1	22	1.96	8	2.07
Q9-16 183.6	<0.01	5.5	<0.1	1.71	0.16	<0.01	0.15	<0.01	9.59	4.74	32.5	<0.1	3.92	0.3	44.1	8.02
Q9-16 191.3	0.05	3.1	0.7	1.84	0.27	<0.01	0.47	0.04	5.81	64.2	18.8	<0.1	16.3	0.88	40.6	11.5
Q9-16 199.6	<0.01	6.5	4.3	1.56	0.65	<0.01	0.16	<0.01	6.01	4.53	130	<0.1	4.48	0.31	28.9	4.15
Q9-16 214.6	<0.01	5.6	<0.1	0.69	0.43	<0.01	0.09	0.02	1.39	0.34	31.5	<0.1	1.98	0.1	38	1.7
Q9-16 217.2	<0.01	7	<0.1	1.35	0.62	<0.01	0.16	0.07	2.12	0.56	53.2	<0.1	2.49	0.13	28.9	2.58
EL 09-797.7	0.04	0.8	1.3	2.37	0.46	<0.01	0.39	0.04	4.92	205	6.9	<0.1	9.55	0.58	5.4	4.68
EL-09-823.7	<0.01	6	2.3	0.47	1.2	<0.01	0.05	<0.01	1.68	1.94	86.8	<0.1	1.29	0.12	27.2	2.25
RI-46-570.1	<0.01	0.5	<0.1	0.44	0.15	<0.01	0.04	<0.01	3.31	0.69	2	<0.1	0.64	0.05	2.8	0.9
RI-80-454.5	<0.01	3.3	<0.1	1.35	1	<0.01	0.16	<0.01	0.97	0.82	20.1	<0.1	3.35	0.22	3.4	5.38
MAC 207.511.1	<0.01	3	0.2	1.68	0.12	<0.01	0.22	0.01	15.4	18.2	66.6	<0.1	7.24	0.41	5.8	11
MAC 207.664.8	<0.01	0.2	<0.1	0.67	0.04	<0.01	0.05	<0.01	3.69	3.73	1.3	<0.1	0.78	0.03	2.1	3.4

Sample Number	SRC Total Digestion Q-ICPMS Finish																
	Ag ppm	Be ppm	Bi ppm	Cd ppm	Co ppm	Cs ppm	Cu ppm	Dy ppm	Er ppm	Eu ppm	Ga ppm	Gd ppm	Hf ppm	Ho ppm	Mo ppm	Nb ppm	Nd ppm
A94-040D	0.52	1.6	0.2	0.5	6.95	10.6	4.3	5.61	3.13	1.17	20.9	7.6	19.7	1.13	11.9	30.3	40.2
I57 114.5	0.15	2.6	0.5	<0.1	12.9	0.4	2.1	4.15	1.83	0.1	41.6	4.8	2.8	0.73	0.61	4.3	16.9
Q6-66 131.2	0.42	4.9	<0.1	0.1	8.76	2.2	1.7	3.26	1.4	1.19	31.5	7.2	5.6	0.56	0.81	16.9	38.4
Q6-66 149.7	0.45	4.8	1.2	0.1	19.8	3.7	3.7	2.03	0.9	1.03	36.4	4.8	5.6	0.35	7.43	19	29.3
Q6-66 164.2	0.06	4	0.2	<0.1	1.26	2	109	3.95	1.12	1.04	20	9.6	4.4	0.54	0.54	1.2	37.5
Q6-66 170.9	0.65	7.4	1	0.2	35.9	2.2	4.4	4.08	1.7	0.68	27.7	8.1	7.1	0.71	4.36	22.7	42.2
Q6 67 104.4	0.3	6.1	0.3	0.1	42.8	0.4	1.3	3.89	2.48	1.21	16.4	7.2	5.1	0.85	0.58	14.6	61.5
Q6-72 108.7	0.4	4.5	0.4	0.1	14.9	13.3	1.4	3.07	1.5	0.73	30.4	6.6	5.2	0.56	0.46	9	37
Q6-72 114.5	0.38	3.5	1.1	0.2	3.34	1.5	6.4	5.49	2.48	0.63	19.2	5.9	7.5	0.98	0.3	17.6	16.4
Q6-72 117.2	1.08	7.4	6.9	0.2	110	2	22.5	2.86	1.5	0.82	28	4.7	5.9	0.55	8.71	6.3	28.9
Q7-16 266.8	0.07	3.1	0.5	<0.1	5.72	4.5	58.9	8.62	5.4	1.42	18.1	16.7	2.2	1.83	0.86	2.5	93.8
Q9-16 183.6	0.35	11.2	0.7	0.1	27	4.4	7.4	2.65	1.57	0.69	30.1	5.7	5.5	0.52	0.39	16.5	47.2
Q9-16 191.3	0.46	6.7	4.9	0.2	29.5	2.5	51.8	4.4	2.17	0.76	22.9	5.9	5.7	0.84	2.87	7.2	21.4
Q9-16 199.6	1.87	7	1.6	0.3	147	5.8	360	2.49	1.35	1.26	16.3	5.1	4.9	0.48	24.9	5.1	32.3
Q9-16 214.6	0.23	5.6	0.3	<0.1	14.1	5.8	11.6	1.91	0.7	1.46	16.7	5	4.2	0.29	1.19	6.9	30.4
Q9-16 217.2	0.26	7	0.2	0.1	26.8	7.8	4.3	3.67	1.88	1.61	21.2	7	5.1	0.66	1.36	11.8	41.1
EL 09-797.7	0.08	8.6	1.6	0.2	7.75	2.3	16	4.4	1.93	1.89	22.6	9.1	11.7	0.73	0.49	1.5	62
EL-09-823.7	0.46	4.2	0.6	0.2	17.6	9.2	53.2	2.61	0.98	1	17.4	6.2	5.4	0.4	22.3	18.1	37.9
RI-46-570.1	0.21	2.9	0.2	<0.1	3.97	1	2.7	0.4	0.2	0.74	26.2	1.7	0.4	0.07	0.2	9	9.4
RI-80-454.5	0.16	6.5	0.3	0.1	48.7	0.8	69	4.52	2.7	1.33	30.8	5.6	4.4	0.93	0.3	8.9	16.4
MAC 207.511.1	0.13	6.1	0.5	0.1	16	1.8	26.6	3.15	1.72	0.88	30.9	3.7	6.2	0.63	1.42	5	18.8
MAC 207.664.8	0.08	0.5	<0.1	<0.1	3.3	0.3	23.7	0.61	0.28	0.46	8.4	2.2	3.4	0.1	0.34	1.5	14.7

Sample Number	SRC Total Digestion Q-ICPMS Finish continued																
	Ni ppm	Pb^{204} ppm	Pb^{206} ppm	Pb^{207} ppm	Pb^{208} ppm	Pb_{SUM} ppm	Pr ppm	Rb ppm	Sc ppm	Sm ppm	Sn ppm	Ta ppm	Tb ppm	Th ppm	U ppm	V ppm	W ppm
A94-040D	2.7	0.363	66.4	12.7	17.4	96.9	12.3	342	6.5	7.7	5.45	2.65	0.89	29.6	171	28.6	1.7
I57 114.5	11.9	0.031	2.02	0.604	2.91	5.56	5.8	17.7	22.4	4.8	7.04	1.07	0.73	44.1	12.3	7.7	1.7
Q6-66 131.2	58.8	0.018	2.15	0.454	1.91	4.52	11.6	92.7	18.9	7.7	1.62	1.5	0.65	23.5	11	128	1.3
Q6-66 149.7	35.1	0.094	4.88	1.63	5.33	11.9	8.4	267	16	6.1	2.46	1.62	0.4	24.4	17.8	153	3
Q6-66 164.2	2.2	0.683	28.9	11.8	38	79.4	10.9	142	1.3	10.7	2.05	0.27	0.94	68	180	1.3	1.2
Q6-66 170.9	68.5	0.09	6.06	1.77	6.52	14.4	12	70.5	12.6	8.6	2.04	1.65	0.81	30.2	21.3	133	2.6
Q6 67 104.4	53.7	0.039	2.9	0.829	2.63	6.4	18.5	3.1	12.4	9	1.62	1.6	0.59	20.3	25.2	67.2	4.2
Q6-72 108.7	73.8	0.075	2.51	1.35	4.16	8.09	11.2	247	16.8	7.3	2.59	1.14	0.62	20.6	6.58	153	6
Q6-72 114.5	13.6	0.026	5.04	0.773	2.21	8.04	4.9	40	3.6	5.2	4.55	2.99	0.95	25.6	23.5	26.9	2.1
Q6-72 117.2	118	0.132	7.82	2.29	7.3	17.5	8.8	47.3	17.2	5.2	0.87	0.67	0.5	21.7	16.4	329	1.8
Q7-16 266.8	6.9	0.852	15.1	12.7	36.6	65.3	27.6	331	49.5	19.7	3.86	0.93	1.52	102	27	29	1
Q9-16 183.6	96.9	0.023	2.61	0.443	1.87	4.95	13.8	43	19.5	8.1	0.87	1.76	0.44	22.1	10	133	2.1
Q9-16 191.3	35.9	0.363	11.4	5.93	17.8	35.5	6	72.5	8.6	5.3	1.33	0.99	0.79	13.1	74.4	76.5	1.5
Q9-16 199.6	91.7	0.373	10.4	6.2	18.1	35.1	9.7	134	10.9	5.9	1.74	0.7	0.44	15	10.2	245	2.1
Q9-16 214.6	17.4	0.174	3.56	2.65	7.19	13.6	9.2	141	10.8	5.7	1.34	0.49	0.41	14.2	6.12	75.2	0.9
Q9-16 217.2	35.5	0.209	4.02	3.13	8.68	16	12	177	15.4	7.8	1.54	1.19	0.63	17	4.18	101	1.1
EL 09-797.7	34.1	0.065	13.5	2.05	3.68	19.3	19.4	51.6	6	11.6	3.64	0.37	0.78	11.7	212	39.5	2.4
EL-09-823.7	127	0.196	4.8	3.13	8.27	16.4	11	245	14.1	7.1	4.18	1.21	0.52	14	9.18	238	2.7
RI-46-570.1	11.8	0.046	1.1	0.698	1.91	3.75	2.7	78.9	5.7	2.3	2.95	1.42	0.1	4.9	0.95	38.1	1.4
RI-80-454.5	112	0.179	3	2.68	6.13	12	4.2	17.5	42.9	4	6.93	0.79	0.78	2.18	2.8	310	0.4
MAC 207.511.1	138	0.06	9.98	1.41	3.38	14.8	5.8	56.1	18.2	3.6	1.24	0.56	0.49	20.8	42.4	368	4.1
MAC 207.664.8	10.5	0.034	1.44	0.61	1.75	3.83	4.4	28.5	3.4	2.7	0.33	0.17	0.14	8.69	8.65	14.1	0.5

Sample Number	Total Digestion Q-ICPMS contd…		
	Y ppm	Yb ppm	Zn ppm
A94-040D	30.5	2.92	84
I57 114.5	23.7	1.71	112
Q6-66 131.2	15.9	1.14	16
Q6-66 149.7	9.6	0.77	44
Q6-66 164.2	15.2	0.7	67
Q6-66 170.9	19.9	1.34	33
Q6 67 104.4	26.2	2.18	40
Q6-72 108.7	15.5	1.32	105
Q6-72 114.5	28.5	2.61	7
Q6-72 117.2	15.5	1.45	23
Q7-16 266.8	50.9	6.29	10
Q9-16 183.6	14.3	1.5	48
Q9-16 191.3	27.4	1.91	41
Q9-16 199.6	13.4	1.31	42
Q9-16 214.6	7.7	0.55	75
Q9-16 217.2	18	1.87	48
EL 09-797.7	22.4	1.88	47
EL-09-823.7	10	0.77	61
RI-46-570.1	2	0.21	16
RI-80-454.5	25.6	2.66	19
MAC 207.511.1	19.6	1.68	12
MAC 207.664.8	2.7	0.26	3

APPENDIX B
WOLLASTON EAGLE PROJECT DRILLHOLES

All drillhole images are extracted from the SRC Wollaston EAGLE and EAGLE 2 Projects

(Annesley et al., 1995, 1996, 1998, 1999). Red dots denote sample location.

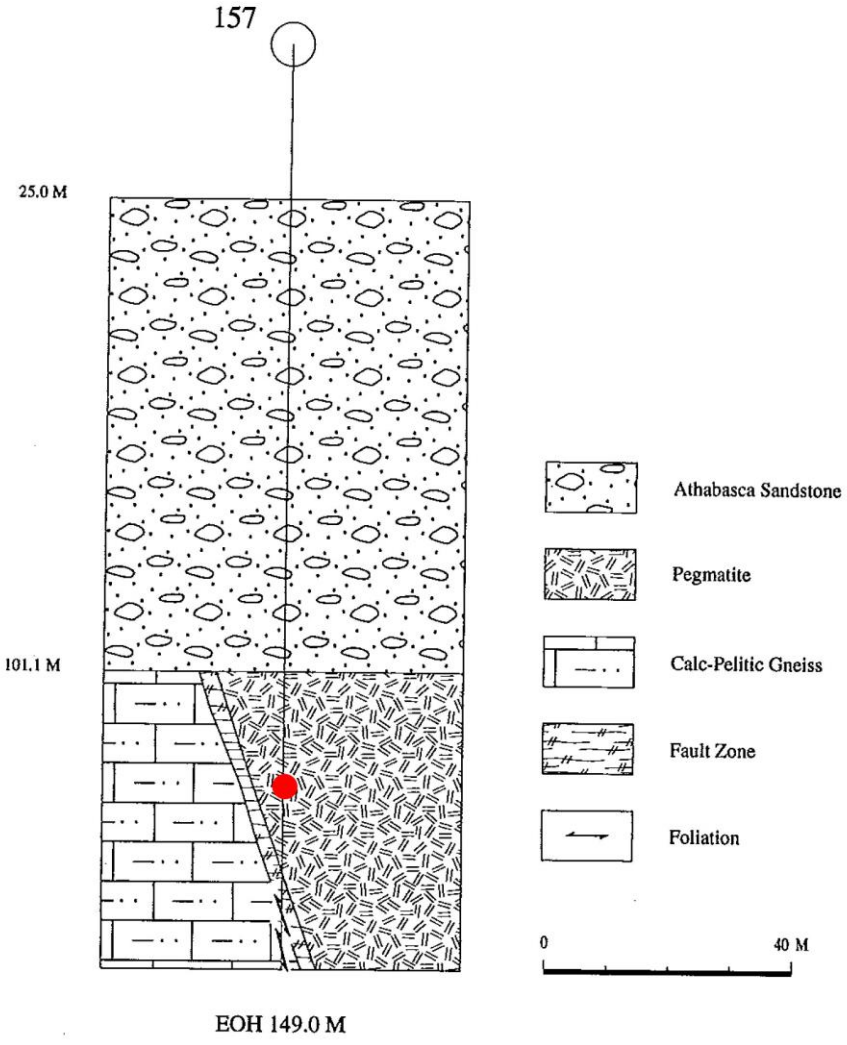

Cross-section of DDH 157.

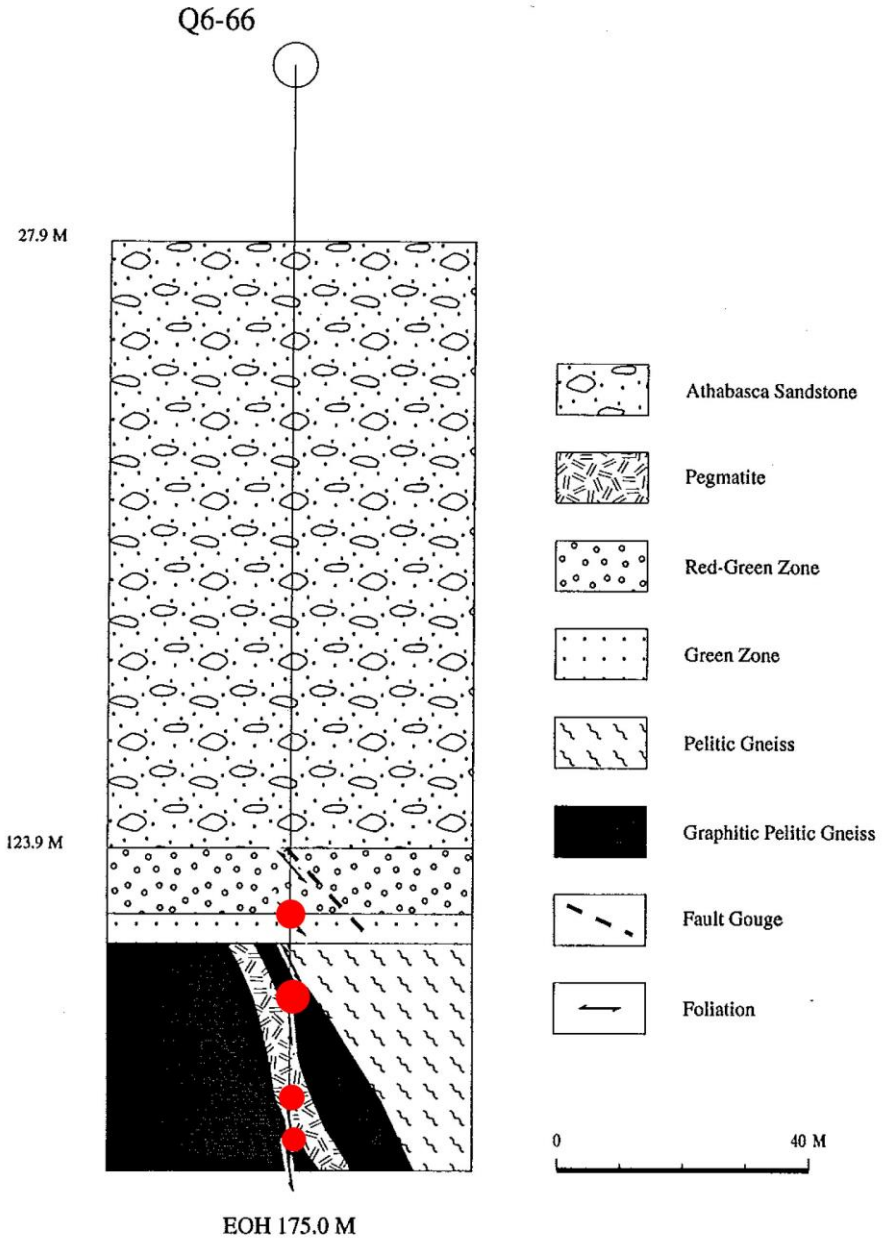

Cross-section of DDH Q6-66.

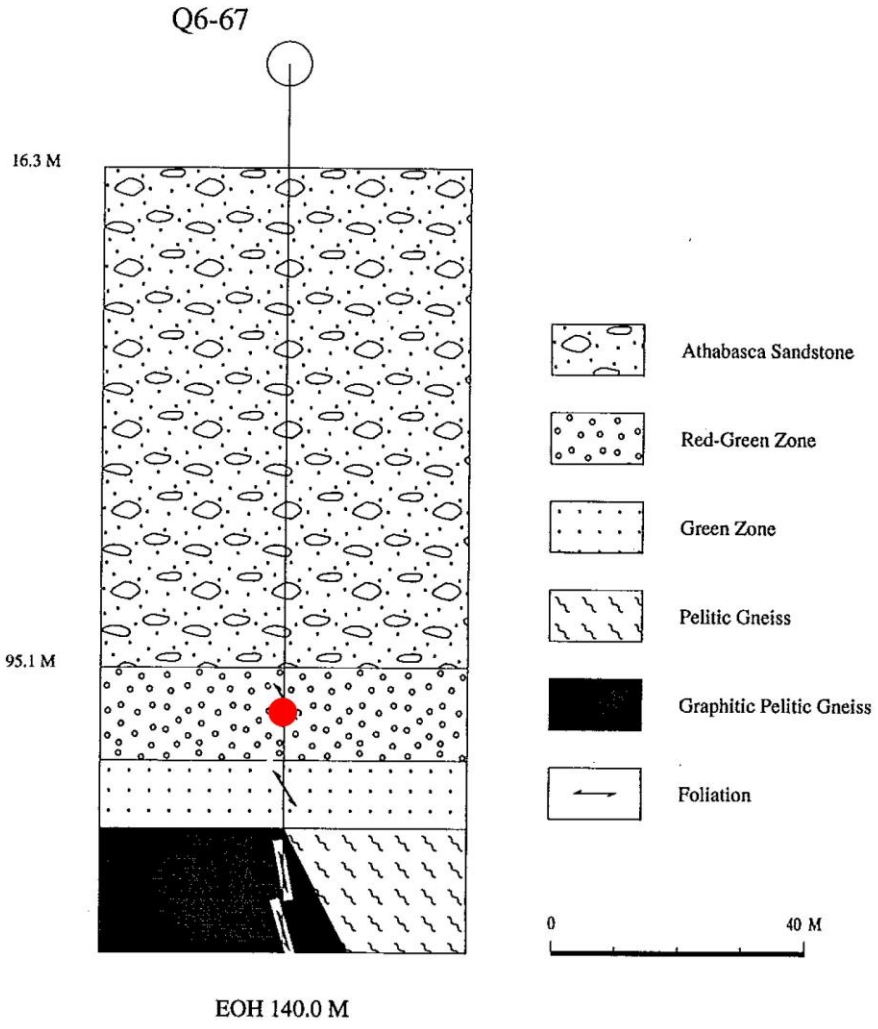

Cross-section of DDH Q6-67.

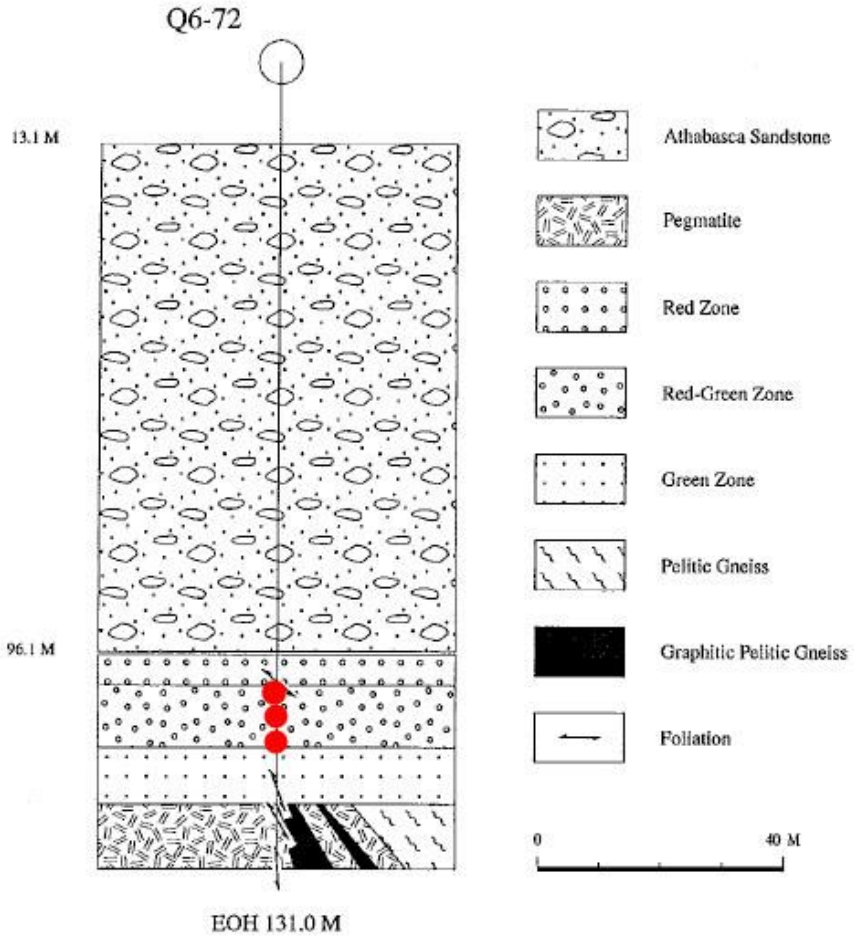

Cross-section of DDH Q6-72.

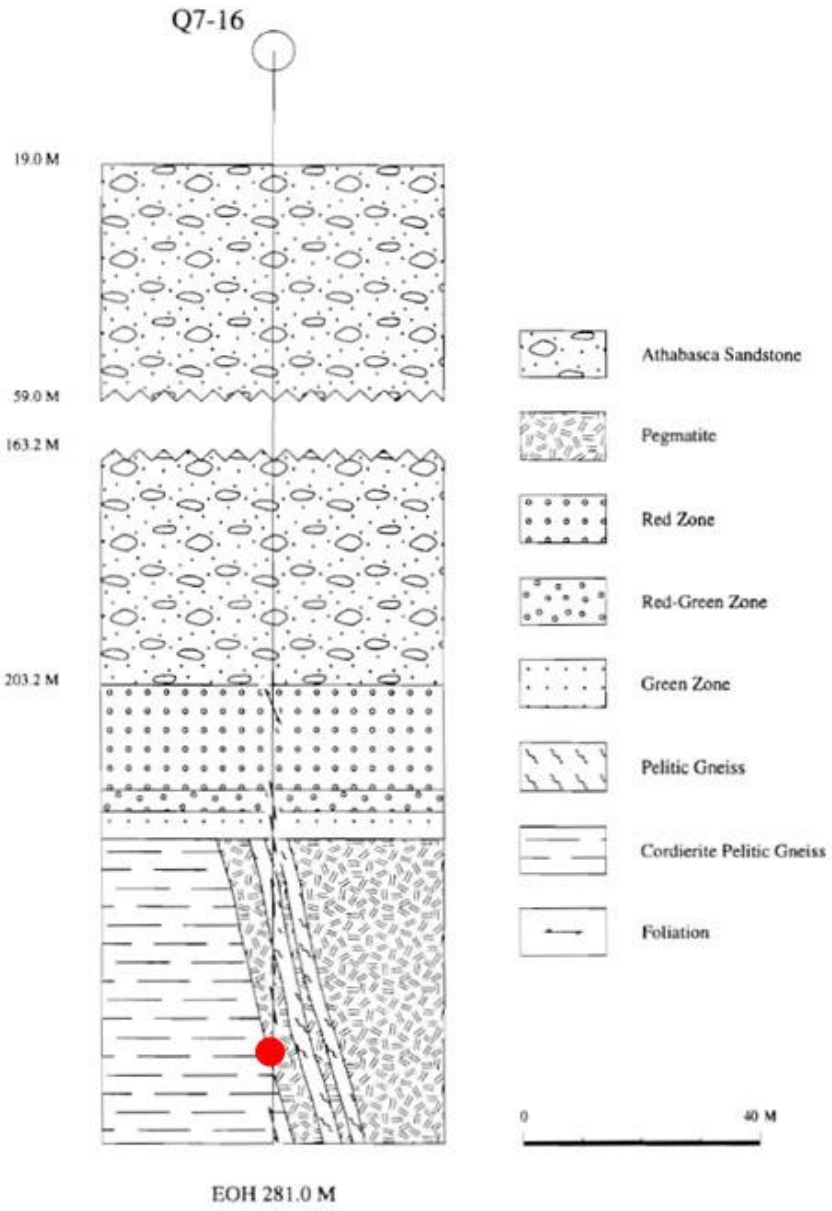
Q7-16
19.0 M
59.0 M
163.2 M
203.2 M
Athabasca Sandstone
Pegmatite
Red Zone
Red-Green Zone
Green Zone
Pelitic Gneiss
Cordierite Pelitic Gneiss
Foliation
0
40 M
EOH 281.0 M

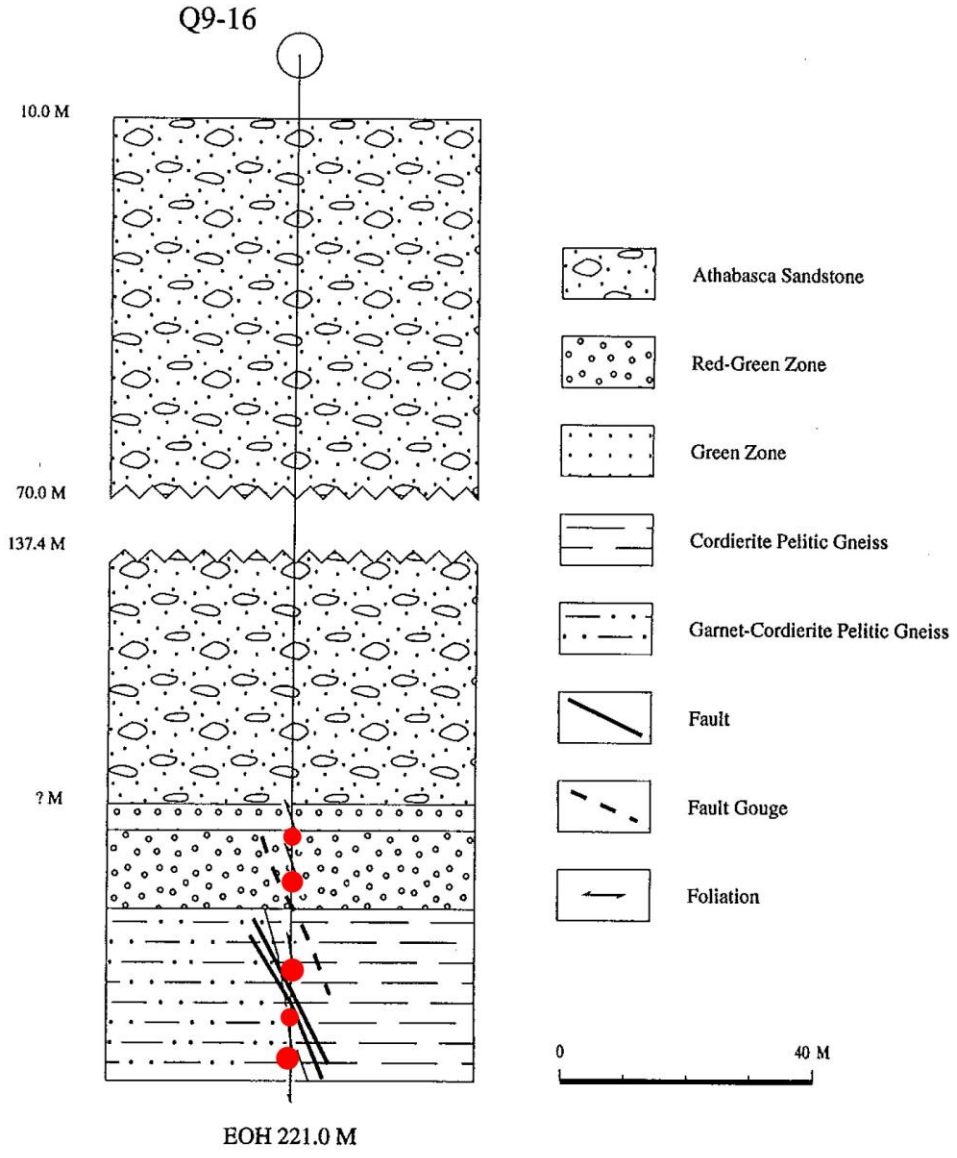

Cross-section of DDH Q9-16.

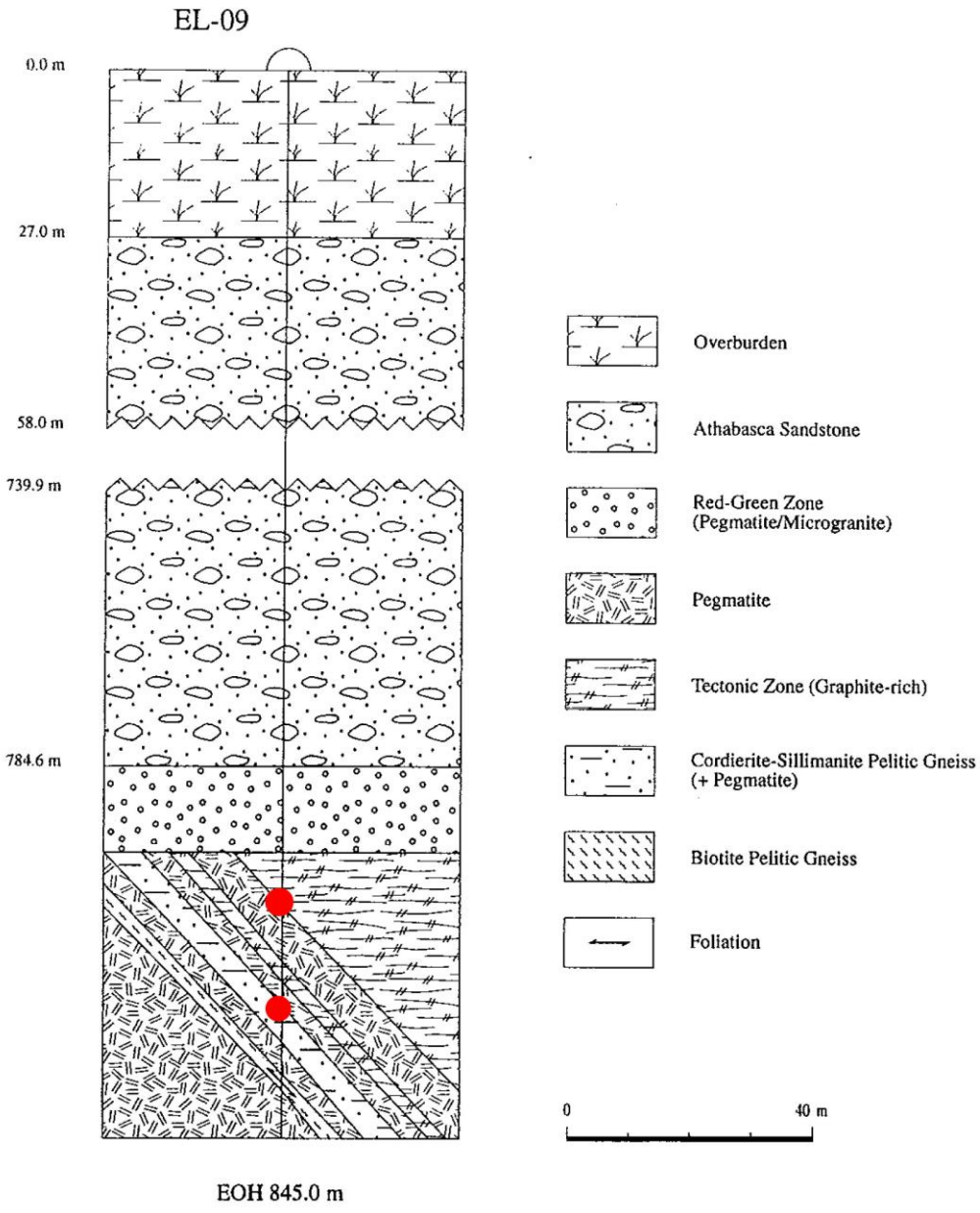

Cross-section of DDH EL-09.

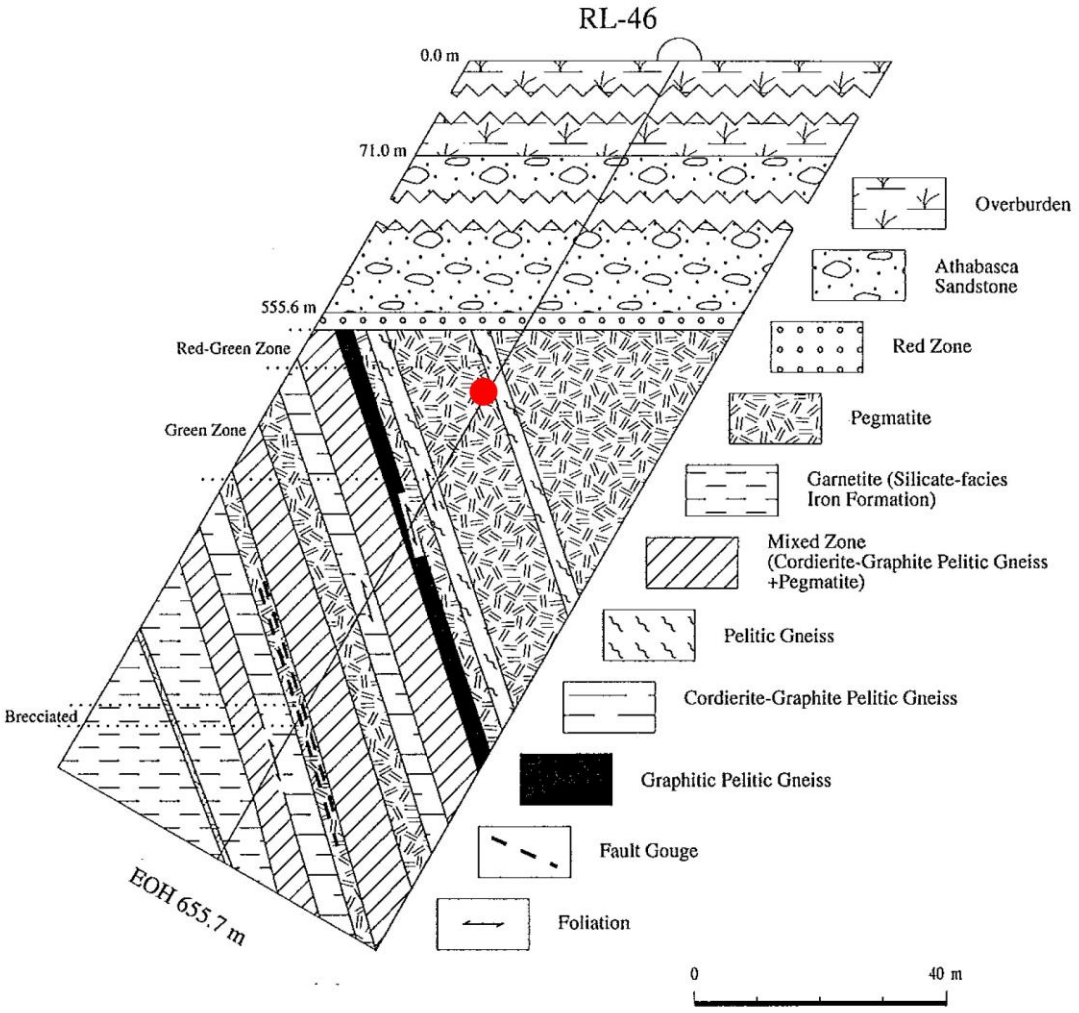

Cross-section of DDH RL-46.

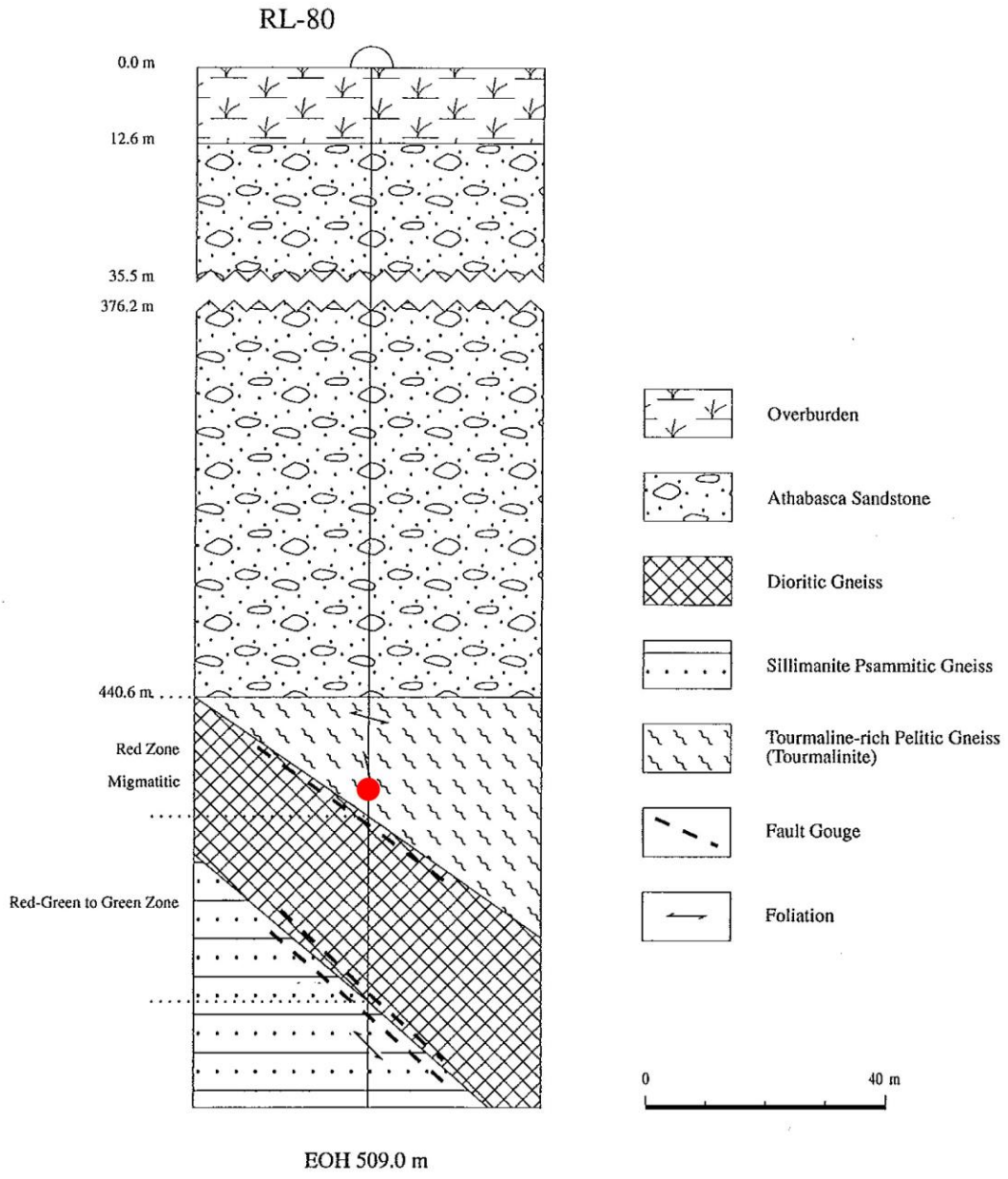

Cross-section of DDH RL-80.

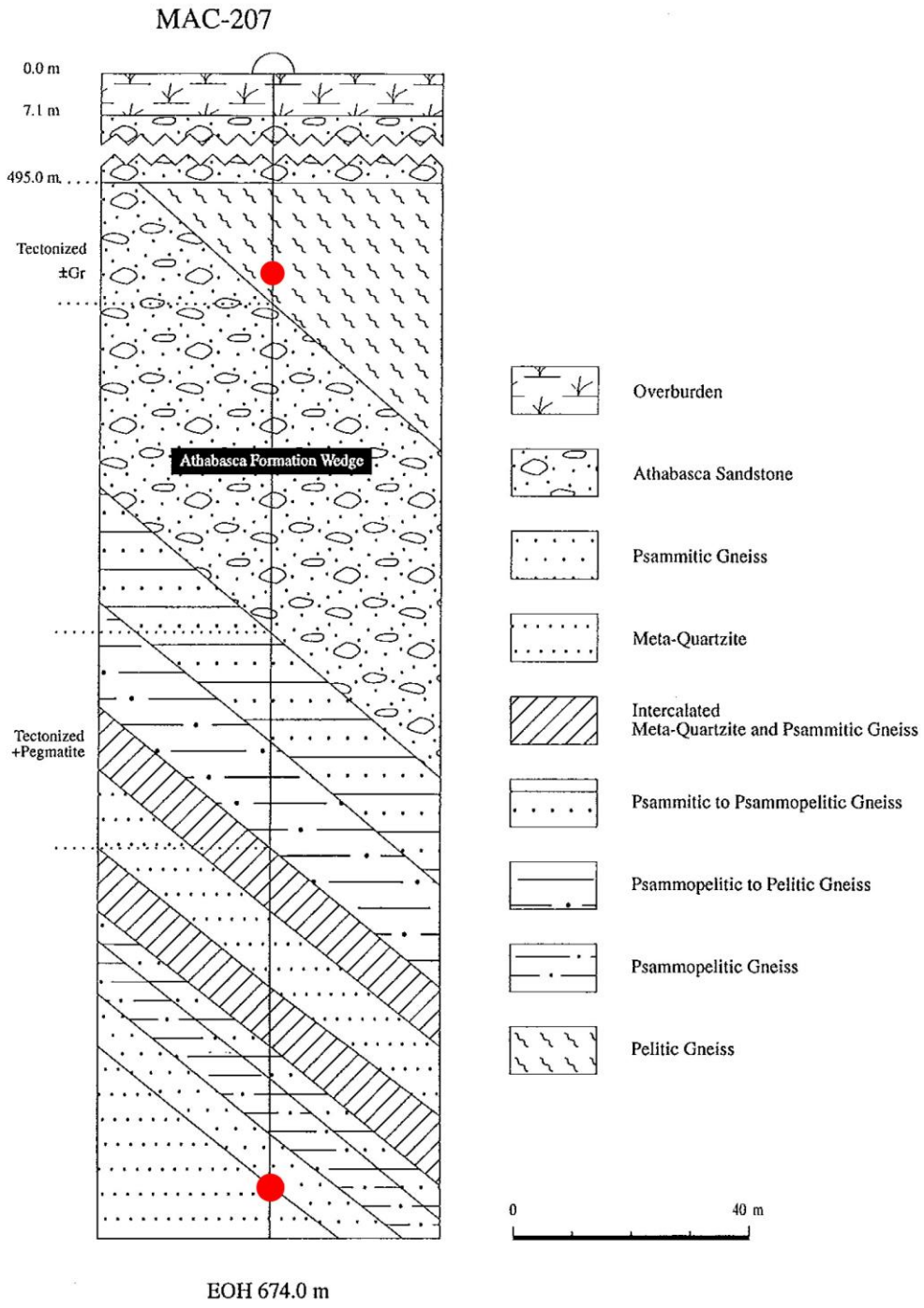

Cross-section of DDH MAC-207.